

# Structural Behavior of R-UHPFRC – RC Composite Slabs

THÈSE N° 6841 (2015)

PRÉSENTÉE LE 8 DÉCEMBRE 2015

À LA FACULTÉ DE L'ENVIRONNEMENT NATUREL, ARCHITECTURAL ET CONSTRUIT  
LABORATOIRE DE MAINTENANCE, CONSTRUCTION ET SÉCURITÉ DES OUVRAGES  
PROGRAMME DOCTORAL EN GÉNIE CIVIL ET ENVIRONNEMENT

ÉCOLE POLYTECHNIQUE FÉDÉRALE DE LAUSANNE

POUR L'OBTENTION DU GRADE DE DOCTEUR ÈS SCIENCES

PAR

**Maléna BASTIEN MASSE**

acceptée sur proposition du jury:

Prof. I. Smith, président du jury  
Prof. E. Brühwiler, Dr E. Denarié, directeurs de thèse  
Prof. W. Kaufmann, rapporteur  
Prof. D. Redaelli, rapporteur  
Prof. T. Keller, rapporteur



ÉCOLE POLYTECHNIQUE  
FÉDÉRALE DE LAUSANNE

Suisse  
2015



*A toutes ces femmes qui ont marché devant moi et qui ont ouvert le chemin...*



*Le béton est bien méphistobélique mais l'on peut s'en arranger.*

– Rudy Ricciotti. L'architecture est un sport de combat. 2013.



# Foreword

---

Reinforced Concrete (RC) structural elements such as slabs of bridges, parkings or industrial buildings, often do not show satisfactory performance in terms of structural behaviour and durability when exposed to increased concentrated high mechanical loading. In order to improve both existing RC elements, cost-effective novel concepts and technologies must be developed.

Ultra-High Performance Fiber Reinforced cement-based Composite materials (UHPFRC) have excellent mechanical properties. Cast as a relatively thin layer on an existing RC slab to form a monolithic composite element, UHPFRC acts as an external reinforcement, increasing both the bending and shear resistance. An additional benefit is that UHPFRC has extremely low permeability and thus serves as waterproofing layer protecting the slab from environmental influences.

In Switzerland, this novel technology is applied for more than 10 years. These applications are based on a targeted research activity by the MCS group. The present doctoral thesis by Maléna Bastien Masse is part of this more than 16 year-long research effort. Earlier theses showed that adding a layer of UHPFRC with/without steel reinforcing bars allows for significant increase of the structural resistance of RC members offering in this way effective strengthening solutions.

In her doctoral thesis, Maléna Bastien Masse investigates the structural behaviour of R-UHPFRC – RC composite slabs subjected to combined bending and shear. She explores the advantages of this novel structural system for effective strengthening of existing RC slabs. She conducted her research by means of an experimental campaign and thorough analytical modelling. Experimental results gave insight into hitherto unknown structural failure modes which in turn provided the basis for the analytical modelling according to the theory of plasticity. In addition, she addressed the topic of fiber orientation in UHPFRC.

The thesis topic is relevant and challenging since it shows additional more refined ways towards even more effective use of UHPFRC for the improvement of RC slabs. The present thesis delivers useful results in view of practical application.

Maléna Bastien Masse provides the proof of her capabilities to conduct a scientific study and to solve complex scientific problems. In the name of the whole MCS Team, I thank her for her constant and thorough investment to the thesis topic as well as for her professional skills and personal qualities.

Lausanne, November 2015

Professor Eugen Brühwiler





# Remerciements

---

Cette thèse a bénéficiée de la contribution de plusieurs personnes qui m'ont à un certain moment conseillée et encouragée et que je tiens ici à remercier sincèrement.

Tout d'abord je suis reconnaissante envers Prof. Eugen Brühwiler, mon directeur de thèse, qui est une source d'inspiration par sa façon de porter les projets et le BFUP. Son savoir et sa vision ont évidemment marqué mon travail pour le mieux. Il m'a également permis de participer à des projets diverses qui ont enrichi m'on expérience. Je veux aussi souligner la contribution du Dr Emmanuel Denarié qui a agi comme co-directeur de ma thèse, avec qui j'ai eu de longues discussions sur le BFUP et qui m'a beaucoup aidée et conseillée.

Je remercie les membres du jury pour leurs commentaires et questions qui ont permis d'améliorer la thèse : Prof. Walter Kaufmann, Prof. Dario Redaelli et Prof. Thomas Keller. Je remercie également le Prof. Ian Smith pour avoir présidé l'examen de thèse d'une main de maître.

Ce travail comprend une large étude expérimentale réalisée au laboratoire des structures de l'EPFL qui est pourvu d'une super équipe technique sans laquelle rien n'aurait été possible. En particulier je veux mentionner l'aide de Sylvain Demierre, Frédérique Dubugnon, Gérald Rouge et Gilles Guignet ainsi que tous les étudiants qui m'ont aidé lors de mes essais. Merci également à Jürgen Einpaul et à Fabio Brantschen pour m'avoir montré le fonctionnement du bâti de poinçonnement.

Le MCS ne serait probablement pas le même sans le support logistique et administratif qui a été fourni par deux personnes au courant de ma thèse : Christine Benoit et Florence Grandjean. Merci à toutes les deux d'avoir fait en sorte que tout se passe toujours bien mais aussi pour les discussions plus générales sur la vie en Suisse.

Au MCS, j'ai également eu la chance d'avoir des collègues exceptionnels. D'abord, Dr Talayeh Noshiravani, dont le travail précède le mien, a été une source d'inspiration par sa personnalité et la rigueur de son travail. Je remercie le Dr Hamid Sadouki qui a réalisé des analyses numériques de mes essais. Ensuite, je dois nommer Vasileios Grigoriou, Christophe Loraux, Dr Hadi Kazemi-Kamyab, Dr Mark Treacy, Dr Tohru Makita, Dr Marina Rocha et Dr Alexis Kalogeropoulos pour toutes les discussions sur le BFUP, les structures et la vie ainsi que pour les pauses café et les repas partagés. Et enfin, merci à tous les autres membres du groupe actuels et anciens, visiteurs, doctorants et étudiants au master, qui font du MCS ce qu'il est.

Au sein de l'EPFL j'ai bénéficié de l'expertise variée de nombreux amis. Je dois beaucoup à Jürgen Einpaul avec lequel j'ai eu d'innombrables conversations sur le poinçonnement des dalles de béton armé et sur la course à pied! Je le remercie aussi, ainsi que Dr Stefan Lips, Dr Hadi Kazemi-Kamyab et Galina Argirova, pour m'avoir aidé à préparer l'examen de thèse.

Merci aussi à toutes ces personnes qui ont rendu la vie à l'EPFL plus agréable, par des repas, des pauses café et des sorties... Un merci plus particulier à Aurelia Cuba Ramos pour toutes

## REMERCIEMENTS

les discussions sur la recherche de l'équilibre dans la vie et pour la traduction du résumé de la thèse en allemand!

Je n'aurais probablement pas débuté un doctorat si je n'avais pas été initié au monde des BFUP par le Prof. Jean-Philippe Charron, il y a 9 ans déjà. Je le remercie de m'avoir poussé vers le captivant monde de la recherche.

Je dois aussi énormément à ma famille, et plus particulièrement à mes parents Marc et Lise, qui m'ont encouragée tout au long de mes études en Génie civil ainsi que dans tous mes projets même si cela signifiait me laisser partir loin de Montréal.

Enfin, je remercie mon partenaire Peter Andrea Glauser de m'avoir accompagné pendant les hauts et les bas de ce doctorat. Il a su m'aider à rationaliser pendant les moments de panique et il m'a aidé à développer mes passions à côté de la thèse. Merci pour toutes les découvertes et tous les moments de joies partagées. Merci d'être simplement là.

Lausanne, novembre 2015

Maléna Bastien Masse

# Summary

---

The application on existing Reinforced Concrete (RC) slabs of cast-on-site Ultra-High Performance Fiber Reinforced cement-based Composite (UHPFRC) layers is an efficient reinforcement technique, currently spreading. The thin layer of UHPFRC, with or without steel rebars, serves as a tensile reinforcement for the RC slab, creating a composite element. This thesis combines material and structural engineering to study the behavior and resistance of two-way spanning composite slabs, with a certain focus on punching shear resistance.

When analysing the behavior of composite elements, the effect of fiber orientation on the in-plane tensile response of the UHPFRC layer needs to be accounted for. Theoretical tools are derived herein to analyze the complementarity of fiber orientation in perpendicular directions and determine the average effect of fiber orientation on fiber efficiency at pull-out. A comprehensive material testing campaign on a strain-hardening UHPFRC is carried out on specimens with various thicknesses and casting processes. The most likely fiber orientation in a layer of UHPFRC for the casting method considered herein is finally estimated with the results of the theoretical and experimental work and a representative tensile response is scaled accordingly.

An experimental campaign is carried out on six composite slabs without transverse reinforcement. The parameters of the tests include the thickness of the UHPFRC layer and the amount of reinforcement in it. The punching shear resistance of all composite slabs is higher than the resistance of the reference RC slab. The layer of UHPFRC increases the rigidity of the slab and provides added shear resistance to the cracked RC section by out-of-plane bending accompanied by limited or inexistent Near Interface Cracking (NIC) in the concrete section prior to failure. By doing so, it allows more deformation to take place in the RC section before punching shear failure. This results in rotations at maximum resistance close to what is observed for the reference RC slab.

An analytical model is then developed to predict the global bending behavior of the composite slab and the punching shear resistance. A multilinear moment-curvature relation for composite sections is used to calculate the force-rotation curve of a slab. The intersection between this curve and a deformation based composite failure criterion predicts the punching shear resistance. This criterion combines the concrete and the UHPFRC layer contributions. The latter resists to punching shear by out-of-plane bending over a limited length. This mechanism induces tensile stresses perpendicularly to the interface with the concrete. The contribution of the UHPFRC layer to the punching shear resistance thus depends on the tensile strength of concrete.

In the final section of the work, a description of the parameters influencing the shear resistance of composite elements is done. With the tools developed in this work, the effects of fiber orientation in a layer can be mastered and the analytical models allow to simply verify the resistance of a composite section.

**Keywords:** UHPFRC, Fiber orientation, Fiber efficiency, Tensile response, Composite slab, Punching shear, Strengthening, Critical shear crack, Near interface cracking.



# Résumé

---

L'ajout d'une couche de Béton Fibré à Ultra-Haute Performance (BFUP) sur une dalle de béton armé existante est une méthode de renforcement efficace de plus en plus utilisée en Suisse et ailleurs. La mince couche de BFUP, avec ou sans barres d'armature, sert de renforcement en traction pour la dalle, créant ainsi une section composée. Cette thèse combine la science des matériaux et des structures afin d'étudier le comportement et la résistance d'une dalle composée bidirectionnelle, avec une certaine attention portée sur la résistance au poinçonnement.

L'effet de l'orientation des fibres sur la réponse en traction dans le plan d'une couche de BFUP doit être considéré lors de l'étude du comportement d'une dalle composée. Des outils théoriques sont dérivés pour analyser la complémentarité de l'orientation des fibres dans les deux directions perpendiculaires du plan et pour définir l'effet moyen de cette orientation sur l'efficacité des fibres à l'arrachement. Une campagne d'essais de caractérisation d'un BFUP écrouissant est réalisée sur des éprouvettes avec différentes épaisseurs et méthodes de fabrication. Le coefficient d'orientation des fibres le plus probable dans une couche de BFUP, pour les méthodes de mise en place considérées ici, est enfin estimé et la réponse en traction est définie en fonction.

Une campagne d'essais sur six dalles composées sans renforcement d'effort tranchant est réalisée. Les paramètres d'essais sont l'épaisseur de la couche de BFUP et son taux d'armature. La résistance au poinçonnement de toutes les dalles composées est plus grande que celle de la dalle de béton armé de référence. La couche de BFUP augmente la rigidité flexionnelle de la dalle et contribue à la résistance au poinçonnement par un mécanisme de flexion hors-plan accompagné par le développement très limité d'une fissuration horizontale dans le béton, près de l'interface. Ainsi, la couche de BFUP permet à la section de béton armé de se déformer d'avantage avant la rupture et la rotation de la dalle à sa résistance maximale est proche de celle qui a été mesurée pour la dalle de béton armé.

Un modèle analytique est développé pour prédire le comportement global en flexion de la dalle composée et sa résistance au poinçonnement. Une relation moment-courbure multilinéaire est utilisée pour calculer la courbe force-rotation de la dalle. L'intersection entre cette courbe et un critère de rupture composé basé sur l'état de déformation de la dalle donne la résistance au poinçonnement. Ce critère combine la contribution du béton et celle de la couche de BFUP. Celle-ci résiste au poinçonnement par un mécanisme de flexion qui se développe sur une courte longueur. Ce mécanisme induit des contraintes de traction perpendiculairement à l'interface avec le béton. La contribution de la couche de BFUP à la résistance au poinçonnement est donc fonction de la résistance à la traction du béton.

Dans la dernière partie de cette thèse, une description des paramètres influençant la résistance à l'effort tranchant des éléments composés est faite. Avec les outils développés, les effets d'orientation de fibres dans une couche de BFUP peuvent être maîtrisés tandis que les outils analytiques permettent de simplement vérifier la résistance de la dalle composée.

**Mots-clés :** BFUP, Orientation des fibres, Efficacité des fibres, Comportement en traction, Dalle composée, Poinçonnement, Renforcement, Fissure critique, Fissuration près de l'interface.



# Zusammenfassung

---

Das Aufbringen von vor Ort gegossenem, ultra-hochleistungsfähigem Faserbeton (UHFB) auf bereits existierenden Decken aus Stahlbeton (StB) ist eine effiziente Verstärkungstechnik, die immer mehr an Bedeutung gewinnt. Die dünne Schicht aus UHFB, mit oder ohne Stahlbewehrungsstäbe, dient als Zugbewehrung des Verbundbauteils. In der vorliegenden Arbeit werden Ansätze aus der Werkstoff- und der Tragwerks-Bautechnik kombiniert, um das Verhalten und den Widerstand der Verbundbauteile zu untersuchen, wobei ein besonderes Augenmerk auf den Durchstanzwiderstand gerichtet wird.

Bei der Untersuchung des mechanischen Verhaltens von Verbundtragwerken muss der Einfluss der Faserorientierung auf das Zugverhalten der UHFB-Schicht berücksichtigt werden. In dieser Arbeit werden theoretische Modelle hergeleitet, um die Komplementarität der Faserorientierung in den orthogonalen Richtungen zu analysieren und den gemittelten Einfluss der Faserorientierung beim Ausziehen zu bestimmen. Umfangreiche Materialprüfungen an Fest-UHFB werden durchgeführt, wobei die Proben in Dicke und der Art des Gießverfahrens variieren. Die in einer UHFB-Schicht am wahrscheinlichsten auftretende Faserorientierung, für das hier berücksichtigte Gießverfahren, wird schließlich anhand der Ergebnisse aus den theoretischen Betrachtungen und den experimentellen Versuchen abgeschätzt, und ein repräsentatives Zugverhalten wird dementsprechend skaliert.

Eine experimentelle Testreihe an sechs Verbunddecken ohne Querverstärkung wird durchgeführt. Als Testparameter werden die Dicke der UHFB-Schicht und der Anteil an Bewehrungsstahl gewählt. Der Durchstanzwiderstand ist für alle untersuchten Verbunddecken höher als der Widerstand der Referenzdecke. Die UHFB-Schicht erhöht die Steifigkeit der Decke und führt zu einem zusätzlichem Schubwiderstand im gerissenen StB-Abschnitt aufgrund des Biege- und Schubwiderstands der UHFB-Schicht, mit der in manchen Fällen eine Rissbildung nahe der Grenzfläche einhergeht, bevor es zum Bauteilversagen kommt. Durch diesen Mechanismus können im StB-Abschnitt höhere Verformungen aufgenommen werden, bevor es zum Durchstanzversagen kommt.

Ein analytisches Modell wird entwickelt, um das globale Biegeverhalten der Verbunddecke und den Durchstanzwiderstand vorzuberechnen. Die Verwendung einer multi-linearen Beziehung zwischen Moment und Krümmung für den Verbundquerschnitt ermöglicht es die Kraft-Krümmungs-Kurve der Decke zu berechnen. Den Durchstanzwiderstand wird danach als Schnittpunkt dieser Kurve mit einem verformungsbasierten Versagenkriterium für Verbundbauteile erhalten. Dieses Kriterium kombiniert die Anteile des Betons und der UHFB-Schicht. Letztere widersetzt sich dem Durchstanzschub durch einen Biege- und Schubwiderstand der UHFB-Schicht, der sich entlang einer begrenzten Länge bildet. Dieser Mechanismus verursacht Zugspannungen senkrecht zur Beton-UHFB-Grenzfläche. Der Beitrag der UHFB-Schicht am Durchstanzwiderstand hängt daher von der Zugfestigkeit des Betons ab.

Der abschließende Teil dieser Arbeit enthält eine Beschreibung der Parameter, die den Schubwiderstand des Verbundtragwerks beeinflussen. Mit den Methoden, die in dieser Arbeit entwickelt wurden, kann der Einfluss der Faserorientierung abgeschätzt werden, und

## ZUSAMMENFASSUNG

die analytischen Modelle ermöglichen es, den Widerstand eines Verbundabschnitts auf eine einfache Art nachzuprüfen.

**Stichworte:** UHFB, Faserorientierung, Fasereffizienz, Zugverhalten, Verbunddecken, Durchstanzwiderstand, Festigkeitssteigerung, kritischer Schubriss, Versagen nahe der Grenzfläche.



# Table of Contents

---

<b>Foreword</b> .....	<b>v</b>
<b>Remerciements</b> .....	<b>vii</b>
<b>Summary</b> .....	<b>ix</b>
<b>Résumé</b> .....	<b>xi</b>
<b>Zusammenfassung</b> .....	<b>xiii</b>
<b>Table of Contents</b> .....	<b>xv</b>
<b>List of Figures</b> .....	<b>xxi</b>
<b>List of Tables</b> .....	<b>xxv</b>
<b>Introduction</b> .....	<b>1</b>
<b>1 Context</b> .....	<b>3</b>
<b>2 Motivation</b> .....	<b>4</b>
2.1 Conceptual idea .....	4
2.2 Background .....	6
2.2.1 Overview .....	6
2.2.2 UHPFRC properties.....	6
2.2.3 Structural behavior of RU-RC elements .....	6
<b>3 Problem statement</b> .....	<b>7</b>
<b>4 Objectives</b> .....	<b>8</b>
<b>5 Scope</b> .....	<b>8</b>
<b>6 Outline</b> .....	<b>9</b>
<b>7 References</b> .....	<b>10</b>

**Paper I Effect of Fiber Orientation on the In-Plane Tensile Response of UHPFRC Reinforcement Layers..... 13**

**1 Introduction..... 15**

**2 Tensile response of UHPFRC..... 16**

2.1 Overview .....16

2.2 Ultimate tensile strength .....16

2.2.1 Equation.....16

2.2.2 Fiber orientation factor.....16

2.2.3 Fiber efficiency factor .....17

2.2.4 Maximum fiber pull-out stress .....18

2.3 Tensile hardening response .....18

**3 Stereological analysis..... 19**

3.1 Overview .....19

3.2 Fiber orientation in orthogonal directions.....20

3.2.1 Two dimensional case (2D) .....20

3.2.2 Three dimensional case (3D) .....21

3.2.3 Relations for orthogonal directions .....22

3.3 Average efficiency factor.....24

**4 Material characterization..... 25**

4.1 Overview .....25

4.2 Testing program .....25

4.3 Test results .....27

4.3.1 Bending response.....27

4.3.2 Tensile response.....29

4.4 Modelling results .....30

4.5 Discussion .....31

4.5.1 Analysis of test results.....31

4.5.2 Recent literature data.....31

4.5.3 Interpretation .....32

**5 Validation of the stereological analysis ..... 33**

5.1 Overview .....33

5.2 Fiber orientation in orthogonal directions.....33

5.2.1 Validation with test results .....33

5.2.2 Average relation .....33

5.2.3 Generalization .....36

5.3 Average efficiency factor.....36

**6 Application to a UHPFRC layer..... 38**

6.1 Overview .....38

6.2 Slab elements .....38

6.3 Average fiber orientation factors.....39

6.4 Representative tensile response .....39

**7 Conclusions ..... 40**

**8 References..... 41**

<b>Paper II Experimental Investigation on Punching Resistance of R-UHPFRC – RC Composite Slabs .....</b>	<b>45</b>
<b>1 Introduction .....</b>	<b>47</b>
<b>2 Background.....</b>	<b>48</b>
2.1 Punching shear resistance of RC slabs without transverse reinforcement.....	48
2.2 Strengthening methods.....	48
2.3 Shear resistance of RU-RC composite beams .....	49
<b>3 Experimental investigations .....</b>	<b>50</b>
3.1 Test specimens.....	50
3.2 Material properties .....	51
3.3 Test setup and procedure.....	53
<b>4 Experimental results and discussion .....</b>	<b>54</b>
4.1 Force-rotation response and failure mode .....	54
4.2 Cracking patterns.....	57
4.3 Deflections, deformations and strains .....	58
4.3.1 Thickness variation and UHPFRC cracking .....	58
4.3.2 Slab deformation.....	59
4.3.3 Shear deformation .....	61
4.3.4 Concrete strains.....	61
4.4 Contribution of the UHPFRC layer to punching shear resistance .....	62
4.5 Post-peak remaining resistance .....	63
<b>5 Comparison with resistance models for RC Slabs .....</b>	<b>64</b>
5.1 Overview.....	64
5.2 Yield-line method.....	64
5.3 Critical shear crack theory.....	64
<b>6 Conclusions.....</b>	<b>65</b>
<b>7 References.....</b>	<b>66</b>
<b>Paper III Composite Model for Predicting the Punching Resistance of R-UHPFRC – RC Composite Slabs.....</b>	<b>69</b>
<b>1 Introduction .....</b>	<b>73</b>
<b>2 Model parameters .....</b>	<b>75</b>
2.1 Material constitutive laws .....	75
2.1.1 Concrete .....	75
2.1.2 Steel.....	75
2.1.3 UHPFRC.....	76
2.2 Tension chords .....	76
2.2.1 Overview .....	76
2.2.2 RC tension chord.....	77
2.2.3 RU tension chord.....	77
2.2.4 RU-RC tension chord .....	78

<b>3</b>	<b>Force-rotation behavior .....</b>	<b>78</b>
3.1	Assumed bending behavior .....	78
3.2	Moment-curvature relations .....	79
3.2.1	RC section.....	79
3.2.2	RU-RC composite section.....	81
3.3	Direct method.....	84
<b>4</b>	<b>Punching shear resistance .....</b>	<b>88</b>
4.1	Composite failure criterion.....	88
4.2	Concrete contribution .....	88
4.3	UHPFRC layer contribution .....	89
4.4	Validity of the model.....	90
4.5	Punching shear failure and post-peak resistance.....	91
<b>5</b>	<b>Model validation .....</b>	<b>91</b>
5.1	Slab specimens.....	91
5.1.1	Geometry .....	91
5.1.2	Material properties.....	92
5.2	Results .....	94
<b>6</b>	<b>Post-installed UHPFRC layer.....</b>	<b>96</b>
6.1	Overview .....	96
6.2	Moment-curvature relations .....	96
6.3	Force-rotation behavior and punching shear failure .....	98
<b>7</b>	<b>Conclusions .....</b>	<b>100</b>
<b>8</b>	<b>References.....</b>	<b>101</b>

**Paper IV Contribution of R-UHPFRC Strengthening Layers to the Shear**

<b>Resistance of RC Elements .....</b>	<b>105</b>	
<b>1</b>	<b>Introduction.....</b>	<b>109</b>
<b>2</b>	<b>Background .....</b>	<b>110</b>
2.1	Shear transfer mechanism in RC elements.....	110
2.2	Bending behaviour of a composite section.....	110
<b>3</b>	<b>Shear resistance of RU-RC composite members .....</b>	<b>111</b>
3.1	Shear transfer mechanism in RU-RC composite members.....	111
3.2	Analytical model.....	112
3.2.1	Overview.....	112
3.2.2	Concrete contribution.....	113
3.2.3	Shear reinforcement contribution.....	113
3.2.4	R-UHPFRC layer contribution .....	113
3.3	Validation with test results.....	114
3.3.1	Overview and specimens.....	114
3.3.2	Cantilever beams.....	116
3.3.3	Continuous beams.....	117
3.4	Parametric study.....	118

3.5	Design example.....	119
<b>4</b>	<b>Punching shear resistance of composite slabs .....</b>	<b>121</b>
4.1	Punching shear resistance of RU-RC composite slabs.....	121
4.2	Analytical model.....	122
4.2.1	Overview.....	122
4.2.2	Composite failure criterion.....	122
4.2.3	Force-rotation behavior.....	123
4.3	Parametric study.....	124
4.4	Design example.....	125
<b>5</b>	<b>Discussion.....</b>	<b>127</b>
<b>6</b>	<b>Conclusions.....</b>	<b>128</b>
<b>7</b>	<b>References.....</b>	<b>128</b>
 <b>Conclusions .....</b>		 <b>131</b>
<b>1</b>	<b>Overview .....</b>	<b>133</b>
<b>2</b>	<b>Summary of contributions .....</b>	<b>133</b>
2.1	Representative tensile response of a UHPFRC layer .....	133
2.2	Experimental investigation on the punching shear resistance of composite slabs 134	
2.3	Modelling the behavior and punching shear resistance of composite slabs .....	134
2.4	Influence of parameters on the shear resistance of composite sections .....	135
<b>3</b>	<b>Perspectives and future works .....</b>	<b>136</b>
3.1	UHPFRC properties .....	136
3.2	Structural behavior of RU-RC elements.....	137
3.3	Reinforcing with UHPFRC .....	138
<b>4</b>	<b>References.....</b>	<b>138</b>
 <b>Appendix A Characterization of the UHPFRC S3-13 .....</b>		 <b>141</b>
 <b>Appendix B Punching Tests on R-UHPFRC-RC Composite Slabs without Shear Reinforcement.....</b>		 <b>143</b>
 <b>Curriculum Vitae.....</b>		 <b>145</b>



# List of Figures

---

## Introduction

Figure 1 (a) Tensile behavior of UHPFRC; (b) Quarter of composite slab element.....	4
Figure 2 The present work placed in the context of previous research [I.10, 11, 13-19] .....	5
Figure 3 Flexure-shear failure of a composite beam [I.15] .....	7
Figure 4 Structure of the thesis .....	9

## Paper I Effect of Fiber Orientation on the In-Plane Tensile Response of UHPFRC Reinforcement Layers

Figure 1 Typical composite slab element with bending and shear actions.....	15
Figure 2 Fiber efficiency depending on pull-out angle, adapted from [1.16, 19] .....	17
Figure 3 Meso-mechanical model for UHPFRC tensile hardening response, adapted from [1.22]: (a) individual contributions to the crack-opening response; (b) distributed micro-cracks .....	18
Figure 4 Position of a fiber: (a) in 2D plan; (b) in 3D volume, adapted from [1.10, 25] .....	20
Figure 5 Possible range of angles in the quadrant: (a) 1-2; (b) 2-3 .....	20
Figure 6 Relation between orientation factors in orthogonal directions .....	23
Figure 7 Relation between orientation and efficiency factors .....	25
Figure 8 Test specimens for series III, IV and V .....	27
Figure 9 Bending tests results for UHPFRC S3-13: (a to d): force-displacement curves; (e) result of the inverse analysis on series I .....	28
Figure 10 Tensile test results for UHPFRC S3-13 .....	30
Figure 11 Orientation factors in orthogonal directions and experimental data .....	35
Figure 12 Relation between orientation and efficiency factors and experimental data.....	37
Figure 13 Geometry of composite slab specimens PBM [1.30].....	38

## Paper II Experimental Investigation on Punching Resistance of R-UHPFRC – RC Composite Slabs

Figure 1 (a) Typical RU-RC composite cross-section and notations [2.2]; (b) Constitutive law of UHPFRC [2.3].....	47
Figure 2 Flexure-shear failure of a RU-RC composite beam [2.7] .....	49
Figure 3 Schematic test setup: (a) PBM series; (b) SAMD series [2.19].....	54

Figure 4 Normalized force-rotation curves.....	55
Figure 5 Fully developed cracking pattern on cut sections of the slabs at the end of the test and position of the thickness measurements .....	56
Figure 6 Fully developed cracking pattern of the top tensile faces at the end of the tests.....	57
Figure 7 Change of thickness of the slab in two locations (Ep01 and 02) and radial displacements of the UHPFRC layer (UT01) as a function of the normalized force .....	59
Figure 8 Deflections of PBM1 and PG19: (a) top and bottom deformed shapes; (b) central deflections as a function of the normalized force .....	60
Figure 9 Shear deformation: (a) definition [2.21]; (b) measurements at column face as a function of the normalized force for selected specimen.....	61
Figure 10 Bending of the UHPFRC layer and shear deformations at column face .....	62
Figure 11 Post-peak behaviour of selected slabs as a function of the normalized force.....	63

### **Paper III Composite Model for Predicting the Punching Resistance of R-UHPFRC – RC Composite Slabs**

Figure 1 (a) Typical RU-RC composite slab element; (b) Resisting mechanisms for composite slabs [3.2].....	73
Figure 2 (a) Efforts in slab sector; (b) assumed behavior of slab; (c) calculation of punching shear resistance with a failure criterion, adapted from [3.12] .....	74
Figure 3 Constitutive laws: (a) UHPFRC in compression; (b) concrete in compression [3.13]; (c) steel .....	75
Figure 4 UHPFRC tensile law .....	76
Figure 5 Moment-curvature relations: (a) RC section [3.12]; (b) RU-RC section.....	80
Figure 6 Sectional distributions of strains, stress and forces .....	81
Figure 7 UHPFRC resisting mechanism.....	89
Figure 8 Moment-curvature behavior of an R-UHPFRC layer .....	90
Figure 9 Geometry for (a) square test slab; (b) axisymmetric circle slab.....	92
Figure 10 Experimental force-rotation curves versus model predictions .....	94
Figure 11 (a) Moment-curvature relation for a composite section with a post-installed UHPFRC layer; (b) Related sectional distributions of strains, stress and forces .....	97
Figure 12 Force-rotation behavior for a composite section with a post-installed UHPFRC layer.....	98



## **Paper IV Contribution of R-UHPFRC Strengthening Layers to the Shear Resistance of RC Elements**

Figure 1 Example of structures submitted to combined bending and shear: (a) cantilevers on a box girder bridge; (b) cantilever floor in a building; (c) flat slabs on columns .....	109
Figure 2 (a) Typical RU-RC composite cross-section [4.2]; (b) Schematic tensile behavior of UHPFRC [4.7].....	109
Figure 3 Multilinear moment-curvature relation for composite RU-RC sections .....	111
Figure 4 Flexure-shear failure mechanisms of composite RU-RC member, adapted from [4.8] .....	112
Figure 5 Moment distribution for the two test setups, adapted from [4.5, 21]: (a) cantilever beams; (b) continuous beams .....	114
Figure 6 Relation between span-to-depth ratio and shear strength.....	119
Figure 7 Design example: Chillon viaducts box girders cross-section, adapted from [4.23]	121
Figure 8 Punching shear resistance of composite RU-RC slabs [4.9]: (a) failure mechanisms; (b) calculation of punching shear resistance with a failure criterion .....	122
Figure 9 Influence of UHPFRC layer parameters on the punching resistance .....	125
Figure 10 Design example: floor plan .....	126



# List of Tables

---

## **Introduction**

Table 1 UHPFRC types [I.20] .....	6
-----------------------------------	---

## **Paper I Effect of Fiber Orientation on the In-Plane Tensile Response of UHPFRC Reinforcement Layers**

Table 1 Testing program for UHPFRC S3-13.....	26
Table 2 Main results of the characterization campaign on UHPFRC S3-13 .....	29
Table 3 Parameters for the meso-mechanical model for UHPFRC S3-13 .....	30
Table 4 Review of recent ultimate tensile strength results for UHPFRC.....	32
Table 5 Review of experimental fiber orientation measurements .....	34
Table 6 Calculations of fiber orientation factor.....	35
Table 7 Review of experimental fiber orientation measurements and related tensile strength .....	37
Table 8 Fiber orientation and tensile responses for layers of UHPFRC S3-13.....	39

## **Paper II Experimental Investigation on Punching Resistance of R-UHPFRC – RC Composite Slabs**

Table 1 Main parameters of test series.....	51
Table 2 Tested material properties.....	52
Table 3 Main test results.....	55
Table 4 Comparison to flexural capacity .....	64

## **Paper III Composite Model for Predicting the Punching Resistance of R-UHPFRC – RC Composite Slabs**

Table 1 Expressions for the quadrilinear moment-curvature relation for an RC section [3.12] .....	80
Table 2 Expressions for the multilinear moment-curvature relation for an RU-RC composite section.....	85
Table 3 Equation of forces on the composite section at different stages of the moment-curvature relation.....	86
Table 4 Comparison between test results or layered model predictions to multilinear model predictions.....	87

Table 5 Parameters of composite slab test series [3.2] .....92

Table 6 Average material properties [3.2].....93

Table 7 Experimental test results versus model predictions .....95

Table 8 Modified expressions for the multilinear moment-curvature relation of composite section with a post-installed UHPFRC layer.....99

Table 9 Equation of forces on the composite section with a post-installed UHPFRC layer100

**Paper IV Contribution of R-UHPFRC Strengthening Layers to the Shear Resistance of RC Elements**

Table 1 Geometry and steel ratios of the tested composite beams.....115

Table 2 Updated material properties of the tested composite beams.....116

Table 3 Comparison between test results and predictions for composites beams in a cantilever configuration .....117

Table 4 Comparison between test results and predictions for continuous composite beams .....118

Table 5 Reference values for parametric study on shear resistance of composite beams .....119

Table 6 Main parameters for the shear design example on the Chillon viaduct cross-section .....120

Table 7 Reference values for parametric study on punching shear resistance of composite slabs .....124

Table 8 Main parameters for the punching shear design example .....127

# Introduction

---



## 1 Context

The transportation network (road and railway) includes structures such as bridges, tunnels, retaining walls, parking buildings and transport stations. The importance of these structures for our society can be analysed through the general sustainability definition: (1) economic development, (2) social and cultural value and (3) environmental impacts.

Transportation infrastructure and, more generally, the built environment have a high initial cost for our society, but then brings significant added value for the economy and social life. Closing or restricting the circulation or use of a bridge or building at any point within a network always has a user cost. To allow unrestricted utilization, even for increasing traffic and loads, structures should be built for very long service life, if not forever [I.1]. When maintenance is needed, it should be done in ways that will increase this service life and with methods that significantly reduce the need to disrupt circulation.

Structures also have a cultural, historical and esthetical value. They can be considered as pieces of art, as recently proposed by Men  trety [I.2]: “their design and construction require the creative work of engineers, put into practice through their experience, skill and common sense.” A structure is a unique solution to a technical problem, representative of the period in which it was built, and as such, needs to be preserved. At the same time, they serve the society as a connexion to other regions and a passing point and as so have a strong social value.

Finally, the environmental impacts of the construction industry are known to be very large. The building material sector represents 5 to 10% of the total anthropogenic CO<sub>2</sub> emissions and consumes 60% of the extracted raw materials [I.3, 4]. To reduce these environmental impacts and conserve our resources, the use of raw materials and energy utilization in transforming and transporting them should be more and more limited.

New structures must thus be built with innovative methods, using less resources and more durable materials, to limit the need for rehabilitation during the service life. The development of new high performance materials allow a rethinking of the way structures are designed. High performance cementitious materials have higher CO<sub>2</sub> emissions per cubic meter, but the volume of material needed to construct a given structural element is reduced. With the Life Cycle Assessment (LCA) methodology, it was shown that the use of high performance concrete instead of normal strength concrete for the construction of a new bridge reduces the greenhouse gas emissions for material production by up to 50% [I.4].

However, erecting a new bridge or building where one already exists is questionable. In most cases, a new-build has a higher economic and environmental cost than maintaining the existing one and also implies destroying a “piece of art”. At the same time, transportation infrastructure of western developed countries is ageing while traffic volumes keep increasing. By developing methods to correctly examine existing structures, such as the monitoring of structures, interventions can often be limited and even proven to be unnecessary [I.5]. When reinforcement is indeed needed, it should be done in a way that will improve the performance of the structure for future traffic demand, without modifying its original aspect and esthetics, and avoiding or limiting circulation restrictions.

As for new structures, high performance materials can be used in an efficient way for reinforcement. In recent years, the use of thin layers of Ultra-High Performance Fiber Reinforced cement-based Composite (UHPFRC) for the strengthening of existing structures has been actively developed and shown to be an efficient and durable method [I.6, 7]. This technique is currently spreading and respects the economic, artistic and environmental considerations previously exposed. The application of a UHPFRC layer on a slab can be done in a very short time frame, thus limiting the need to restrict traffic and for costs equivalent or lower to conventional reinforcement methods [I.1, 8]. Using LCA methodology, it was also demonstrated that the use of a UHPFRC layer for the reinforcement of a bridge deck slab has a lower environmental impact than conventional methods, as it reduces the need for further rehabilitation during the service life of the structure and limits the need for traffic deviation [I.9].

The targeted use of high performance material such as UHPFRC is part of the answer for the development and improvement of our bridges and buildings, as it allows the building and strengthening of structures in a more cost effective, creative and durable way.

## 2 Motivation

### 2.1 Conceptual idea

UHPFRC is composed of a very compact cementitious matrix combined with a high amount of short straight steel fibers. The orientation of these fibers and their efficiency at pull-out governs the tensile behavior of UHPFRC [I.10, 11], characterized by strain-hardening and softening phases (Figure 1a). UHPFRC also has a very low permeability, which is preserved even when it is submitted to tensile strains within its hardening domain [I.12].

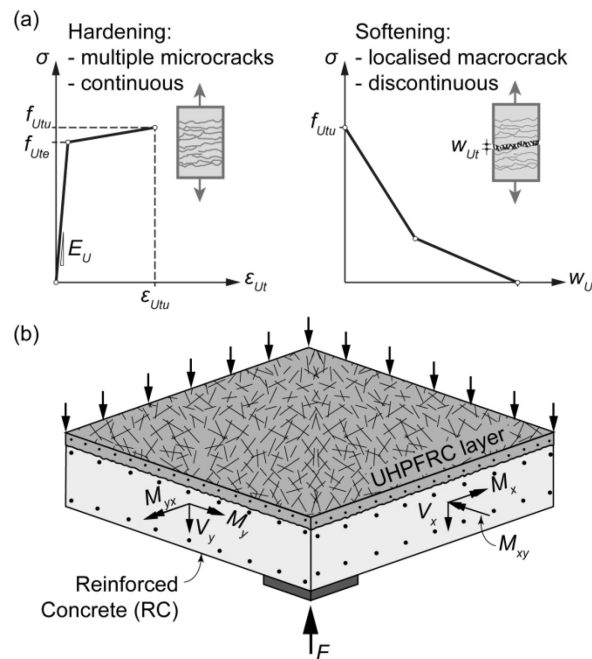
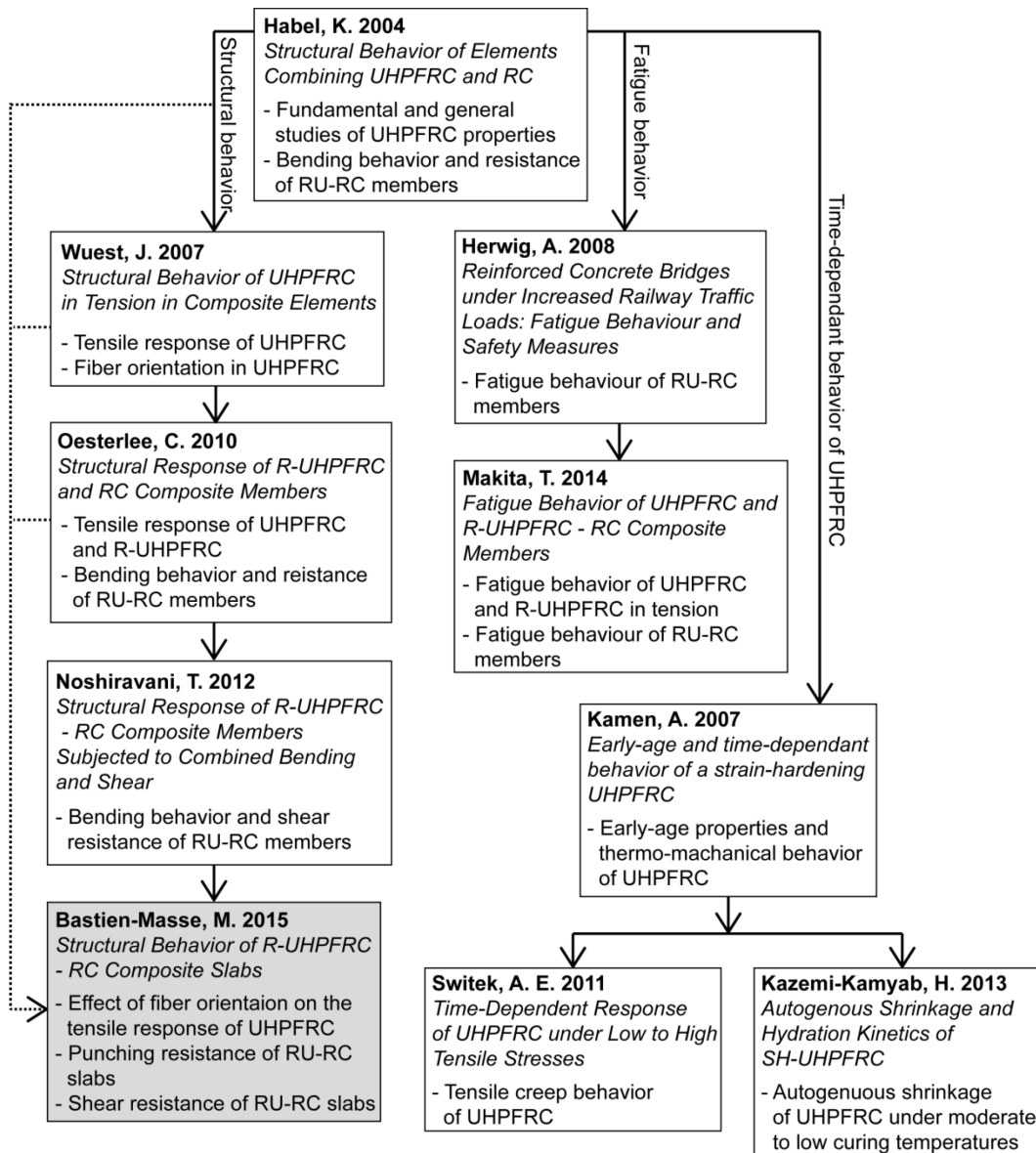


Figure 1 (a) Tensile behavior of UHPFRC; (b) Quarter of composite slab element



Because of these outstanding properties, UHPFRC is adequate for rehabilitation of Reinforced Concrete (RC) structures. Placed on the top of a RC element, UHPFRC layers, reinforced (or non-reinforced) with small diameter steel rebars (R-UHPFRC), serve as an external tensile reinforcement, creating a composite RU-RC section (Figure 1b). The layers have a typical thickness of between 25 and 50 mm and are cast in place over a concrete surface roughened by high-pressure water jetting.



**Figure 2** The present work placed in the context of previous research [I.10, 11, 13-19]

With one R-UHPFRC layer, at least three beneficial effects are achieved. Firstly, with its low permeability, the layer serves as a waterproofing for the RC section below, protecting it from the ingress of detrimental substances such as water and chlorides. Secondly, the high tensile deformability and strength of UHPFRC combined with steel rebars significantly increases the bending and shear resistance of the section [I.11, 13, 15]. Thirdly, the addition of a R-UHPFRC layer increases the fatigue life of the element [I.16]. This thesis will focus on the second point, the behavior and resistance of composite RU-RC slabs. The work is a

continuation of 16 years of research on the topic at MCS-EPFL which resulted in 7 theses (Figure 2).

## 2.2 Background

### 2.2.1 Overview

The design of composite RU-RC sections combines both material and structural engineering. In a first step, the UHPFRC mechanical properties need to be known. In particular, the tensile response of the material must be identified. The global structural behavior of a composite RU-RC member is then studied through experimental campaigns that serve the development of analytical models. These models, with the correct material properties, can be used to predict the behavior and resistance of composite members.

### 2.2.2 UHPFRC properties

UHPFRCs typically have a modulus of elasticity  $E_U$  between 40 and 60 GPa and a compressive strength higher than 120 MPa [I.20]. In the Swiss guidelines for UHPFRC, three types of UHPFRC are defined according to their tensile properties: elastic limit strength  $f_{Ute}$ , tensile strength  $f_{Utm}$  and extent of hardening in tension  $\varepsilon_{Utm}$  (Table 1). Type U0 does not present a hardening domain, while types UA and UB are hardening UHPFRCs.

**Table 1 UHPFRC types [I.20]**

UHPFRC type	U0	UA	UB
$f_{Ute}$ [MPa]	$\geq 7.0$	$\geq 7.0$	$\geq 10.0$
$f_{Utm}/f_{Ute}$	$\geq 0.7$	$\geq 1.1$	$\geq 1.2$
$\varepsilon_{Utm}$ [‰]	$f_{Utm}/E_U$	$\geq 1.5$	$\geq 2.0$

To define these tensile properties and categorize a given mix, tensile tests must be carried, as was done by many authors [I.13, 21-23]. However, only a few have linked the results to the fiber orientation in the specimen [I.10, 11, 24, 25]. Moreover, in most cases, tensile or bending tests are done on individually cast specimens with fiber orientation and dispersion not representative of what can be expected in a layer of UHPFRC cast over a large slab. To accurately predict the resistance of a composite section, representative UHPFRC tensile properties must be identified, taking into account the effect of fiber orientation and efficiency.

### 2.2.3 Structural behavior of RU-RC elements

The bending behavior of composite sections has been thoroughly studied with experimental campaigns which showed that the composite section behaves monolithically when submitted to pure bending efforts [I.11, 13]. The layer of R-UHPFRC increases the flexural rigidity and bending resistance of the section. The experimental results then served the development of analytical models to predict the bending behavior and resistance of a composite section. A sectional analysis was proposed using plane section theory and assuming a rigid bond between all elements [I.13]. The multiple layers of tensile reinforcements (UHPFRC layer,

steel rebars in the RC section and the layer) add to the complexity of the bending resistance prediction, as their yield strength is reached for different levels of bending efforts.

To complete the study of composite members, Noshiravani [I.15] undertook a large experimental campaign on composite beams submitted to combined bending and shear. These tests showed that the development of an inclined flexure-shear crack in the RC section is accompanied by softening of the concrete below the RU-RC interface (Figure 3). This Near Interface Cracking (NIC) modifies the shear transfer between the RC section and the R-UHPFRC layer, and alters the structural behavior and failure mode of the composite member. Based on these observations and using the theory of plasticity, Noshiravani developed an analytical model to predict the structural behavior of a member submitted to NIC using an elastic-plastic fictitious hinge. A collapse mechanism to predict the flexure-shear resistance of a composite beam was also developed. According to this mechanism, the R-UHPFRC layer contributes to the shear resistance by out-of-plane bending over the NIC zone. To apply this collapse mechanism and the fictitious hinge model, an exact knowledge of the state of cracking in the composite beam, such as the length of NIC, is needed.

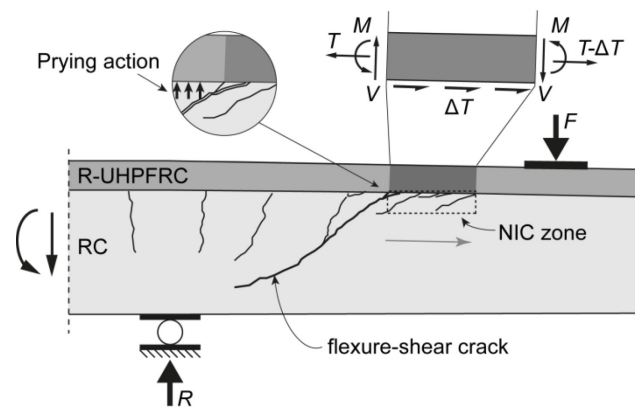


**Figure 3 Flexure-shear failure of a composite beam [I.15]**

The structural behavior of composite RU-RC beams has been well studied and can be reproduced with the available analytical models. However, little work has been done on the behavior of two-way spanning composite slabs. Wuest [I.10] submitted two composite slabs to a point force to study their punching shear resistance. These test showed that final failure occurs due to the punching shear failure of the RC section but no analytical formulation was proposed to evaluate the contribution of the R-UHPFRC layer to the punching shear resistance. Is the out-of-plane bending resistance of the R-UHPFRC layer activated as for the punching shear resistance of composite slabs?

### 3 Problem statement

Previous research on composite RU-RC elements focused on the behavior of beams and one-way slabs and the effect of fiber orientation in the UHPFRC layer was never implicitly included in the structural analysis. Also, there is currently no model to evaluate the punching shear resistance of composite slabs. The present work will extend the existing models to the cases of slabs with the following research questions:

- What is the representative tensile response of a UHPFC layer cast on a two-way spanning slab?
- How does an R-UHPFRC layer contribute to the punching shear resistance of a RC slab? Are the same or similar mechanism activated in the layer as for shear resistance of composite RU-RC beams?

## 4 Objectives

This thesis combines material and structural engineering with the aim of giving analytical tools for the prediction of the bending, shear or punching shear resistance of composite RU-RC slabs. There are five specific objectives:

1. to establish a method to define the representative tensile response of a UHPFRC layer cast on a slab, taking into account fiber orientation and efficiency;
2. to investigate the structural behavior of a composite RU-RC slab submitted to a point force;
3. to develop a model to take into account the contribution of a UHPFRC layer to the punching shear resistance of a composite RU-RC slab;
4. to systematise the prediction of the bending resistance of a composite section based on the strength of all tensile reinforcements;
5. to further study the contribution of a UHPFRC layer to the shear resistance of a RC section and the parameters influencing it.

## 5 Scope

This thesis studies the case of UHPFRC layers cast on RC sections and submitted to tensile stresses and strains. The case of a composite section with a UHPFRC layer submitted to compressive stresses or strains is not addressed in this work.

The fiber orientation in the layer and its effect on the tensile strength are examined. The UHPFRC material studied herein is considered to have strain-hardening behavior for most fiber orientations (type UA in Table 1). The UHPFRC mix design and its time-dependant behavior are not addressed as it has been covered by previous research [I.17-19].

Once the representative tensile strength of a UHPFRC layer is known, the focus is placed on quasi-static structural behavior of composite slabs submitted to combined bending and shear, with the aim of determining the ultimate resistance of the element and its failure mode. The specific case of elements submitted to point forces is considered but it is expected that the conclusions can be extended to uniformly distributed forces. The fatigue life of a composite section is not within the scope of this work.

The work is limited to the case of thin layers that have a thickness of between 20 and 50 mm. The ratio between the UHPFRC layer and the RC section thicknesses is between 10 and 25%.

## 6 Outline

The work is presented as four distinct papers that have been published or submitted to internationally peer-reviewed journals. It is divided between material and structural investigations as developed in Figure 4. Within both parts, experimental results are used to develop and validate the analytical models.

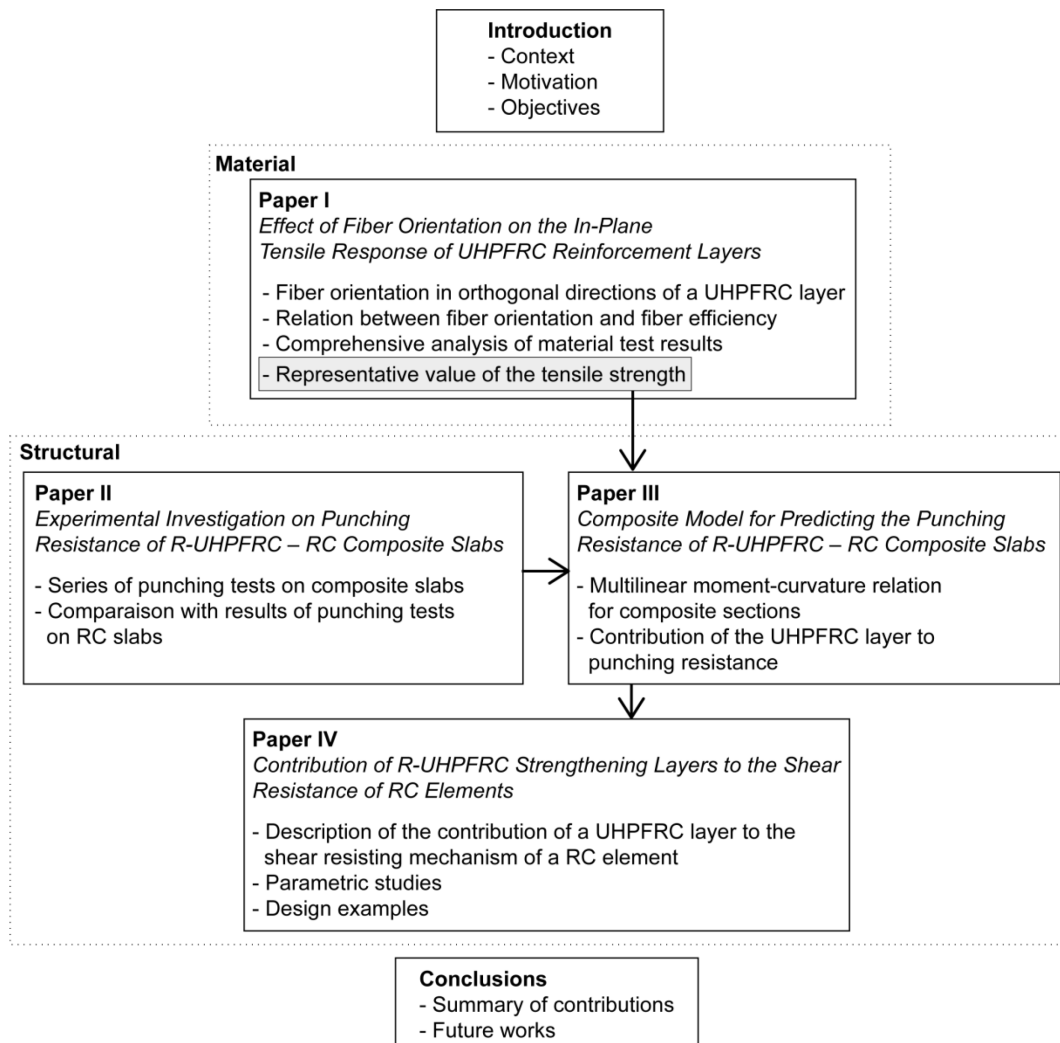


**Figure 4 Structure of the thesis**

The four papers are as follows:

- I. Effect of Fiber Orientation on the In-Plane Tensile Response of UHPFRC Reinforcement Layers (Revised version submitted to Cement and Concrete Composite) – This paper treats objective 1.

- II. Experimental Investigation on Punching Resistance of R-UHPFRC – RC Composite Slabs (Published in Materials and Structures) – This paper treats objective 2.
- III. Composite Model for Predicting the Punching Resistance of R-UHPFRC – RC Composite Slabs (Submitted to Engineering Structures) – This paper treats objectives 3 and 4.
- IV. Contribution of R-UHPFRC Strengthening Layers to the Shear Resistance of RC Elements. (Submitted to Structural Engineering International) – This paper treats objective 5.

The conclusion chapter summarizes the main contributions of each paper and gives an outlook for future research. Finally, the thesis is complemented by two test reports presented in the appendices:

- A. Characterization of the UHPFRC S3-13: test report with the complete results of the material characterization campaign carried out on the UHPFRC mix used within this work;
- B. Punching Tests on R-UHPFRC-RC Composite Slabs without Shear Reinforcement: test report with the complete measurements carried out on each of the tested composite slabs.

## 7 References

- [I.1] Brühwiler E. Bridge “examineering” or how monitoring and UHPFRC improve the performance of structures. In: Chen A, Frangopol D, Ruan X, editors. IABMAS Conference ‘Bridge Maintenance, Safety, Management and Life Extension’; Shanghai: CRC Press; 2014. p. 15-28.
- [I.2] Menétrey P. ArtStructures. Structural Engineering International. 2015;25(2):121.
- [I.3] Zabalza Bribián I, Valero Capilla A, Aranda Usón A. Life cycle assessment of building materials: Comparative analysis of energy and environmental impacts and evaluation of the eco-efficiency improvement potential. Building and Environment. 2011;46(5):1133-40.
- [I.4] Habert G, Arribe D, Dehove T, Espinasse L, Le Roy R. Reducing environmental impact by increasing the strength of concrete: quantification of the improvement to concrete bridges. Journal of Cleaner Production. 2012;35:250-62.
- [I.5] Treacy MA, Brühwiler E. A direct monitoring approach for the fatigue safety verification of construction joint details in an existing post-tensioned concrete box-girder bridge. Engineering Structures. 2015;88:189-202.
- [I.6] Brühwiler E, Denarié E. Rehabilitation and Strengthening of Concrete Structures Using Ultra-High Performance Fibre Reinforced Concrete. Structural Engineering International. 2013;23(4):450-7.
- [I.7] Denarié E, Brühwiler E. Cast-on-site UHPFRC for improvement of existing structures - Achievements over the last 10 years in practice and research. In: Reinhardt H, Parra-Montesinos GJ, Garrecht H, editors. HPRCC-7: 7th RILEM Workshop on High Performance Fiber Reinforced Cement Composites Stuttgart: RILEM; 2015.

- [I.8] Brühwiler E, Bastien-Masse M, Mühlberg H, Houriet B, Fleury B, Cuennet S, et al. Strengthening the Chillon viaducts deck slabs with reinforced UHPFRC. IABSE Conference 'Structural Engineering: Providing Solutions to Global Challenges'; Geneva: IABSE; 2015. p. 1171-8.
- [I.9] Habert G, Denarié E, Šajna A, Rossi P. Lowering the global warming impact of bridge rehabilitations by using Ultra High Performance Fibre Reinforced Concretes. *Cement and Concrete Composites*. 2013;38:1-11.
- [I.10] Wuest J. Comportement structural des bétons de fibres ultra performants en traction dans des éléments composés. Doctoral thesis EPFL no. 3987. Lausanne: Ecole Polytechnique Fédérale de Lausanne; 2007; 244 p.
- [I.11] Oosterlee C. Structural Response of Reinforced UHPFRC and RC Composite Members. Doctoral thesis EPFL no. 4848. Lausanne: Ecole Polytechnique Fédérale de Lausanne; 2010; 136 p.
- [I.12] Charron JP, Denarié E, Brühwiler E. Permeability of ultra high performance fiber reinforced concretes (UHPFRC) under high stresses. *Materials and Structures*. 2007;40(3):269-77.
- [I.13] Habel K. Structural behaviour of elements combining ultra-high performance fibre reinforced concretes (UHPFRC) and reinforced concrete. Doctoral thesis EPFL no. 3036. Lausanne: Ecole Polytechnique Fédérale de Lausanne; 2004; 195 p.
- [I.14] Herwig A. Reinforced concrete bridges under increased railway traffic loads fatigue behaviour and safety measures. Doctoral thesis EPFL no. 4010. Lausanne: Ecole Polytechnique Fédérale de Lausanne; 2008; 120 p.
- [I.15] Noshiravani T. Structural Response of R-UHPFRC - RC Composite Members Subjected to Combined Bending and Shear. Doctoral Thesis EPFL no. 5246. Lausanne: Ecole Polytechnique Federale de Lausanne; 2012; 188 p.
- [I.16] Makita T. Fatigue behaviour of UHPFRC and R-UHPFRC - RC composite members. Doctoral thesis EPFL no. 6068. Lausanne: Ecole Polytechnique Fédérale de Lausanne; 2014; 148 p.
- [I.17] Kamen A. Comportement au jeune âge et différé d'un BFUP écrouissant sous les effets thermomécaniques. Doctoral Thesis EPFL no. 3827. Lausanne: Ecole Polytechnique Fédérale de Lausanne; 2007; 246 p.
- [I.18] Switek AE. Time-Dependent Response of Ultra High Performance Fibre Reinforced Concrete (UHPFRC) under Low to High Tensile Stresses. Doctoral Thesis EPFL no. 4899. Lausanne: Ecole Polytechnique Federale de Lausanne; 2011; 200 p.
- [I.19] Kazemi Kamyab H. Autogenous Shrinkage and Hydration Kinetics of SH-UHPFRC under Moderate to Low Temperature Curing Conditions. Doctoral Thesis EPFL no. 5681. Lausanne: Ecole Polytechnique Federale de Lausanne; 2013; 295 p.
- [I.20] SIA. CT 2052 : Béton fibré ultra-performant (BFUP) - Matériaux, dimensionnement et exécution. Zürich: Société suisse des Ingénieurs et Architectes; 2015.
- [I.21] Graybeal BA, Baby F. Development of direct tension test method for ultra-high-performance fiber-reinforced concrete. *ACI Materials Journal*. 2013;110(2):177-86.
- [I.22] Wille K, El-Tawil S, Naaman AE. Properties of strain hardening ultra high performance fiber reinforced concrete (UHP-FRC) under direct tensile loading. *Cement and Concrete Composites*. 2014;48:53-66.
- [I.23] Kwon S, Nishiwaki T, Kikuta T, Mihashi H. Development of ultra-high-performance hybrid fiber-reinforced cement-based composites. *ACI Materials Journal*. 2014;111(3):309-18.
- [I.24] Hollmann C, Wille K. Influence of fiber orientation on the properties of strain hardening ultra-high performance fiber reinforced concrete (UHPFRC) under direct tensile loading. In: Zingoni

A, editor. *Research and Applications in Structural Engineering, Mechanics & Computation: Fifth International Conference on Structural Engineering, Mechanics & Computation*; Cape Town: CRC Press; 2013. p. 1721-6.

[I.25] Ferrara L, Ozyurt N, di Prisco M. High mechanical performance of fibre reinforced cementitious composites: the role of “casting-flow induced” fibre orientation. *Materials and Structures*. 2011;44(1):109-28.



# Paper I

## Effect of Fiber Orientation on the In-Plane Tensile Response of UHPFRC Reinforcement Layers

---

**Reference:** Bastien-Masse M, Denarié E, Brühwiler E. Effect of Fiber Orientation on the In-Plane Tensile Response of UHPFRC Reinforcement Layers. *Revised version submitted to Cement and Concrete Composite on September 28<sup>th</sup> 2015.*

### Abstract

The application on existing Reinforced Concrete (RC) slabs of cast-on-site Ultra-High Performance Fiber Reinforced cement-based Composite (UHPFRC) layers is a very efficient reinforcement technique, currently spreading. For the design of these tensile reinforcement UHPFRC layers with thicknesses of between 25 and 50 mm, a representative in-plane tensile response of the UHPFRC has to be determined considering the effects of fiber orientation. To do so, theoretical analysis tools are derived to (1) analyze the relation between fiber orientations in perpendicular directions and (2) determine the average effect of fiber orientation on fiber efficiency at pull-out. A comprehensive material testing campaign of a strain-hardening UHPFRC is then carried out on specimens with various thicknesses and casting processes and a meso-mechanical model is calibrated on the results. The results of this campaign as well as results taken from the literature are used to validate the theoretical developments. Finally, the most likely fiber orientation in a layer of UHPFRC for the casting method considered herein is estimated based on the results of the theoretical developments and the material characterization and a representative tensile response is estimated using the calibrated meso-mechanical model.

**Keywords:** Ultra-High Performance Fiber Reinforced cement-based Composite (UHPFRC), Reinforcement, Fiber orientation, Fiber efficiency, Tensile response, Representative values.

## List of Symbols

### Latin upper case

$A$	Area
$A_f$	Area of the cross-section of a fiber
$E_m$	Modulus of elasticity of the UHPFRC matrix
$E_f$	Modulus of elasticity of the fibers
$E_U$	Modulus of elasticity of UHPFRC
$F$	Measured force during bending test
$F_u$	Maximum measured force during bending test
$G_m$	Matrix fracture energy
$L$	Total span in the bending test setup
$V$	Volume fraction
$V_f$	Volume fraction of fibers in UHPFRC mix
$V_m$	Volume fraction of matrix in UHPFRC mix
$X$	Material property

### Latin lower case

$b$	width of bending test specimens
$d_f$	diameter of fiber
$f_{sf}$	maximum tensile strength of a fiber
$f_{Ute}$	elastic tensile strength of UHPFRC
$f_{Um}$	tensile strength of UHPFRC
$h_U$	height of UHPFRC layer; thickness of UHPFRC test specimens
$h_c$	height of the reinforced concrete section
$l_f$	fiber length
$l_{mes}$	length of measuring base for tensile tests
$n_f$	number of fibers crossing a plane
$x, y, z$	coordinates of the fiber tip

### Greek lower case

$\gamma_m$	partial factor for material properties
$\gamma_U$	partial factor for UHPFRC properties
$\Delta$	mid-span deflection measured during bending tests
$\Delta l$	displacement between two points measured during tensile tests
$\varepsilon_{Uel}$	strain in UHPFRC at elastic tensile strength
$\varepsilon_{Um}$	strain in UHPFRC at tensile strength
$\theta$	angle between the fiber and axis 1
$\mu_{oi}$	fiber orientation factor in direction $i$
$\mu_1$	fiber efficiency factor
$\sigma_{Ut}$	tensile stress in UHPFRC
$\tau_f$	maximum pullout stress of a straight fiber embedded in UHPFRC
$\varphi$	angle between the projection of the fiber in plane 2-3 and axis 2

## 1 Introduction

Fiber orientation governs to a very large extent the tensile mechanical response (strength and deformability) of cement-based composites reinforced with discontinuous short steel fibers [1.1-3] such as Ultra-High Performance Fiber Reinforced cement-based Composite (UHPFRC) [1.4, 5]. In a given element, fiber orientation depends on the geometry of the element, the casting process and the mix proportions (fiber type and volume, matrix volume). Fiber orientation must be considered: (1) in the analysis of experimental test results on UHPFRC, (2) in the design and the fabrication of structural elements with UHPFRC, and more generally speaking (3) in the design of appropriate methodologies of characterization of those materials.

Cast-in-place UHPFRC layers with typical thickness of between 25 and 50 mm serve as tensile reinforcement for Reinforced Concrete (RC) elements with deficient resistance, creating composite elements (Figure 1). In such applications, UHPFRC layers resist bending and shear actions on the composite structures by both their in-plane tensile resistance and deformability and out-of-plane bending resistance and rotation capacity [1.6-8]. The in-plane and out-of-plane resistance mechanisms of UHPFRC layers are governed by their in-plane tensile responses.

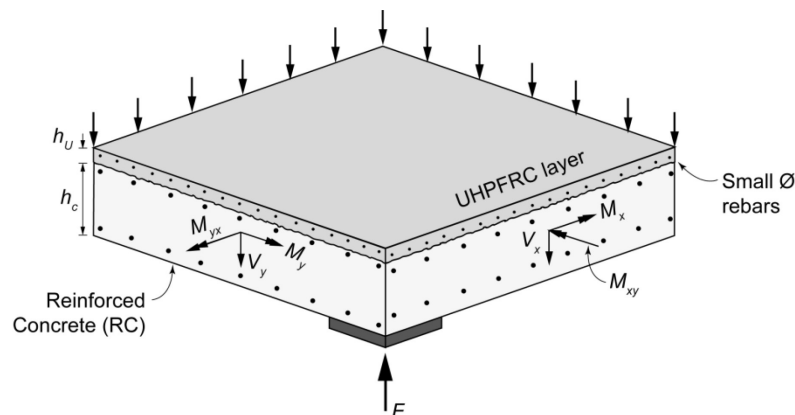


**Figure 1 Typical composite slab element with bending and shear actions**

For a UHPFRC layer cast on a large surface, the in-plane fiber orientation is a priori different in orthogonal directions. The tensile response being influenced by fiber orientation, it will also vary in different directions. It is thus important to be able to predict the relation between these tensile responses.

The main objective of the presented work is to calculate, in a consistent manner, representative values of the UHPFRC tensile strength for the design of a reinforcement layer, using theoretical tools and test results. This is done through a theoretical stereological analysis and a material characterization campaign. First, the relation between fiber orientations in orthogonal directions is determined using stereological tools. Based on this development, the relation between fiber orientation and fiber efficiency is established. Second, an extensive testing programme on a specific UHPFRC mix is presented and the results are analysed based on fiber orientation and fiber efficiency. The test results are used to calibrate a meso-mechanical model used to predict the tensile response of this material

based on the composition of the mix and fiber orientation. This model takes into account the interaction between the fibers and the matrix at the mesoscale. Finally, the theoretical work is validated with experimental results and representative values of the in-plane fiber orientation and tensile strength are defined for a UHPFRC reinforcement layer.

## 2 Tensile response of UHPFRC

### 2.1 Overview

The tensile response of UHPFRC is characterized by elastic, hardening if applicable, and softening phases. The magnitude of these phases strongly depends on the matrix tensile strength, fibrous mix and fiber orientation. It can be estimated by various methods: inverse analysis of bending test results, direct tensile tests, meso-mechanical models, etc.

In the following, the different parameters influencing the tensile strength of UHPFRC  $f_{Utu}$  are described and a meso-mechanical model for the prediction of the complete tensile response of the material is briefly described.

### 2.2 Ultimate tensile strength

#### 2.2.1 Equation

The tensile strength of UHPFRC is often estimated using equation 1, proposed in a close form by different authors [1.2, 9]:

$$f_{Utu} = \mu_0 \mu_1 \tau_f V_f \frac{l_f}{d_f} \quad (1)$$

This equation takes into account the orientation and efficiency factors of fibers,  $\mu_0$  and  $\mu_1$ , the fiber volume fraction  $V_f$ , the maximum pull-out stress of the fibers  $\tau_f$  and the aspect ratio of the fibers  $l_f/d_f$ .

#### 2.2.2 Fiber orientation factor

The fiber orientation factor  $\mu_0$  is the probability that a fiber will cross a given section [1.10] as obtained by the ratio between the number of fibers crossing a unit surface  $n_f$  and the total number of fibers per unit volume (equation 2) [1.1, 11, 12]. Assuming that the concentration of fibers is homogeneous, the number of fibers per unit volume is the ratio between the area of the cross-section of a fiber  $A_f$  and the fiber volume fraction  $V_f$ .

$$\mu_0 = n_f \frac{A_f}{V_f} \quad (2)$$

The value of  $\mu_0$  varies between zero when no fibers cross the section and one when all the fibers are perpendicular to it. It can be calculated using stereology and geometric probability theory.

Together with the fiber efficiency factor  $\mu_1$  described in the next paragraph, the fiber orientation factor  $\mu_0$  quantifies the contribution of the fibers to the tensile response of the

material in the direction perpendicular to the section. A higher orientation factor will result in an improved tensile response and a higher tensile strength in the considered direction. However, simultaneously, in perpendicular directions, the tensile properties drop accordingly and vice-versa.

### 2.2.3 Fiber efficiency factor

When fibers are not aligned with the loading direction, they are pulled out from the matrix in a direction different from their axis. The efficiency factor  $\mu_l$  is the ratio between the pull-out forces of an inclined fiber and a perfectly aligned one and thus depends on the orientation angle  $\theta$  of the fiber towards the direction of loading. The effect of the angle at pull out has been studied experimentally in [1.13-15] for various types of fibers (straight, deformed or hooked) and mixes and fully described elsewhere [1.16]. These experimental results were used to propose different simplified functions to relate  $\mu_l$  to the angle  $\theta$  [1.17-19]. The one proposed by Oesterlee [1.19] is given by equation 3 and illustrated in Figure 2 along with some main experimental results.

$$\theta \leq \frac{\pi}{3} (60^\circ) \rightarrow \mu_l = 1 \quad (3a)$$

$$\frac{\pi}{3} (60^\circ) < \theta \leq \frac{\pi}{2} (90^\circ) \rightarrow \mu_l = -\left(\frac{6\theta}{\pi}\right) + 3 \quad (3b)$$

This relation is assumed to be valid for a wide range of stiff fiber types (straight, deformed and hooked) and mixes including UHPFRC.

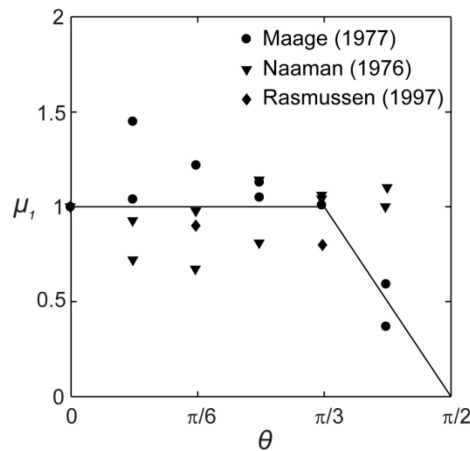


**Figure 2 Fiber efficiency depending on pull-out angle, adapted from [1.16, 19]**

The fiber efficiency factor  $\mu_l$  depends on the orientation angle of each fiber crossing the studied surface. An average value can be used in equation 1 and a constant value of 0.833 was proposed in [1.19], regardless of the implied fiber orientation factor  $\mu_0$ . However, the average efficiency factor depends on the distribution of fiber orientation angles. A relation can thus be established between the average value of  $\mu_l$  and  $\mu_0$ . This will be done using stereological principles, in paragraph 3.3.

### 2.2.4 Maximum fiber pull-out stress

The maximum pull-out resistance of a fiber  $\tau_f$  was measured for UHPFRC mixes by some authors. Wuest [1.5] measured a value of 6.9 MPa for fibers sizes (length/diameter) of 10/0.2 mm, while Behloul [1.4], Wille and Naaman [1.20] and Orange et al. [1.21] respectively reported values of 7.5 MPa for fibers of 13/0.16mm, 8.7 MPa for fibers of 13/0.2 mm and 10 MPa for fibers of 5/0.2 mm.

### 2.3 Tensile hardening response

Various models exist to predict the tensile hardening-softening response based on the composition of the UHPFRC mix and the fiber orientation and efficiency factors. Wuest et al. [1.22] developed a meso-mechanical model for the prediction of the full tensile response of UHPFRC (Figure 3).

The model is described in details in the works by Wuest [1.5, 22] and Oesterlee [1.19]. It consists of two parts. In the first part, the fibre bridging force for a cross-section is calculated based on fiber debonding and pull-out processes and taking into account the fiber orientation and average fiber efficiency factors. This sectional analysis provides a stress-crack opening relation. It is then combined with the matrix softening response and the prestress already present in the fibers before first cracking to obtain the total stress crack-opening response (Figure 3a). In the second part, this response is assigned to predefined potential microcracks along the specimen (Figure 3b). The stress in the specimen is then incremented. Potential microcracks are activated if the stress exceeds the elastic limit strength of the matrix  $f_{Ute}$  which is randomly distributed over the specimen using a normal distribution. The stress is continually increased until one of the microcracks reaches its maximum strength and enters the softening behavior. Successive microcracks spacing is regulated according to the model by Aveston et al. [1.23], modified to account for fiber orientation.

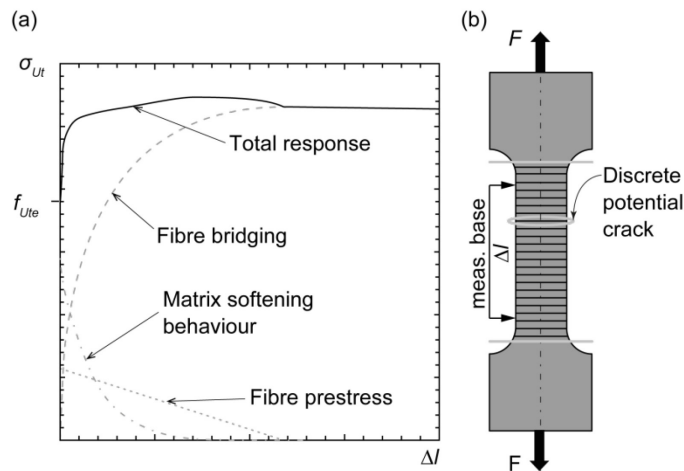


**Figure 3 Meso-mechanical model for UHPFRC tensile hardening response, adapted from [1.22]: (a) individual contributions to the crack-opening response; (b) distributed micro-cracks**

The main input parameters of this model are:

- tensile strength  $f_{sf}$  and modulus of elasticity  $E_f$  of fibers,
- fiber length  $l_f$  and diameter  $d_f$

- fiber volume fraction  $V_f$ ,
- maximum pull-out stress of fibers  $\tau_f$ ,
- fiber orientation factor  $\mu_0$ ,
- average fiber efficiency factor,  $\overline{\mu_1}$
- modulus of elasticity of the material  $E_U$ ,
- modulus of elasticity of the matrix  $E_m$ ,
- matrix fracture energy  $G_m$ .

For a given UHPFRC mix, the fiber characteristics (tensile strength  $f_{sf}$  and modulus of elasticity  $E_f$ ) and fiber volume fraction  $V_f$  are known. The matrix fracture energy  $G_m$  is supposed to be 10 J/m<sup>2</sup> for standard UHPFRC mixes as proposed by Wuest [1.5]. The elastic modulus of the UHPFRC  $E_U$  can be measured and using the law of mixtures, the modulus of elasticity of the matrix  $E_m$  can be calculated:

$$E_U = V_f E_f + V_m E_m \quad (4)$$

Once the entire parameters specific to the mix are known, this model can be used to determine the tensile response for various fiber orientation factors.

### 3 Stereological analysis

#### 3.1 Overview

When studying a reference plane or volume, the orientation factor  $\mu_0$  can be defined in all the principal directions using stereological principles and geometric probabilities. To do so, the position of the fiber is described with the angles it makes towards the different directions (Figure 4), also called orientation angles. A uniform distribution of all the possible positions is considered within certain range of angles (Figure 5). Finally, by varying the ranges of angles, the relation between the orientation factors in orthogonal directions can be calculated for the 2D and 3D cases, as will be demonstrated in the following paragraphs. Using the equations developed to predict the orientation factor for a given range of angles and equation 3, it is also possible to obtain the average value of the fiber efficiency factor  $\overline{\mu_1}$  and its relation with the orientation factor  $\mu_0$ .

In [1.24], probability density distributions of the orientation angle of fibers were measured on individually cast small dogbone specimens. These experimental distributions show that fiber orientation angle distribution over a section is complex and varies greatly. However, these results also show that it is safe to ignore extreme angles when calculating the fiber orientation factor as these angles have a very low probability of appearing in an actual distribution. Based on these observations, it was decided to consider a uniform distribution of all the possible positions of the fiber between two limit angles ( $\theta_a$  and  $\theta_b$ ). This hypothesis generalizes the following development calculation.

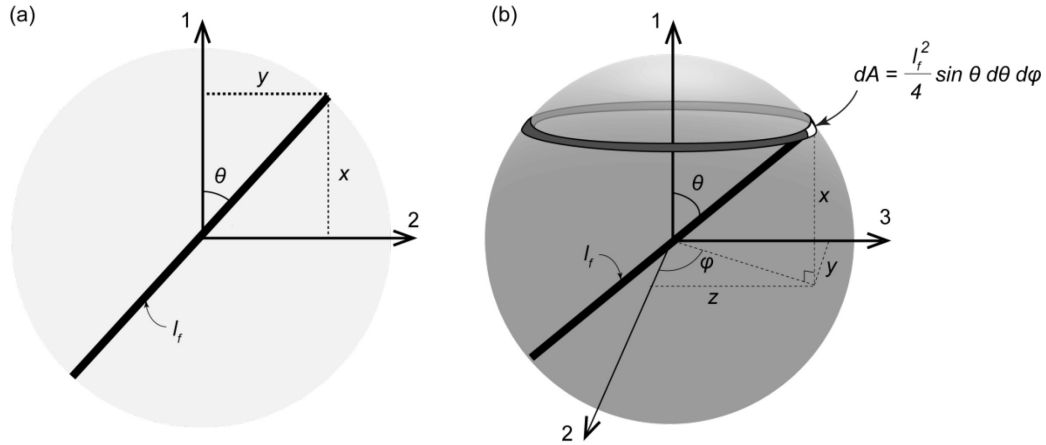


Figure 4 Position of a fiber: (a) in 2D plan; (b) in 3D volume, adapted from [1.10, 25]

### 3.2 Fiber orientation in orthogonal directions

#### 3.2.1 Two dimensional case (2D)

The perfect two-dimensional (2D) case is when all fibers are lying in parallel planes. The orientation factor in the third direction perpendicular to the considered plane is equal to zero. As illustrated in Figure 4a, in 2D, all possible orientations of a fiber describe a circle around its center. The position of the fiber is defined by  $x$  and  $y$ , the distances between the center of the fiber and the plane where fiber orientation is calculated, and the angle  $\theta$  between the fiber and axis 1. To get all the possible combinations of orientation factors, the minimum and maximum values of  $\theta$ ,  $\theta_a$  and  $\theta_b$ , are varied within the quadrant (Figure 5a), supposing a uniform distribution between these two values.

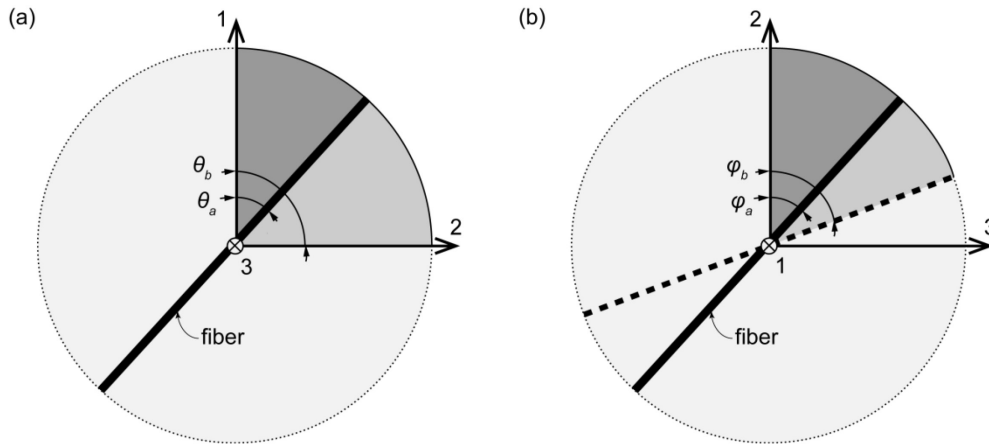


Figure 5 Possible range of angles in the quadrant: (a) 1-2; (b) 2-3

The variables  $x$ ,  $y$  and  $\theta$  are supposed random and independent. They have the following density functions. Variable  $y$  has the same density function as  $x$ .

$$f(x) = \frac{2}{l_f} \text{ for } 0 \leq x \leq \frac{l_f}{2} \quad (5a)$$

$$f(\theta) = \frac{1}{\theta_b - \theta_a} \text{ for } \theta_a \leq \theta \leq \theta_b \quad (5b)$$



$$f(x, \theta) = \frac{2}{l_f \cdot (\theta_b - \theta_a)} \quad (5c)$$

For a given position of the fiber, the maximum values of  $x$  and  $y$  are given by equation 6.

$$x \leq \frac{l_f}{2} \cos \theta \quad (6a)$$

$$y \leq \frac{l_f}{2} \sin \theta \quad (6b)$$

Therefore, the 2D fiber orientation in directions 1 and 2 is obtained as follows:

$$\mu_{01} = \int_{\theta_a}^{\theta_b} \int_0^{\frac{l_f}{2} \cos \theta} f(x, \theta) dx d\theta = \int_{\theta_a}^{\theta_b} \int_0^{\frac{l_f}{2} \cos \theta} \frac{2}{l_f \cdot (\theta_b - \theta_a)} dx d\theta = \frac{\sin \theta_b - \sin \theta_a}{\theta_b - \theta_a} \quad (7a)$$

$$\mu_{02} = \int_{\theta_a}^{\theta_b} \int_0^{\frac{l_f}{2} \sin \theta} f(y, \theta) dy d\theta = \int_{\theta_a}^{\theta_b} \int_0^{\frac{l_f}{2} \sin \theta} \frac{2}{l_f \cdot (\theta_b - \theta_a)} dy d\theta = \frac{\cos \theta_a - \cos \theta_b}{\theta_b - \theta_a} \quad (7b)$$

In the perfectly 2D case, when the fiber can take any orientation in a plane and angles  $\theta_a$  and  $\theta_b$  are respectively equal to 0 and  $\pi/2$  the orientation factor is equal to  $2/\pi$  (0.64) in both directions, as also demonstrated by other authors [1.12, 26].

### 3.2.2 Three dimensional case (3D)

As illustrated in Figure 4b, in the three-dimensional (3D) case, all possible orientations of a fiber describe a sphere around its center. The position of the fiber is defined by distances  $x, y$  and  $z$  and the angles  $\theta$  and  $\varphi$ . As for the 2D case, the maximum and minimum values of angles  $\theta$  and  $\varphi$  are varied within the quadrant (Figure 5). The probability that the fiber makes an angle  $\theta$  with axis 1 is proportional to the portion of the ring of area  $dA$  located within  $d\varphi$  [1.25]:

$$dA = \frac{l_f^2}{4} \sin \theta d\theta d\varphi \quad (8a)$$

$$A = \int_{\varphi_a}^{\varphi_b} \int_{\theta_a}^{\theta_b} \frac{l_f^2}{4} \sin \theta d\theta d\varphi = \frac{l_f^2}{4} \cdot (\varphi_b - \varphi_a) \cdot (\cos \theta_a - \cos \theta_b) \quad (8b)$$

$$p(\theta, \varphi) = \frac{dA}{A} = \frac{\sin \theta}{(\varphi_b - \varphi_a) \cdot (\cos \theta_a - \cos \theta_b)} d\theta d\varphi \quad (8c)$$

Based on this probability function, the density functions of the three variables  $x, \theta$  and  $\varphi$ , are given by equations 9. Once more, variables  $y$  and  $z$  have the same density function as variable  $x$ .

$$f(x) = \frac{2}{l_f} \text{ for } 0 \leq x \leq \frac{l_f}{2} \quad (9a)$$

$$f(\theta, \varphi) = \frac{\sin \theta}{(\varphi_b - \varphi_a) \cdot (\cos \theta_a - \cos \theta_b)} \text{ for } \theta_a \leq \theta \leq \theta_b \text{ and } \varphi_a \leq \varphi \leq \varphi_b \quad (9b)$$

$$f(x, \theta, \varphi) = \frac{2 \sin \theta}{l_f \cdot (\varphi_b - \varphi_a) \cdot (\cos \theta_a - \cos \theta_b)} \quad (9c)$$

For a given position of the fiber, the maximum values of  $x$ ,  $y$  and  $z$  are given by equations 10.

$$x \leq \frac{l_f}{2} \cos \theta \quad (10a)$$

$$y \leq \frac{l_f}{2} \sin \theta \cos \varphi \quad (10b)$$

$$z \leq \frac{l_f}{2} \sin \theta \sin \varphi \quad (10c)$$

The orientation factor in each direction is then obtained as follows:

$$\mu_{01} = \int_{\varphi_a}^{\varphi_b} \int_{\theta_a}^{\theta_b} \int_0^{\frac{l_f}{2} \cos \theta} \frac{2 \sin \theta}{l_f \cdot (\varphi_b - \varphi_a) \cdot (\cos \theta_a - \cos \theta_b)} dx d\theta d\varphi$$

$$\mu_{01} = \frac{(\cos 2\theta_a - \cos 2\theta_b)}{4 \cdot (\cos \theta_a - \cos \theta_b)} \quad (11a)$$

$$\mu_{02} = \int_{\varphi_a}^{\varphi_b} \int_{\theta_a}^{\theta_b} \int_0^{\frac{l_f}{2} \sin \theta \cos \varphi} \frac{2 \sin \theta}{l_f \cdot (\varphi_b - \varphi_a) \cdot (\cos \theta_a - \cos \theta_b)} dy d\theta d\varphi$$

$$\mu_{02} = \frac{[2 \cdot (\theta_b - \theta_a) + \sin 2\theta_a - \sin 2\theta_b]}{4 \cdot (\varphi_b - \varphi_a) \cdot (\cos \theta_a - \cos \theta_b)} \cdot (\sin \varphi_b - \sin \varphi_a) \quad (11b)$$

$$\mu_{03} = \int_{\varphi_a}^{\varphi_b} \int_{\theta_a}^{\theta_b} \int_0^{\frac{l_f}{2} \sin \theta \sin \varphi} \frac{2 \sin \theta}{l_f \cdot (\varphi_b - \varphi_a) \cdot (\cos \theta_a - \cos \theta_b)} dz d\theta d\varphi$$

$$\mu_{03} = \frac{[2 \cdot (\theta_b - \theta_a) + \sin 2\theta_a - \sin 2\theta_b]}{4 \cdot (\varphi_b - \varphi_a) \cdot (\cos \theta_a - \cos \theta_b)} \cdot (\cos \varphi_a - \cos \varphi_b) \quad (11c)$$

In the perfect 3D case, the fibers are randomly and uniformly distributed in the volume and equally probable to take any angle towards a considered direction. In this case, angles  $\theta_a$  and  $\theta_b$  are respectively equal to 0 and  $\pi/2$  and angles  $\varphi_a$  and  $\varphi_b$  are also equal to 0 and  $\pi/2$ . The orientation factor in all the directions is thus equal to 0.5, as also demonstrated by other authors [1.12, 26].

### 3.2.3 Relations for orthogonal directions

Figure 6 shows the curves that relate the orientation factor  $\mu_{0i}$  in one direction  $i$  and the ratio  $\mu_{01}/\mu_{02}$ . Using these curves, if the orientation factor is known for one direction, it can be defined for the second direction of the plane. The curves are calculated in two steps using equations 7 and 11 for the 2D and 3D cases:

1.  $\theta_a = 0, \theta_b \in [0, \frac{\pi}{2}]$
2.  $\theta_a \in [0, \frac{\pi}{2}], \theta_b = \frac{\pi}{2}$

In 2D, the orientation factor in direction 3,  $\mu_{03}$ , is equal to 0. For the 3D case, angles  $\varphi_a$  and  $\varphi_b$  are equal to respectively 0 and  $\pi/2$ , meaning that  $\mu_{03}$  is equal to the fiber orientation factor in direction 2,  $\mu_{02}$ . This grey curve for the 3D case has been previously calculated by Breyse et al. [1.27] and is considered to be a limit of all the possible combination of orientation factors in the 3 directions. Cases where the orientation factors in directions 2 and 3 are not equal would fall between the 2D and 3D curves shown in Figure 6.

The following points must be noted:

1. Unidirectional case (1D): shown with a circle in Figure 6, it is the case when  $\mu_{02} = 1$  and  $\mu_{01} = \mu_{03} = 0$ ;
2. Isotropy in a plan (2D): shown with the triangle, it happens when two of the orientation factors are equal to  $2/\pi$ :
  - For the 2D case (black curve), when  $\mu_{01}/\mu_{02} = 1$ .
  - For the 3D case (grey curve), when the angles  $\theta_a$  and  $\theta_b$  are both equal to  $\pi/2$ , all fibers are laying in the plan formed by axis 2 and 3. Thus:  $\mu_{02} = \mu_{03} = 2/\pi$ ,  $\mu_{01} = 0$  and  $\mu_{01}/\mu_{02} = 0$ .
3. Isotropy in a volume (3D): shown with a square, the orientation factors in all directions are equal to 0.5.

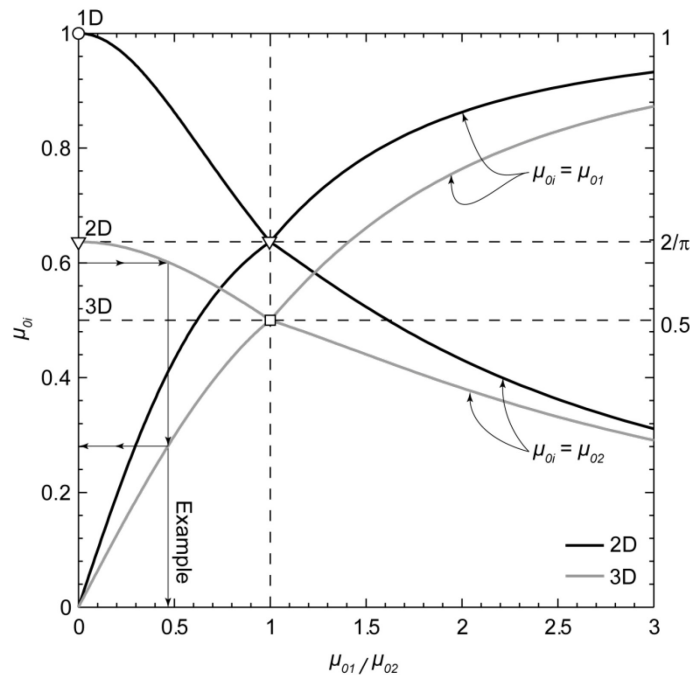


**Figure 6 Relation between orientation factors in orthogonal directions**

The use of this graph is illustrated by an example shown with the arrows in Figure 6. If the orientation factor in direction 2,  $\mu_{02}$ , is known to be 0.6, it is possible to directly find the value of the orientation factor in direction 1,  $\mu_{01}$ , and the ratio  $\mu_{01}/\mu_{02}$  which are 0.28 and 0.47 respectively.

These curves and the equations to calculate them can be used to estimate the relation between fiber orientation factors in the orthogonal directions of a UHPFRC layer. The curves presented here are general boundary cases including the 2D case never demonstrated elsewhere. Moreover, the equations proposed give for the first time a general calculation procedure and can be used to evaluate any other anisotropic case. This will be demonstrated in paragraph 5.

### 3.3 Average efficiency factor

As presented in paragraph 2.2.3, the efficiency factor  $\mu_l$  is different for every single fiber and depends on its orientation angle  $\theta$  towards the direction of loading. Foster [1.28] calculated the average efficiency factor for the 3D isotropic case assuming that fibers with an incidence higher than  $\pi/3$  ( $60^\circ$ ) have no contribution to strength. Using the equations developed in paragraph 3.2, it is possible to obtain the average effect of fiber efficiency  $\overline{\mu_1}$  and its relation with the orientation factor  $\mu_0$ . For the 2D case, equation 7a is multiplied by the function describing  $\mu_l$ :

$$\mu_0 \overline{\mu_1} = \frac{1}{\theta_b - \theta_a} \int_{\theta_a}^{\theta_b} \mu_1(\theta) \cos \theta \, d\theta \quad (12)$$

The same procedure is use for the 3D case and using equation 11a the following relations is obtained:

$$\mu_0 \overline{\mu_1} = \frac{1}{\cos \theta_a - \cos \theta_b} \int_{\theta_a}^{\theta_b} \mu_1(\theta) \sin \theta \cos \theta \, d\theta \quad (13)$$

These equations are general and can be applied to any function  $\mu_1(\theta)$  relating the efficiency factor to the angle  $\theta$ . Herein, the function given by equation 3 (paragraph 2.2.3) is adopted and the efficiency of fibers with angles of incidence larger than  $\pi/3$  is linearly diminished until it reaches zero. The relations between the orientation factor  $\mu_0$  and the average efficiency factor  $\overline{\mu_1}$  calculated with this function are given in Figure 7. This relation between  $\mu_0$  and the average efficiency factor  $\overline{\mu_1}$  must be used when modeling the tensile response of UHPFRC, as presented in paragraph 2.3.

In Figure 7, three zones of influence of the average efficiency factor can be defined:

1.  $\mu_0 < 0.280$ : The average efficiency factor  $\overline{\mu_1}$  is directly proportional to  $\mu_0$ . In this case, the average efficiency factor has a strong influence on the value of the tensile strength calculated with equation 1.
2.  $0.280 \leq \mu_0 < 0.827$  (2D) or  $0.750$  (3D): The influence of the average efficiency on the tensile strength decreases.
3.  $\mu_0 \geq 0.827$  (2D) or  $0.750$  (3D): The average efficiency factor  $\overline{\mu_1}$  is equal to one and has no more influence on the tensile strength. All fibers are efficient for these high values of orientation factors.

The average efficiency factor was also calculated for the perfect 2D and 3D cases. When the fibers are uniformly distributed in a plan (2D,  $\mu_0 = 2/\pi$ ) or a volume (3D,  $\mu_0 = 0.5$ ), the average efficiency factor  $\overline{\mu_1}$  is equal to 0.955 and 0.914 respectively.

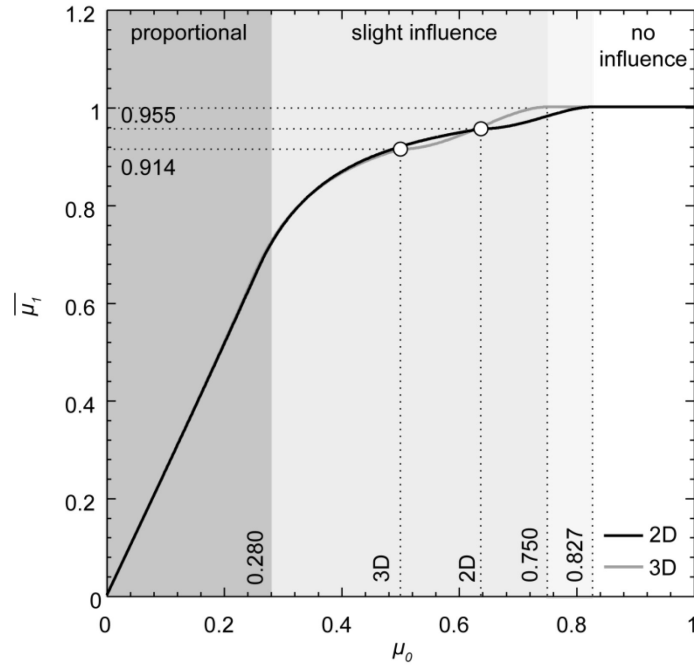


Figure 7 Relation between orientation and efficiency factors

## 4 Material characterization

### 4.1 Overview

A complete characterization campaign was carried out on a UHPFRC mix also used to fabricate layers of composite slabs (Figure 1) [1.29, 30]. This UHPFRC is an industrial premix containing 3% volume of 13/0.16 mm straight steel fibers and identified herein as S3-13. At 28 days, it has an average modulus of elasticity of 44.5 GPa and an average compressive strength of 151 MPa, measured on cylinders of 70 mm diameter.

The experimental campaign was designed to study the response of S3-13 under bending and direct tension for geometries close to the intended application. The objective of this experimental campaign was to (1) identify the range of possible tensile response and their relation with the geometry and fabrication method of the specimens, (2) identify the fiber orientation factor related to a given tensile strength using equation 1 and the relation with the efficiency factor (Figure 7) and (3) calibrate the meso-mechanical model presented in paragraph 2.3.

### 4.2 Testing program

Different fabrication methods and specimen types were used for this characterization campaign in order to get a full overview of the bending and tensile response of S3-13. To be representative of the UHPFRC layer cast on concrete slabs in practice, the thickness of the specimens was varied between 25 and 50 mm. The bending tests were carried out on rectangular specimens while the tensile test specimens were dog-bones. The specimens were

either cast individually in molds or cut out from square or rectangular plates. Table 2 gives an overview of the different types of specimens used for this characterization campaign.

**Table 2 Testing program for UHPFRC S3-13**

Test series	Dimensions [mm]	$h_V$ [mm]	Number of tested specimens	Fabrication	
<b>Bending on plates</b>	I	500×200	50	4	Molded rectangular plate
	II		30	5	Molded rectangular plate
	III	500×100	50	10	5 plates cut out from a 580×580×50 mm square plate
<b>Tension on dog-bones</b>	IV	850×100	50	11	4 dog-bones cut out from a 1000×1000×50 mm square plate
	V	490×50	25	6	2 dog-bones cut out from a 500×200×25 mm rectangular plate

Square plates were used to fabricate the bending test specimens of series III and the tensile test specimens of series IV (Figure 8). These square plates were cast in pairs using a similar procedure to that was used for the fabrication of the overlay on the composite slabs, placing the material from one side to the other using an overhead bucket. For a pair of plates, 4 or 5 specimens are cut out in parallel to the principal casting direction in one case (series A) and perpendicularly in the other case (series B). This way, it is possible to study the effect of the casting procedure on the tensile properties in orthogonal directions and the variability of the behavior in a plate.

For test series I, II and V, rectangular plates were used. In this case, the material was placed along the long side of the plate. These specimens were then either used directly for the bending tests (series I and II) or two tensile dog-bone specimens were cut out of them for tensile tests (series V, Figure 8c). In both cases, only the properties in the longitudinal direction, the casting direction, were tested. Due to the geometry and casting process of the specimens, it is supposed that they have fibers that are more oriented towards the longitudinal direction.

The four-point bending tests were performed on a universal servo-hydraulic testing machine with a capacity of 200 kN. The total span of the bending test setup ( $L$ ) was 420 mm and the supports allowed free displacement of the specimen along its longitudinal axis. The loading points were 140 mm apart. The test was displacement controlled and two transducers placed on a measuring frame on each side of the specimen measured the deflection in the center of the span.

The tensile tests were also done in universal testing machines: a universal servo-hydraulic testing machine with a capacity of 1000 kN for series IV and a universal electromechanical testing machine with a capacity of 250 kN for series V. The wider heads of the dog-bone specimens (Figure 8) were reinforced with aluminium plates and held in place by clamping jaws. These tests were also displacement controlled and transducers were used to measure the deformation and crack openings of the specimen. The measuring base was 350 mm for the larger tensile tests (series IV) and 140 mm for the smaller specimens (series V).

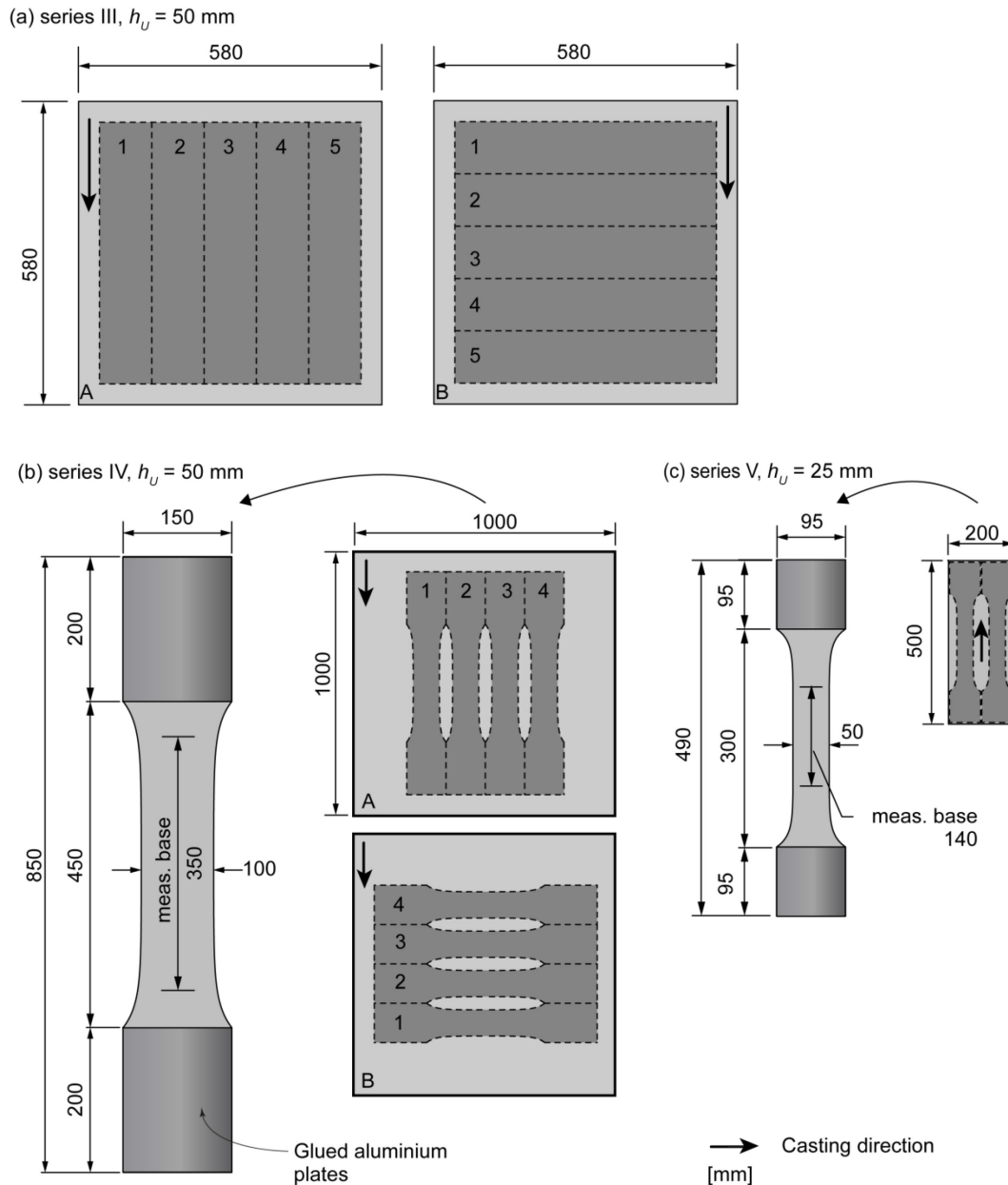
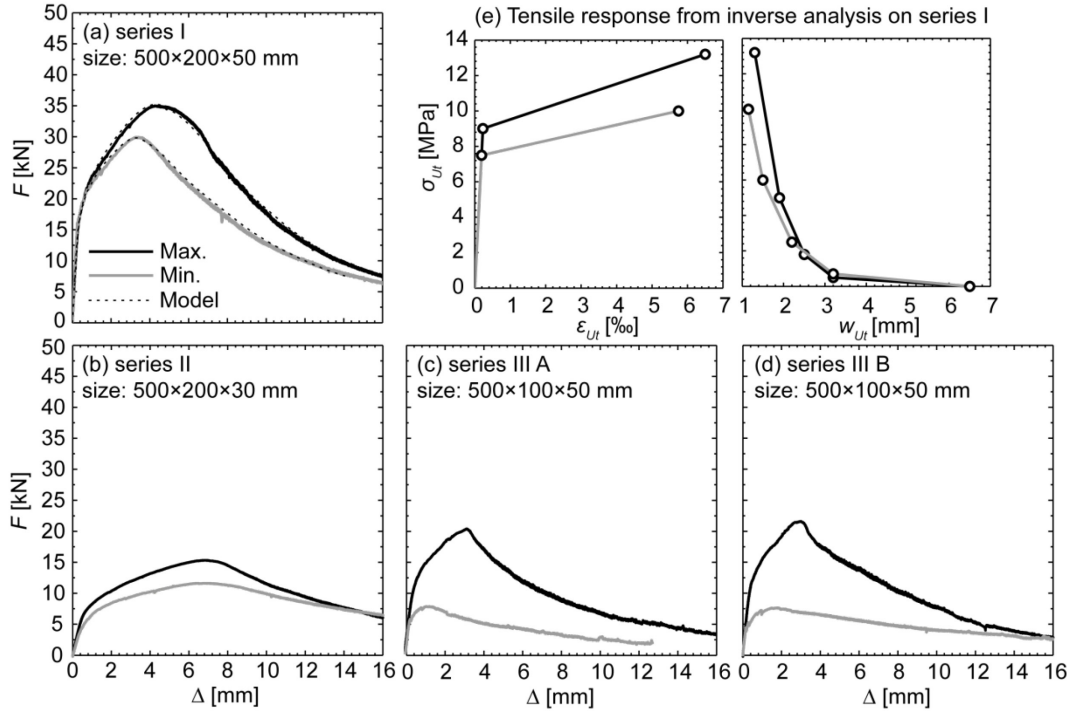


Figure 8 Test specimens for series III, IV and V

## 4.3 Test results

### 4.3.1 Bending response

The maximum and minimum force-deflection curves of all the bending test series are given in Figure 9. The bending tests of series I were modelled using a Non Linear Finite Element (NLFE) code [1.31]. The software used was MLS and the model was based on the smeared crack model with bulk energy dissipation. The test results of series I were very well reproduced by the model as shown by the dotted lines in Figure 9. This inverse analysis using a NLFE model gave an estimation of the maximum and minimum tensile response for specimens of series I. The main values of these tensile responses are given in the first line of Table 3 and the full response is shown in Figure 9e.



**Figure 9 Bending tests results for UHPFRC S3-13: (a to d): force-displacement curves; (e) result of the inverse analysis on series I**

The NLFE models used to reproduce the bending behavior of series I showed that for a specimen thickness between 25 and 50 mm, with a span of 420 mm, under 4-point bending and for strain hardening UHPFRC, at maximum force ( $F_u$ ), the position of the neutral axis of a bending specimen is approximately at 82% of the thickness ( $h_U$ ) from the extreme tensile fiber. According to these observations, the tensile strength of the material  $f_{Utu}$  can be predicted with  $F_u$  by supposing a rectangular distribution of the tensile stresses and a triangular elastic distribution of the compression stresses:

$$f_{Utu} = \frac{F_u \cdot L}{2.61 \cdot b \cdot h_U^2} \quad (14)$$

Using this equation, the maximum tensile strength  $f_{Utu}$  can be estimated for all bending test series in a straight forward manner using only the recorded peak force. With the values of  $f_{Utu}$ , it is then possible to calculate the values of the fiber orientation factors  $\mu_0$  using equation 1 (paragraph 2.2.1). All these results are given in Table 3. For these calculations, the value of the fiber efficiency  $\mu_1$  was determined using Figure 7. A value of 6.7 MPa was used for pull-out resistance of a fiber  $\tau_f$  as proposed for a similar mix by Oesterlee [1.19] and based on the tests by Wuest [1.5].

Series I and II were both cast in molds and differ only by the thickness of the specimens (50 or 30 mm). The average calculated values of  $f_{Utu}$  for these series are of 11.7 MPa and 13.4 MPa respectively (Table 3). This shows that thinner specimens tend to have higher tensile strengths and thus, a higher fiber orientation. For series III, the calculated values of  $f_{Utu}$  are globally lower. As expected, the value of  $f_{Utu}$  is higher for plate A (9.3 MPa) than for plate B (8.1 MPa). For both plates, the range of measured tensile strengths, between the maximum and minimum values, is larger than for series I and II. Thus, in a square plate, the



average tensile strength is lower and the variability of fiber orientation is higher than in an individually cast specimens.

**Table 3 Main results of the characterization campaign on UHPFRC S3-13**

Series		$f_{Ute}$ [MPa]	$\varepsilon_{Uel}$ [‰]	$f_{Utu}$ [MPa]	$\varepsilon_{Utu}$ [‰]	$f_{Utu}/f_{Ute}$	$\mu_0$	$\bar{\mu}_1$
I (inverse analysis - FEM)	Min.	7.5	0.19	10.0	5.80	1.33	0.64	0.95
	Max.	9.0	0.23	13.2	6.50	1.47	0.81	1.00
	<b>Average</b>	<b>8.3</b>	<b>0.21</b>	<b>11.7</b>	<b>6.15</b>	<b>1.40</b>	<b>0.73</b>	<b>0.98</b>
I (meso- mech. model)	Min.	6.6	0.17	9.8	2.79	1.49	0.63	0.95
	Max.	8.5	0.21	12.6	4.45	1.48	0.78	0.88
	<b>Average</b>	<b>7.8</b>	<b>0.20</b>	<b>11.7</b>	<b>4.08</b>	<b>1.50</b>	<b>0.73</b>	<b>0.98</b>
II (meso- mech. model)	Min.	8.1	0.20	11.8	4.15	1.46	0.74	0.98
	Max.	9.8	0.24	14.4	5.06	1.47	0.88	1.00
	<b>Average</b>	<b>9.2</b>	<b>0.23</b>	<b>13.4</b>	<b>4.69</b>	<b>1.45</b>	<b>0.82</b>	<b>1.00</b>
IIIA (meso- mech. model)	Min.	3.4	0.09	5.2	0.54	1.51	0.37	0.85
	Max.	9.2	0.23	13.5	4.76	1.47	0.83	1.00
	<b>Average</b>	<b>6.1</b>	<b>0.15</b>	<b>9.3</b>	<b>2.55</b>	<b>1.51</b>	<b>0.60</b>	<b>0.95</b>
IIIB (meso- mech. model)	Min.	3.4	0.08	5.2	0.55	1.54	0.38	0.85
	Max.	9.7	0.24	14.6	5.08	1.50	0.89	1.00
	<b>Average</b>	<b>5.4</b>	<b>0.13</b>	<b>8.1</b>	<b>1.78</b>	<b>1.52</b>	<b>0.54</b>	<b>0.93</b>
IVA	Min.	6.3	0.27	6.8	1.15	1.08	0.46	0.90
	Max.	7.6	0.40	9.2	2.01	1.22	0.60	0.95
	<b>Average</b>	<b>6.7</b>	<b>0.34</b>	<b>7.8</b>	<b>1.61</b>	<b>1.17</b>	<b>0.52</b>	<b>0.92</b>
IVB	Min.	5.3	0.20	5.5	0.28	1.04	0.39	0.86
	Max.	7.6	0.27	8.8	0.86	1.16	0.57	0.94
	<b>Average</b>	<b>6.6</b>	<b>0.29</b>	<b>7.3</b>	<b>0.79</b>	<b>1.11</b>	<b>0.49</b>	<b>0.91</b>
V	Min.	8.1	0.18	8.1	0.75	1.00	0.53	0.93
	Max.	10.8	0.31	13.4	2.8	1.24	0.82	1.00
	<b>Average</b>	<b>9.1</b>	<b>0.27</b>	<b>10.5</b>	<b>1.65</b>	<b>1.16</b>	<b>0.67</b>	<b>0.96</b>

Notes: - Factors  $\mu_0$  and  $\bar{\mu}_1$  are deduced with equation 1 and Figure 7  
- Values in grey cells are modelling results. All other results are experimental.

#### 4.3.2 Tensile response

The maximum, minimum and average stress-displacement curves for the tensile test series are shown in Figure 10. The main values are given in Table 3. For the specimens of series IV cut out from square plates, the average tensile strength  $f_{Utu}$  and corresponding strain  $\varepsilon_{Utu}$  for the two plates, 7.5 MPa and 1.17‰ respectively, are smaller than what was measured for the specimens of series V cut from the rectangular plates, 10.5 MPa and 1.65‰. These results reflect what was also observed for the bending tests where the specimens cut out from square plates demonstrated weaker behaviors.

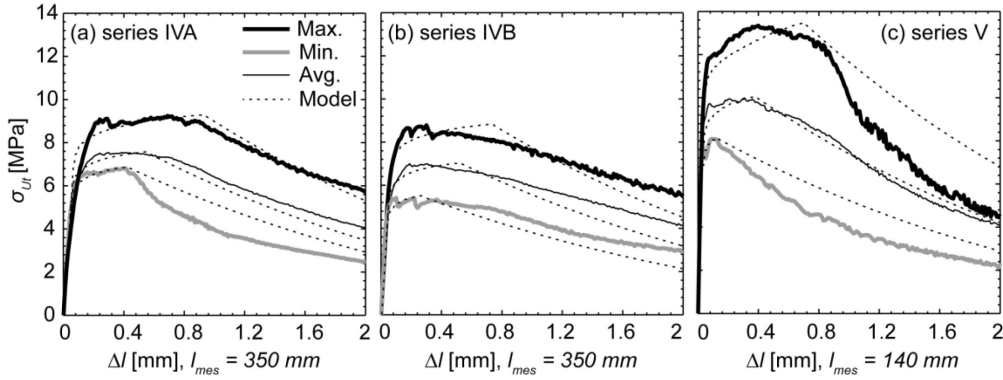


**Figure 10 Tensile test results for UHPFRC S3-13**

As for the bending results, the fiber orientation factor  $\mu_0$  was first estimated using equation 1 (paragraph 2.2.1), taking into account its relation with the efficiency factor  $\mu_l$  (Figure 7). The estimated values of the orientation factor can be found in Table 3 for all tests.

#### 4.4 Modelling results

The model by Wuest et al. [1.22] presented in paragraph 2.3 was calibrated for the UHPFRC mix S3-13. The parameters of the models are known based on the mix proportions or the material characterization campaign and are given in Table 4. The model could reproduce well the tensile test results of series IV and V. The results of this modelling are shown by the dotted lines in Figure 10.

**Table 4 Parameters for the meso-mechanical model for UHPFRC S3-13**

<b>Fibers</b>	$l_f$ [mm]	13
	$d_f$ [mm]	0.16
	$f_{sf}$ [MPa]	2000
	$E_f$ [GPa]	210
	$V_f$ [%]	3
	$\tau_f$ [MPa]	6.7
	$E_U$ [GPa]	40.3
	$E_m$ [GPa]	35.0
	$G_m$ [GPa]	10

Once the model is calibrated with the tensile test results, it is possible to model the full tensile response of bending test series II and III using the calculated values of the ultimate tensile strength  $f_{Um}$  (equation 14) and the orientation factor  $\mu_0$  (equation 1). By doing this, the missing values of elastic limit  $f_{Ue}$  and the maximum hardening strain  $\epsilon_{Um}$  are estimated for these tests without having to carry out a full inverse analysis. These results are given in Table 3.

## 4.5 Discussion

### 4.5.1 Analysis of test results

The bending and tensile test results show the range of possible tensile response of a layer of UHPFRC S3-13 with a thickness of between 25 and 50 mm. The average ultimate tensile strength varies between 13.4 and 7.3 MPa while the average maximum hardening strain varies between 6.15‰ and 0.79‰. This range of performances can be explained by the variation of fiber orientation, which is linked to the different specimen geometries and casting processes that were used here. It is thus important to correctly analyse the test results and identify the fiber orientation in the specimen. The results of the material testing campaign presented here can be separated in two groups for analysis.

First, the results of series II and V, with specimen thicknesses of 30 and 25 mm respectively, are in the higher range of the tensile responses. The average orientation factors for these series are higher than the 0.64 for the 2D isotropic case and the range of results is smaller. With a fiber length  $l_f$  of 13 mm, these specimens had a thickness  $h_U$  close to two times the fiber length ( $h_U \approx 2 \cdot l_f$ ).

Second, the results of series III and IV, with specimens cut out from square plates, allowed to identify the orientation factor in the two principal directions of a 50 mm-thick layer. The average orientation factor in direction 1, corresponding to series IIIB and IVB, was 0.54 and 0.49 respectively. For direction 2, corresponding to series IIIA and IVA, the calculated orientation factors were 0.60 and 0.52 respectively. As will be presented in the next section, these results can be used to identify the representative tensile response of a UHPFRC layer for a structural application.

When preparing specimens by cutting them out of a larger plate, as was done for series III and IV, fiber near the edge of the specimens are also cut and have a shorter length. This modification of the fiber lengths can happen up to a distance of  $l_f/2$  from the cut specimen edge. It is supposed that this has only a small effect on the tensile strength of the specimen as the whole width of the section is participating.

### 4.5.2 Recent literature data

Recently, some authors reported average ultimate tensile strength values up to 20 MPa [1.32, 33] for UHPFRC with variations between maximum and minimum measurements of 1 to 3 MPa. These results are given in Table 5. In the case of Kwon et al. [1.33], a fibrous mix composed of straight (S) and hooked (H) fibers was used, while Wille et al. [1.32] used straight fibers only. With the values of pull-out stress  $\tau_f$  measured by Wille et al. [1.20] for straight and hooked fibers and the relation between the average efficiency factor  $\overline{\mu}_1$  and the orientation factor  $\mu_0$  (Figure 7), supposed valid for both straight and hooked fibers, the orientation factors for those test results are estimated using equation 1. These results are also given in Table 5.

The tensile test specimens used to obtain these results were cast horizontally and had cross sections of 30×30 mm [1.33] and 25×25 mm [1.32]. These very slender specimens induced preferential fiber alignment. All calculated orientation factors are higher than 0.64, the

orientation factor of the perfect 2D isotropic case, which means that orientation factors tend to approach 1D unidirectional case.

**Table 5 Review of recent ultimate tensile strength results for UHPFRC**

Ref.	Cross-section [mm]	Mix	$V_f$ [%]	$l_f$ [mm]	$d_f$ [mm]	$\tau_f$ [MPa]	$f_{U_t}$ [MPa]	$\mu_0$	$\bar{\mu}_1$
Wille et al. [1.32]	25×25	U-S-2	S: 2				15	0.96	1.00
		U-S-2.5	S: 2.5	13	0.2	12	16.5	0.85	1.00
		U-S-3	S: 3				17.8	0.77	0.99
Kwon et al. [1.33]	30×30	S1H0.5	S: 1	6	0.16	12	11.9	1.04	1.00
			H: 0.5	30	0.38	17.6			
		S1H1.0	S: 1	6	0.16	12	12.4	0.70	0.96
			H: 1	30	0.38	17.6			
		S1H1.5	S: 1	6	0.16	12	16.1	0.66	0.96
			H: 1.5	30	0.38	17.6			
		S1H2.0	S: 1	6	0.16	12	20.1	0.65	0.96
			H: 2	30	0.38	17.6			

S : Straight fibers  
H : Hooked fibers

The results presented by these authors [1.32, 33] show that, as expected, a very well oriented specimen can give spectacular results with very large extents of strain hardening, for low  $V_f \cdot \frac{l_f}{d_f}$  values. However, similar mixes with fiber orientations representative of practical applications would yield significantly weaker responses, with very limited or inexistent strain hardening response. These results are thus misleading for practice and design. The orientation factor of the intended application needs to be taken into account and the values must be adjusted accordingly, as will be demonstrated in the next sections.

#### 4.5.3 Interpretation

The tests reviewed here showed that UHPFRC does not have an intrinsic response. It depends on the geometry of the specimen, the casting process as well as the testing method. A large range of results is an indicator of the fabrication method. The lower the fiber orientation factor is, the higher the possible range of results. By using very slender specimens that induce preferential fiber alignment, it is possible to reduce the range of results. On the other side, for very low fiber orientation factors, as obtained in some cases for specimens cut from plates, some fibers are lying perpendicular to the direction of loading. In this case, Oesterlee [1.19] explained that the fibers do not contribute to the tensile capacity but act as a local defect, weakening the specimen and thus increasing the range of possible responses.

Due to this large range of results, it is not suitable to calculate a characteristic value for the tensile strength of UHPFRC based on a coefficient of variation and respecting the 5%-fractile as it is done for other materials in standards. This would yield very low values that are not representative of the actual response of the material. Makita and Brühwiler [1.34] demonstrated that significant local stress redistribution occurs in a UHPFRC specimen, due

to the hardening and softening response of the material. Based on this observation, the representative value for tensile strength  $f_{U_{th,rep}}$  should correspond to the average fiber orientation factor expected in the considered structural element, as will be demonstrated in the next paragraphs. Thus it is important to link the measured values for a specific type of testing (bending or tensile tests) to the actual fiber orientation in the intended application.

## 5 Validation of the stereological analysis

### 5.1 Overview

In the following paragraph, the theoretical relations developed in paragraph 3 are validated using experimental results from the present work and from the literature. Using these experimental results, an average relation between the orientation factors in the in-plane orthogonal directions of a UHPFRC layer is established. This relation can hereafter be used to estimate fiber orientation factor for this specific application.

### 5.2 Fiber orientation in orthogonal directions

#### 5.2.1 Validation with test results

Various authors [1.5, 19, 35] used image analysis to count the fibers on cut sections of UHPFRC specimens and calculate the resulting fiber orientation factor. Table 6 gives detailed information on the various specimen type used by the authors as well as the measured orientation factors. In all cases, the studied elements had a thickness of between 23 and 50 mm, as typical for a layer of UHPFRC on a RC element (Figure 1). Fiber orientation was evaluated in the two orthogonal directions of the plan perpendicular to the thickness. The assumed casting direction of the specimen was set to  $\mu_{02}$ . Wuest [1.5] is the only author who also measured the orientation factors in the third direction and these values are also included in Table 6.

The fiber orientation factors determined with equation1 in paragraph 4.3 for test series III and IV were also included in Table 6. Estimated average fiber orientation factors for plates A and B are supposed to correspond to orthogonal directions and were considered to be  $\mu_{02}$  and  $\mu_{01}$  respectively.

To validate the curves calculated in paragraph 3.2, the measured fiber orientation factors given in Table 6 were then compared to the curves in Figure 11. Most results are found between the two lines showing that these curves are the boundary cases and can be used to study the complementarity of orientation factors in two orthogonal directions.

#### 5.2.2 Average relation

All the results compiled in Table 6 were used to obtain the average orientation factors for specimens with thicknesses typical of a reinforcement layer, between 25 and 50 mm. Various casting method were used to produce all the considered specimens. As explained in paragraph 4.2, the square plates used for series III and IV were cast using a similar procedure to that used for the fabrication of the overlay on the composite slabs. Wuest [1.5] also

measured the fiber orientation factors of the layer of UHPFRC cast with a similar technique on a RC slab (slab SAMD2). Thus, a first average for these similar specimens (highlighted in grey in Table 6) is calculated and indicated in Figure 11 by a grey star. An overall average for all results of Table 6 is also given.

**Table 6 Review of experimental fiber orientation measurements**

Ref.	UHPFRC mix				Specimen		Orientation factors		
	$l_f$ [mm]	$d_f$ [mm]	$V_f$ [%]	$h_U$ [mm]	Fabrication method	ID	$\mu_{01}$	$\mu_{02}$	$\mu_{03}$
Oesterlee [1.19]	13	0.16	3	40	Vertically cast panel, 3000×1500 mm	T2H	0.19	0.79	--
						T6H-1	0.67	0.49	--
						T6H-2	0.74	0.39	--
						T7H-1	0.79	0.36	--
						T2V	0.63	0.53	--
						T4V	0.75	0.55	--
Ferrara et al. [1.35]	13	0.16	1.27	30	Horizontally cast slabs, pouring from 1 point, 1000×500 mm	A	0.44	0.85	--
						B	0.54	0.76	--
Wuest [1.5]	10	0.2	6	50	Horizontally cast dog-bones, 100 mm central width	CM0-98-T4	0.55	0.63	0.24
						CM22-94-T5	0.78	0.60	0.41
	13	0.16	4	50	Horizontally cast rectangular plates, 200 mm central width	CM23-P-T1	0.50	0.71	0.28
						HIFCOM-14-T2	0.35	0.66	0.25
	10	0.2	6	50	Horizontally cast rectangular plates, 200 mm central width	CM0-05-22-TE1	0.74	0.38	0.63
						CM22-3-e	0.51	0.62	0.32
Sect. 4.3	13	0.16	3	50	Reinforcement layer over a RC slab	SAMD2	0.58	0.67	--
						Horizontally cast plates (see Table 2)	III	0.54	0.60
						IV	0.49	0.52	--
					Reinforcement layer	Average	0.53	0.60	--
						Std. dev	0.05	0.08	--
					Overall	Average	0.57	0.59	0.36
						Std. dev	0.16	0.14	0.15

The overall average values of the orientation factor for UHPFRC specimens (Table 6) are used to calculate an average curve with the relations given in paragraph 3.2.2 for the 3D case (equations 11) using the following steps:

1. Angles  $\theta_a$  and  $\varphi_a$  are both fixed at zero.
2. The value of  $\theta_b$  is fitted with equation 11a based on the average value of  $\mu_{01}$ .
3. With equations 11b and c, the value for  $\varphi_b$  that gives the best agreement with the average values of  $\mu_{02}$  and  $\mu_{03}$  is deduced.

4. The average curve is obtained in two steps, as for the general curves. The values of angles  $\theta$  are varied between 0 and  $\pi/2$ , while the angles  $\varphi$  are fixed to the values calculated in the previous steps and given in Table 7.

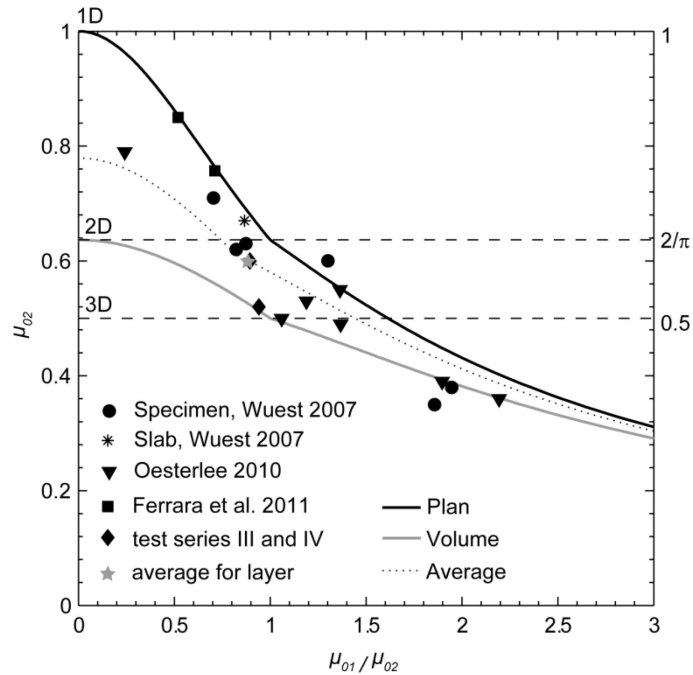


Figure 11 Orientation factors in orthogonal directions and experimental data

Table 7 Calculations of fiber orientation factor

Specimen	Average	CM23-P-T1 [1.5]	CM22-3-e [1.5]
$\theta_a$ [rads]	0	0	0
$\theta_a$ [°]	0	0	0
$\theta_b$ [rads]	$0.44\pi$	$0.48\pi$	$0.48\pi$
$\theta_b$ [°]	78.3	86.4	86.4
$\varphi_a$ [rads]	0	0	0
$\varphi_a$ [°]	0	0	0
$\varphi_b$ [rads]	$0.38\pi$	$0.26\pi$	$0.32\pi$
$\varphi_b$ [°]	67.5	46.8	57.6
$\mu_{01}$	0.60	0.53	0.54
Variation	0.01	0.03	0.03
$\mu_{02}$	0.57	0.69	0.64
Variation	0.00	0.02	0.02
$\mu_{03}$	0.38	0.30	0.35
Variation	0.02	0.02	0.03

The results of the calculations and the variation with the overall average are given in Table 7. The average curve is plotted with a dotted line in Figure 11. The grey star, representing the average values of orientation factors in a layer or plate lies on the dotted line. This average

was obtained for specimen with a maximum thickness to fiber ratio of 5. Results for SAMD2 are shown with a black star in Figure 11. SAMD2 has a thinner layer of 23 mm and the black star lies closer to the black line for the 2D case.

Based on the previous observations, the three curves showed in Figure 11 can be used to relate fiber orientation factors in the orthogonal direction of a layer. They are valid for the following cases:

- The black curve representing the 2D case is valid for thickness approximately equal to two times the fiber length ( $b_U \approx 2 \cdot l_f$ ). In this situation, edge effects will have a stronger influence on fiber orientation and a 2D distribution of fiber can be expected.
- The average dashed curve can be used for a layer thickness between 40 and 60 mm.
- The grey curve for the 3D case can be safely used for thicker UHPFRC layers.

### 5.2.3 Generalization

The procedure explained in steps 1 to 3 was also applied to specimens CM23-P-T1 and CM22-3-e, presented in Table 6 and for which fiber orientation factors were determined in the 3 directions [1.5]. This was done to demonstrate the versatility of the method which applies for various cases and not only for perfectly isotropic cases or cases where the orientation factors equal in direction 2 and 3.

### 5.3 Average efficiency factor

The fiber orientation factors presented in Table 6 were measured using image analysis on specimens on which tensile tests were also done. The tensile strength and the fiber orientation can thus be related and using equation 1 the average fiber efficiency factor can be calculated (Table 8). In a first approximation, maximum pull-out stress of the fibers  $\tau_f$  was taken equal to 8 MPa, which is an average of all the values given in paragraph 2.2.4.

This data is plotted in Figure 12 to validate the relation between fiber orientation factor and the average efficiency factor developed in paragraph 3.3. The cloud of points shows a trend similar to what has been theoretically calculated. Of course, the relation between the fiber orientation factor and the average fiber efficiency factor will strongly depend on the pull-out stress as well as on the chosen relation between the pull-out angle and the fiber efficiency factor. The latter has been defined for various types of fibers and based on experimental data already quite dispersed (Figure 2). Research is needed to define this relation for the specific case of straight fibers and UHPFRC mixes. Nevertheless, the relation established herein allows, in a first step, to define the average efficiency factor for a given fiber orientation factor in a straight forward and systematic manner.



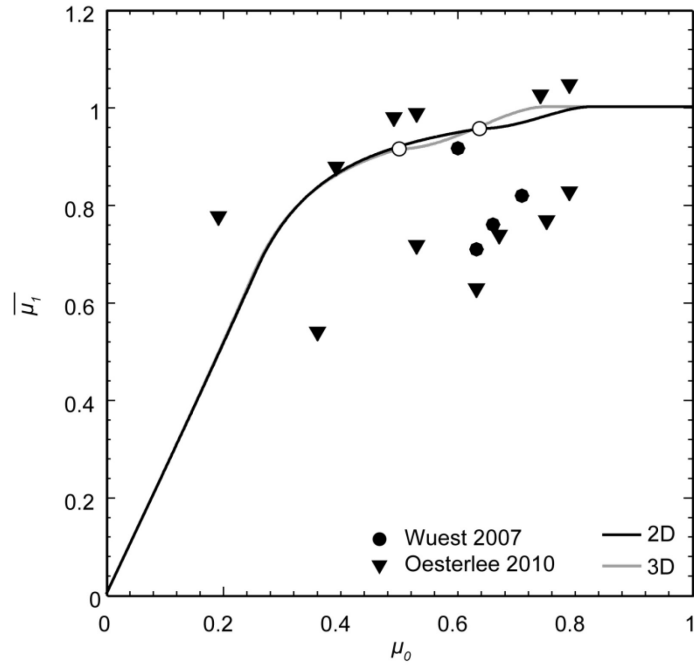


Figure 12 Relation between orientation and efficiency factors and experimental data

Table 8 Review of experimental fiber orientation measurements and related tensile strength

Ref.	Specimen ID	$f_{Uw}$ [MPa]	$\mu_0$	$\bar{\mu}_1$
	T2H	16.1	0.79	1.19
		2.9	0.19	0.89
	T6H-1	9.4	0.49	1.12
		9.7	0.67	0.85
	T6H-2	6.7	0.39	1.01
		14.9	0.74	1.18
[1.19]	T7H-1	3.8	0.36	0.62
		12.8	0.79	0.95
	T2V	7.4	0.53	0.82
		7.7	0.63	0.72
	T4V	14.1	0.55	1.50
		11.2	0.75	0.88
	T6V	12.2	0.50	1.43
		10.2	0.53	1.13
[1.5]	CM0-98-T4	10.7	0.63	0.81
	CM22-94-T5	13.3	0.60	1.06
	CM23-P-T1	14.0	0.71	0.94
	HIFCOM-14-T2	13.0	0.66	0.87

## 6 Application to a UHPFRC layer

### 6.1 Overview

In the following, the results of the analysis in the previous paragraph are used to estimate the representative orientation factors in a layer of UHPFRC cast on a rough concrete substrate. Once the fiber orientation factor is estimated for the considered application, the corresponding tensile response can be found using the calibrated meso-mechanical model.

### 6.2 Slab elements

Four composite slabs, called PBM1-4, were fabricated with a layer of UHPFRC mix S3-13 [1.30], characterized in paragraph 4. The geometry of the slabs and their UHPFRC layers is given in Figure 13. Three slabs had a layer of 50 mm thick (PBM1-3) and one had a thinner layer of 25 mm. All the slabs were cast as described earlier, laying the UHPFRC from one side to the other using an overhead bucket and conventional concrete tools to correctly pull the material and place it over the whole surface. The effect of the roughness of the concrete surface on which the layer is placed is considered to have a negligible effect on the orientation of the fibers. In the layers of 50 mm of slabs PBM2-3, small diameter reinforcement bars were placed. Since in all cases the rebar spacing of 150 mm was relatively large compared to the fiber length, it is also supposed that the rebars only had minor local effects on the orientation.

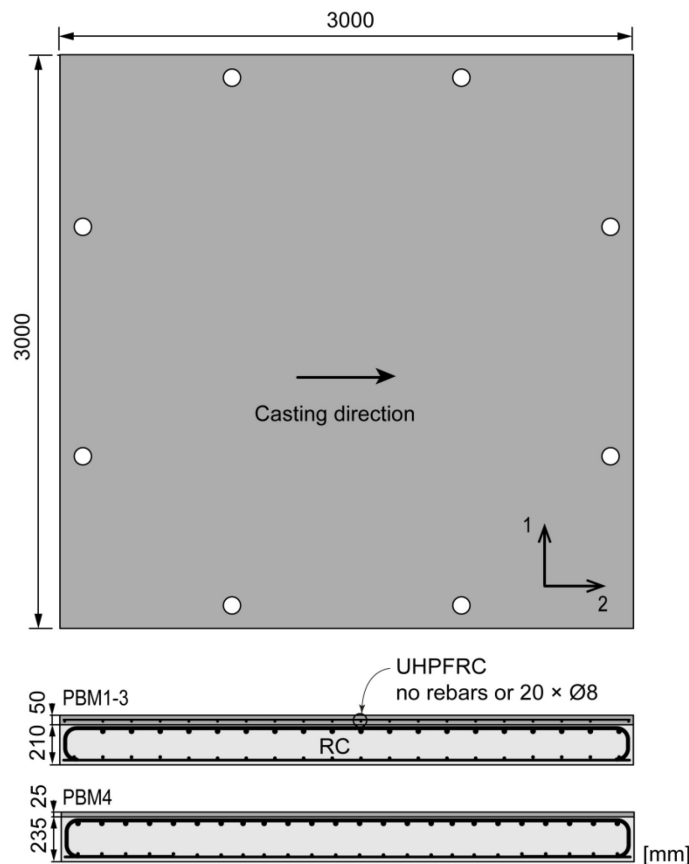


Figure 13 Geometry of composite slab specimens PBM [1.30]

### 6.3 Average fiber orientation factors

Using the average orientation factors obtained for plates or layers cast in similar ways (Table 6) and the meso-mechanical model with the parameters defined in paragraph 4.4, the tensile responses that should be used for the design of a layer made of S3-13 are calculated, see Table 9.

For slabs with a 50-mm layer (PBM1-3), the average values of orientation factors for layers given in the grey line of Table 6 can be directly used. The orientation factors  $\mu_{01}$  and  $\mu_{02}$  for the layer of 50-mm are thus respectively 0.53 and 0.60. Slab PBM4 however has a thinner layer approximately equal to two times the fiber length ( $h_U \approx 2 \cdot l_f$ , see Table 9), as slab SAMD2 had [1.5]. It is thus considered more appropriate to account for the 2D isotropic case. The ratio  $\mu_{01}/\mu_{02}$  obtained with the average values is conserved and reported on the black curve for the 2D isotropic case. The orientation factors for this thinner layer are thus higher, as was observed for the thinner specimens (series II and V) of the material testing campaign. The orientation factors  $\mu_{01}$  and  $\mu_{02}$  for the layer of 25-mm are respectively 0.61 and 0.68.

### 6.4 Representative tensile response

Using the meso-mechanical model calibrated for the mix in paragraph 4.4, the tensile response corresponding to the estimated orientation factors in the layer is obtained. Two tensile responses for a layer of UHPFRC are identified, one in each orthogonal direction. The material response with the highest values is supposed to be in the direction of casting, direction 2. It is not yet clear if this anisotropy has an important influence on the ultimate resistance of a RC element reinforced with a layer of UHPFRC. However, due to the stress and deformation redistribution capacity of UHPFRC [1.34], it is proposed to use the average values to design a UHPFRC layer that will carry loads in both directions. In the case of a one-way slab, it is possible to choose the tensile law that corresponds to the carrying direction.

**Table 9 Fiber orientation and tensile responses for layers of UHPFRC S3-13**

Spec.	$h_U$ [mm]	$l_f$ [mm]	$h_U$ / $l_f$	Direction	$\mu_0$	$f_{Ute}$ [MPa]	$\varepsilon_{Uel}$ [‰]	$f_{Utu}$ [MPa]	$\varepsilon_{Utu}$ [‰]	$f_{Utu}/$ $f_{Ute}$
PBM1-3	50	13	3.8	1	0.53	5.3	0.13	8.0	1.71	1.52
				2	0.60	6.1	0.15	9.3	2.55	1.52
PBM4	25		3.8	1	0.61	6.3	0.16	9.5	2.59	1.49
				2	0.68	7.5	0.19	10.7	2.69	1.42

The orientation factors  $\mu_{01}$  and  $\mu_{02}$  for the layer of 50-mm are thus respectively 0.53 and 0.60, which corresponds to ultimate tensile strengths of 8.0 and 9.3 MPa. Test series II had the highest average orientation factor of 0.82 (see Table 3). This corresponds to an ultimate tensile strength of 13.4 MPa which is significantly higher than the estimated tensile strength in the layer. If the results of this test series would be directly used for the design of the reinforcement layer with UHPFRC S3-13, the resistance would be overestimated. For this reasons, fiber orientation effects need to be considered in the design and execution of elements as well as when analyzing test results.

Representative fiber orientation must be used to scale the tensile response of the material for the design of structural elements. When possible, representative testing can confirm the fiber orientation in the element, as also proposed in the French recommendations [1.36]. However this type of extensive testing is costly. Non-destructive fiber orientation measurement methods offer an alternative to quickly identify the average fiber orientation factors in a large element. These methods include AC-impedance spectroscopy [1.37], electrical resistivity measurement [1.38] or magnetic measurements [1.39, 40].

Scaling the tensile strength of UHPFRC to the correct average fiber orientation and efficiency factors gives the representative value  $f_{Utu,rep}$  which directly takes into account the differences between testing results and expected properties in the layer. By doing so, there is no need to use a characteristic value of the property (see section 4.5.3) and to apply a conversion factor  $\eta$ , as defined in Eurocodes [1.41] and Swiss standards for construction [1.42]. However, to obtain the design value of a material property  $X_d$ , a partial factor  $\gamma_m$  accounting for uncertainties in this property has to be applied (equation 15). Therefore, the representative value  $f_{Utu,rep}$  is divided by a partial factor  $\gamma_U$  to obtain the design tensile strength of UHPFRC  $f_{Utud}$  (equation 16).

$$X_d = \frac{X_{rep}}{\gamma_m} \quad (15)$$

$$f_{Utud} = \frac{f_{Utu,rep}}{\gamma_U} \quad (16)$$

## 7 Conclusions

This paper showed the importance of mastering the effect of fiber orientation when designing with UHPFRC. The representative tensile response of a given UHPFRC mix depends strongly on the fiber orientation which varies with the geometry of the test specimen, the casting process as well as the testing method. The tensile response used for the design of a structural element must be chosen with care keeping in mind the following:

1. A relation between fiber orientation factors in orthogonal directions exists and was developed using stereological principles. Based on this relation and a review of experimental results, average fiber orientation factors in a layer of 50-mm of UHPFRC were identified as 0.53 and 0.60 in the orthogonal direction.
2. The average fiber efficiency factor decreases with the fiber orientation. For orientation factors below 0.28, the average efficiency factor is directly proportional to the fiber orientation factor and thus has a strong influence on the tensile strength of UHPFRC. However, it is equal to 1.0 for orientation factors higher than 0.75. Between the two borders the efficiency factor only has a slight influence on the calculated tensile strength of UHPFRC.
3. Any type of bending or tensile tests can be carried out in order to identify the material's tensile response. The effect of fiber orientation on tensile or bending test results can be identified. Therefore, the material response can be scaled to fit the

average fiber orientation in the intended structural element using equation 1 and the proposed meso-mechanical model for the complete response.

4. There is no intrinsic tensile response for UHPFRC, as it depends on the geometry of the specimen, the casting process as well as the testing method.
5. Average orientation factors should be used to scale the tensile response to the dimensions of the structural elements of the intended application.

## 8 References

- [1.1] Krenchel H. Fibre reinforcement: Theoretical and practical investigations of the elasticity and strength of fibre-reinforced materials. Doctoral thesis. Copenhagen: Akademisk Forlag; 1964; 158 p.
- [1.2] Naaman AE. A Statistical Theory of Strength for Fiber Reinforced Concrete. PhD Thesis. Boston: Massachusetts Institute of Technology; 1972; 196 p.
- [1.3] Soroushian P, Lee C-D. Distribution and orientation of fibers in steel fiber reinforced concrete. *ACI Materials Journal*. 1990;87(5):433-9.
- [1.4] Behloul M. Analyse et modélisation du comportement d'un matériau à matrice cimentaire fibrée à ultra hautes performances du matériau à la structure. Doctoral thesis. Cachan: ENS Cachan; 1996; 180 p.
- [1.5] Wuest J. Comportement structural des bétons de fibres ultra performants en traction dans des éléments composés. Doctoral thesis EPFL no. 3987. Lausanne: Ecole Polytechnique Fédérale de Lausanne; 2007; 244 p.
- [1.6] Habel K, Denarie E, Brühwiler E. Structural Response of Elements Combining Ultrahigh-Performance Fiber-Reinforced Concretes and Reinforced Concrete. *Journal of Structural Engineering*. 2006;132(11):1793-800.
- [1.7] Noshiravani T, Brühwiler E. Experimental investigation on reinforced ultra-high-performance fiber-reinforced concrete composite beams subjected to combined bending and shear. *ACI Structural Journal*. 2013;110(2):251-61.
- [1.8] Brühwiler E, Denarie E. Rehabilitation and Strengthening of Concrete Structures Using Ultra-High Performance Fibre Reinforced Concrete. *Structural Engineering International*. 2013;23(4):450-7.
- [1.9] Hannant PJ. Fibre Cements and Fibre Concretes. England: Wiley & Sons; 1978; 231 p.
- [1.10] Stroeven P. Stereological principles of spatial modeling applied to steel fiber-reinforced concrete in tension. *ACI Materials Journal*. 2009;106(3):213-22.
- [1.11] Krenchel H. Fibre spacing and specific fibre surface. In: Neville AM, editor. *Fibre Reinforced Cement and Concrete: RILEM symposium; 14th to 17th September 1975*; London: Construction Press; 1975. p. 69-79.
- [1.12] Aveston J, Kelly A. Theory of Multiple Fracture of Fibrous Composites. *Journal of Materials Science*. 1973;8(3):352-62.
- [1.13] Maage M. Interaction between steel fibers and cement based matrixes. *Materials and Structures*. 1977;10(5):297-301.
- [1.14] Naaman AE, Shah SP. Pull-out mechanism in steel fiber-reinforced concrete. *Journal of the Structural Division*. 1976;102(8):1537-48.
- [1.15] Rasmussen TV. Time dependent interfacial parameters in cementitious composite materials. Series R 33. Lyngby: Technical University of Denmark; 1997; p.

- [1.16] Pfyl T. Tragverhalten von Stahlfaserbeton. Doctoral thesis ETHZ no. 15005. Zürich: ETH Zürich; 2003; 139 p.
- [1.17] Wille K, Tue NV, Parra-Montesinos GJ. Fiber distribution and orientation in UHP-FRC beams and their effect on backward analysis. *Materials and Structures*. 2013;47(11):1825-38.
- [1.18] Jungwirth J. Zum Tragverhalten von zugbeanspruchten Bauteilen aus Ultra-Hochleistungs-Faserbeton. Doctoral thesis EPFL no. 3429. Lausanne: Ecole Polytechnique Fédérale de Lausanne; 2006; 158 p.
- [1.19] Oesterlee C. Structural Response of Reinforced UHPFRC and RC Composite Members. Doctoral thesis EPFL no. 4848. Lausanne: Ecole Polytechnique Fédérale de Lausanne; 2010; 136 p.
- [1.20] Wille K, Naaman AE. Pullout behavior of high-strength steel fibers embedded in ultra-high-performance concrete. *ACI Materials Journal*. 2012;109(4):479-88.
- [1.21] Orange G, Dugat J, Acker P. Ductal®: New ultra high performance concretes. Damage resistance and micromechanical analysis. In: RILEM, editor. Fifth RILEM symposium on fibre-reinforced concrete (FRC); Lyon: RILEM; 2000. p. 101-11.
- [1.22] Wuest J, Denarié E, Brühwiler E. Model for predicting the UHPFRC tensile hardening response. In: Fehling E, Schmidt M, Stürwald S, editors. Second International Symposium on Ultra High Performance Concrete March 05-07, 2008; Kassel: Kassel University Press; 2008. p. 153-60.
- [1.23] Aveston J, Cooper GA, Kelly A. Single and multiple fracture. Conf Proc of the National Physical Laboratory, Properties of Fiber Composites; Surrey: IPC Science and Technology Press; 1971. p. 15-26.
- [1.24] Kang S-T, Kim J-K. The relation between fiber orientation and tensile behavior in an Ultra High Performance Fiber Reinforced Cementitious Composites (UHPFRCC). *Cement and Concrete Research*. 2011;41(10):1001-14.
- [1.25] Dupont D, Vandewalle L. Distribution of steel fibres in rectangular sections. *Cement and Concrete Composites*. 2005;27(3):391-8.
- [1.26] Stroeven P. The analysis of fibre distributions in fibre reinforced materials. *Journal of Microscopy*. 1977;111(3):283-95.
- [1.27] Breyse D, Attar A, Soulier B, Mesureur B. Modélisation de la réponse en traction du béton renforcé de fibres métalliques. *Materials and Structures*. 1997;30(5):259-68.
- [1.28] Foster SJ. On behavior of high-strength concrete columns: Cover spalling, steel fibers, and ductility. *ACI Structural Journal*. 2001;98(4):583-9.
- [1.29] Bastien-Masse M. Characterization of the UHPFRC S3-13. Test report. Lausanne: Ecole Polytechnique Fédérale de Lausanne; ENAC-MCS;2014.
- [1.30] Bastien-Masse M, Brühwiler E. Experimental Investigation on Punching Resistance of R-UHPFRC – RC Composite Slabs. *Materials and Structures*. 2015: doi:10.1617/s11527-015-0596-4.
- [1.31] Denarié E, Jacomo D, Fady N, Crovez D. Rejuvenation of maritime signalisation structures with UHPFRC. In: F. T, J. R, editors. RILEM-fib-AFGC International Symposium on Ultra-High Performance Fibre-Reinforced Concrete; 2013; Marseille, France: RILEM; 2013. p. 157-66.
- [1.32] Wille K, El-Tawil S, Naaman AE. Properties of strain hardening ultra high performance fiber reinforced concrete (UHP-FRC) under direct tensile loading. *Cement and Concrete Composites*. 2014;48:53-66.
- [1.33] Kwon S, Nishiwaki T, Kikuta T, Mihashi H. Development of ultra-high-performance hybrid fiber-reinforced cement-based composites. *ACI Materials Journal*. 2014;111(3):309-18.
- [1.34] Makita T, Brühwiler E. Tensile fatigue behaviour of ultra-high performance fibre reinforced concrete (UHPFRC). *Materials and Structures*. 2014;47(3):475-91.
- [1.35] Ferrara L, Ozyurt N, di Prisco M. High mechanical performance of fibre reinforced cementitious composites: the role of “casting-flow induced” fibre orientation. *Materials and Structures*. 2011;44(1):109-28.

- [1.36] AFGC. Ultra High Performance Fibre-reinforced Concretes – Recommendations. Paris: Association Française de Génie Civil; 2013; 358 p.
- [1.37] Ozyurt N, Mason TO, Shah SP. Non-destructive monitoring of fiber orientation using AC-IS: An industrial-scale application. *Cement and Concrete Research*. 2006;36(9):1653-60.
- [1.38] Lataste JF, Behloul M, Breyse D. Characterisation of fibres distribution in a steel fibre reinforced concrete with electrical resistivity measurements. *NDT & E International*. 2008;41(8):638-47.
- [1.39] Ferrara L, Faifer M, Toscani S. A magnetic method for non destructive monitoring of fiber dispersion and orientation in steel fiber reinforced cementitious composites—part 1: method calibration. *Materials and Structures*. 2012;45(4):575-89.
- [1.40] Nunes S, Ribeiro F, Carvalho A, Pimentel M, Brühwiler E, Bastien-Masse M. Non-destructive measurements to evaluate fiber dispersion and content in UHPFRC reinforcement layers. In: Pacheco P, Magalhaes F, editors. *Multi-Span Large Bridges*; 01-03 July 2015; Porto, Portugal: Taylor & Francis Group; 2015. p. 1001-8.
- [1.41] CEN. EN 1990 : 2002 : Eurocode – Basis of structural design. Brussels: European Committee of Standardisation; 2002.
- [1.42] SIA. SN 505 260 : Bases pour l'élaboration des projets de structures porteuses. Zurich: Société suisse des Ingénieurs et Architectes; 2013.





## Paper II

### Experimental Investigation on Punching Resistance of R-UHPFRC – RC Composite Slabs

---

**Reference:** Bastien-Masse M, Brühwiler E. Experimental Investigation on Punching Resistance of R-UHPFRC – RC Composite Slabs. *Materials and Structures*: 2015. <http://doi.org/10.1617/s11527-015-0596-4>

#### Abstract

An effective method to strengthen existing Reinforced Concrete (RC) structures is to add a thin layer of Ultra-High Performance Fiber Reinforced cement-based Composite (UHPFRC), with or without steel rebars, over the concrete slab to create a composite element. It was demonstrated by previous test series that this method increases rigidity, bending and shear strength of one-way RC members. This paper presents the results of punching tests on 6 composite slabs without transverse reinforcement. The parameters of the tests included the thickness of the UHPFRC layer and the amount of reinforcement in it. All slabs failed in punching mode with a drop in resistance after maximum resistance was measured. For a layer of 50 mm of UHPFRC, the normalised resistance was at least 1.69 times greater than the normalised resistance of the RC reference slab. The layer of UHPFRC increased the rigidity of the slab and provided added shear resistance to the cracked RC section by out-of-plane bending. By doing so, it allowed more deformation to take place in the RC section before punching shear failure. This results in rotations and deflections at maximum resistance similar to what was observed for the reference RC slab.

**Keywords:** Composite slab, Punching shear, Ultra-High Performance Fiber Reinforced cement-based Composite (UHPFRC), Strengthening, Near interface cracking, Deformation capacity.

## List of Symbols

### Subscripts

$R$	Resistance
$U$	UHPFRC
$c$	concrete
$i$	steel or UHPFRC tensile reinforcement
$sc$	top steel reinforcement layer in RC section
$sU$	steel reinforcement in the R-UHPFRC layer

### Latin upper case

$A$	Area
$B$	side length of slab specimen
$E_{cm,28}$	average modulus of elasticity of concrete at 28 days
$E_{Um,28}$	average modulus of elasticity of UHPFRC at 28 days
$V$	punching shear force
$V_{csct}$	punching shear resistance of the concrete section calculated with CSCT
$V_{flex}$	estimated flexural resistance calculated with yield lines
$V_{res}$	residual shear resistance after punching shear failure

### Latin lower case

$b_0$	critical perimeter for punching shear set at $d_{sc}/2$ from the column face
$c$	side length of column
$d$	flexural depth for a tensile reinforcement: distance from the bottom compression face of the slab to the centroid of the tensile reinforcement
$d_{eff}$	effective flexural depth calculated with the mechanical ratio of each tensile reinforcement
$d_g$	maximum diameter of aggregate
$d_{g0}$	reference aggregate size set at 16 mm
$f$	strength of a material
$f_c$	concrete compressive strength,
$f_{cm,28}$	average concrete compressive strength at 28 days
$f_y$	yield strength of steel reinforcement
$f_{su}$	maximum strength of steel reinforcement
$f_{Ute}$	elastic tensile strength of UHPFRC
$f_{Um}$	tensile strength of UHPFRC
$h$	height
$\Delta b$	change in thickness of a slab
$\Delta l$	change in distance between two points measured by a sensor
$w$	measured deflection of the slab; crack opening
$\Delta w$	shear deformation at the column face

### Greek lower case

$\alpha_c$	minimum angle of the critical shear crack
$\varepsilon_{su}$	strain in steel reinforcement at maximum strength
$\varepsilon_{Um}$	strain in UHPFRC at maximum tensile strength
$\psi$	rotation
$\omega$	mechanical ratio of tensile reinforcement
$\omega_{tot}$	total mechanical ratio of tensile reinforcement

## 1 Introduction

Reinforced Concrete (RC) flat slabs on columns are widely used in building construction for their simplicity to build. However, this type of construction has a basic conceptual flaw as it is prone to punching shear failures around the columns. This particular failure is known to be sudden and can trigger a progressive collapse of the structure [2.1].

To strengthen a RC slab with deficient resistance, it has been proposed to add on the surface a thin layer, 25 to 50 mm in thickness, of Ultra-High Performance Fiber Reinforced cement-based Composite (UHPFRC) with small diameter steel rebars (Figure 1a) [2.2]. This technique modifies the RC slab into an R-UHPFRC – RC (RU-RC) composite slab. The UHPFRC layer reinforced with steel rebar inserts (R-UHPFRC) acts as a tensile reinforcement and increases both bending and shear resistances of the slab.

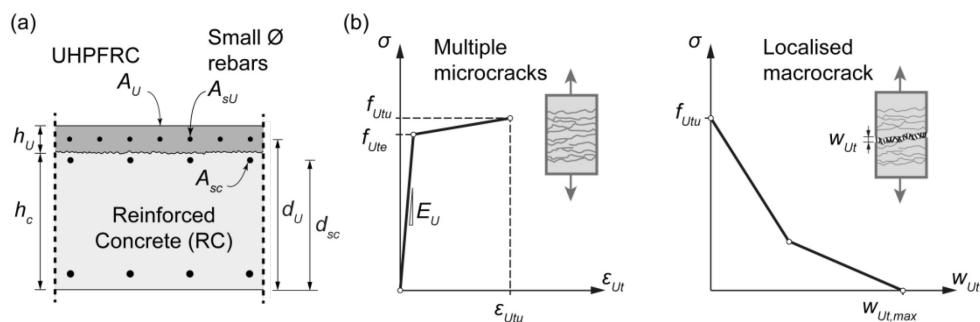


**Figure 1 (a) Typical RU-RC composite cross-section and notations [2.2]; (b) Constitutive law of UHPFRC [2.3]**

UHPFRC is an ultra-high strength material with a very compact cement-based matrix. The high dosage in short straight steel fibers provides this material with outstanding tensile properties and ductility: tensile strength higher than 7 MPa with strain hardening and softening behavior (Figure 1b) [2.3]. The addition of small diameter rebars to create an R-UHPFRC section improves the apparent UHPFRC tensile behavior by increasing the resistance and extending the strain hardening domain [2.4, 5].

The layer of R-UHPFRC is cast in place on the surface of the RC slab. The surface of the concrete must be adequately prepared prior to casting by high-pressure water jetting or sand blasting in order to provide sufficient roughness. This ensures that the composite section will have a monolithic behavior in bending.

One-way RU-RC composite members were tested to study their behavior under bending and shear. Four point bending tests were carried out on composite beams and showed that the layer of UHPFRC significantly increases the bending resistance [2.5]. Moreover, no notable interface cracking was observed between the UHPFRC layer and the RC section prior to failure [2.6]. It is thus supposed that the behavior of composite beams is monolithic when submitted to pure bending moments and design can be done based on the plane-sections hypothesis. RU-RC composite beams were also tested in a cantilever test setup where they were submitted to high shear forces combined with bending [2.7]. These tests showed that the layer of UHPFRC also increases the shear resistance and deformation capacity of a RC beam.

The main goal of this new experimental campaign is to extend the knowledge from one-way to two-way spanning RU-RC composite elements [2.8]. Focus is thus placed on the behavior of RC slabs with no shear reinforcement submitted to point forces with a layer of UHPFRC acting as a two-dimensional tensile reinforcement.

The tests were designed to study the contribution of the UHPFRC layer to punching shear resistance. The main parameter is the total amount of tensile reinforcement which was varied for each test in two ways: (1) variation of the UHPFRC layer thickness; (2) variation of the ratio of steel reinforcement in the UHPFRC layer; (3) specimen size.

No shear reinforcement was used and the ratio of reinforcement in the RC section was kept constant. The tests allowed studying deformation and cracking of the RC section and the UHPFRC layer and global rotation and displacements of the slab.

## **2 Background**

### **2.1 Punching shear resistance of RC slabs without transverse reinforcement**

In order to predict the resistance to punching shear of RU-RC composite slabs, mechanisms that govern the behavior of the RC section must be well understood. It will then be possible to study the influence of the UHPFRC layer on these mechanisms. Parameters that influence the punching shear resistance of a RC slab without transverse reinforcement are the thickness of the slab, the ratio of longitudinal reinforcement and the concrete compressive and tensile strengths.

Punching shear is due to a vertical force acting perpendicularly to the slab, such as the force due to a column. It creates high shear forces that are first carried through an inclined compression strut connecting the point force to the tensile reinforcement at an angle of  $25^\circ$  to  $30^\circ$ . While strains increase, the tensile strength of the concrete is reached and an inclined crack appears along this strut. This is normally observed at 50 to 70% of the punching shear resistance of the slab [2.9]. Stress can still be transferred across the crack due to residual tensile strength and aggregate interlock [2.1, 10, 11]. These mechanisms depend on the opening of the critical shear crack which is proportional to the rotation of the slab. Punching shear failure is sudden and followed by a drop in the resistance of the slab [2.12]. The failure surface has the shape of a truncated cone over the column. Delamination of the cover concrete is also observed.

Slabs with higher reinforcement ratios show higher punching shear resistance but smaller rotations and strains [2.10]. The failure happens before any or limited yielding of the steel reinforcement. Guandalini et al. [2.9] showed that size also has an effect on the punching shear resistance of slabs. Normalized punching shear resistance increases with decreasing slab thickness, but the deformation capacity decreases.

### **2.2 Strengthening methods**

Many methods to strengthen existing flat slabs have been developed to overcome deficient punching shear resistance: enlargement of the support area, post-installed shear

reinforcement, prestressing or increasing the amount of flexural reinforcement [2.13]. This last method can be conducted by casting on the top face of the slab a new layer of reinforced concrete linked to the existing section with shear connectors [2.14]. It is also possible to cast a layer of UHPFRC directly on the prepared existing concrete surface without any mechanical connectors as proposed in this paper or to add externally bonded reinforcements made of steel or fiber-reinforced polymers (FRP).

The use of FRP sheets to increase punching shear resistance has been studied by various authors [2.15-18]. The slabs with added reinforcement have a stiffer behavior. The FRP sheet also delays and controls the development of inclined cracking in the RC slab. As expected for a slab with added flexural reinforcement, the punching shear resistance of the slab reinforced with FRP is higher but smaller rotations at maximum resistance and no yielding of the steel or the external reinforcement is noticed.

### 2.3 Shear resistance of RU-RC composite beams

A test series on RU-RC composite beams submitted to combined bending and shear was realised in [2.7]. It showed that the RU-RC beams have a significantly higher stiffness than their RC reference beams alone and that the maximum resistance is increased by up to 2.77 times. These tests also demonstrated that, if designed adequately, an R-UHPFRC layer can prevent the shear failure expected for the RC beam alone.

If a flexure-shear failure occurs in a composite beam, it is first due to a vertical bending crack in the RC section that develops diagonally towards the support. The widening of this critical crack then creates a prying action on the UHPFRC layer which induces softening of the concrete volume below the interface, starting at the mouth of the crack (Figure 2). This Near Interface Cracking (NIC) leads to a new failure mode [2.7]. Over the NIC zone, the R-UHPFRC layer resists to the prying action by out-of-plane bending in double curvature. The flexure-shear failure finally happens in a sudden manner due to the crushing of the concrete ahead of the inclined crack. It is followed by a drop in the resistance of the beam. Nevertheless, most of the beams that failed in flexure-shear during this test series still reached their maximum bending resistance.

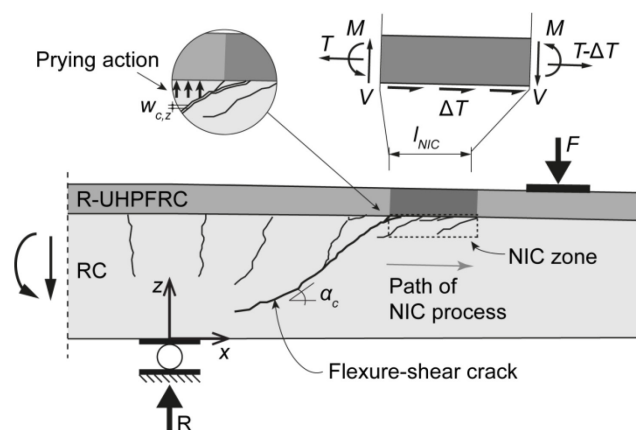


**Figure 2 Flexure-shear failure of a RU-RC composite beam [2.7]**

Since the R-UHPFRC layer increases the mechanical reinforcement ratio of the beam, it would be expected that the flexure-shear failure happens at smaller deflections than the

reference RC beam. However, as a result of the creation of the NIC zone, the deformation and rotation capacity of the composite beam is increased and the deflection at ultimate limit state is between 90 and 100% of the reference beam.

The UHPFRC layer contributes in three ways to shear resistance of a composite beam. First, it hinders the widening of the critical shear crack. Second, it resists to the prying action by bending out-of-plane. Third, the NIC zone modifies the stress fields in the beam and reduces the intensity of the shear stresses that must be carried across the critical shear crack. It is expected that the layer of UHPFRC will contribute to the punching shear resistance of two-way spanning slabs with resisting mechanism similar to those observed for one-way shear resistance (Figure 2).

### 3 Experimental investigations

#### 3.1 Test specimens

A total of six square composite slabs were tested in punching over a column with a square cross section. Two different specimen sizes were used. All presented slabs had orthogonal reinforcement and a standard longitudinal reinforcement ratio in the RC section of 0.75%. Table 1 gives the detailed parameters for each specimen.

In a first series called SAMD and tested by Wuest [2.19], two composite slabs of 200-mm total thickness and 2000-mm side lengths were tested. The thickness of the UHPFRC layer for the two SAMD slabs was respectively 50 and 23 mm, the thicker one being reinforced with high strength steel.

For the second series called PBM, four larger composite slabs were fabricated using similar dimensions as used by Guidotti [2.20] for tests on RC slabs: 260-mm total thickness and 3000-mm side lengths. Three of the composite PBM slabs had a 50-mm thick layer of UHPFRC with a varying amount of reinforcement. The fourth slab had a thinner plain layer of only 25-mm thick.

For a composite slab, the effective flexural depth  $d_{eff}$  and total mechanical reinforcement ratio  $\omega_{tot}$  are calculated with equations 1 and 2 respectively where  $i$  stands for each layer of tensile reinforcement. As seen in Figure 1, the tensile reinforcement of a composite section includes the top steel rebars in the RC section (subscript  $sc$ ), the layer of UHPFRC (subscript  $U$ ) and the steel rebars in the UHPFRC layer (subscript  $sU$ ).

$$d_{eff} = \frac{\sum d_i A_i f_i}{\sum A_i f_i} \quad (1)$$

$$\omega_{tot} = \sum \omega_i = \sum \frac{A_i f_i}{A_c f_c} \quad (2)$$

For every type of tensile reinforcement,  $d_i$  is the distance between the bottom compression face and the centroid of the layer of reinforcement (see notations in Figure 1).  $A_i$  and  $f_i$  are the area per unit length and tensile strength ( $f_y$  for rebars and  $f_{Utu}$  for UHPFRC).  $A_c$  and  $f_c$  are the area per unit length and compressive strength of concrete. All material strengths are given in Table 2.

**Table 1 Main parameters of test series**

Slab	Geometry				Steel in RC		Steel in UHPFRC		Effective reinf.	
	$B$ [mm]	$c$ [mm]	$h_c$ [mm]	$h_U$ [mm]	$d_{sc}$ [mm]	Layout [mm]	Type	Layout [mm]	$d_{eff}$ [mm]	$\omega_{tot}$ [%]
SAMD1*	2000	200	150	50	136	Ø14@150	High strength	Ø10@150	162	20.7
SAMD2*			172	23			--			
PBM1	3000	260	210	50	180	Ø16@150	--	Ø8@150	209	14.5
PBM2							Standard			
PBM3							High strength			
PBM4							--			
PG19*							Ø16@125			
PG20*	Ø20@100	--	--	210	13.4					

\*Tested by [2.19]

\* Tested by [2.20]

All presented slabs also had layers of compression reinforcement at the bottom of the RC sections, with spacing as the top reinforcement. This reinforcement was made of Ø14-mm bars for slabs SAMD and of Ø10-mm for slabs PBM and PG19 and 20, the reference RC slabs.

The results of the PBM series were compared to chosen reference RC specimens PG19 and 20 tested by Guidotti [2.20]. All PBM slabs had an effective flexural depth  $d_{eff}$  close to 210 mm which is the flexural depth  $d_{sc}$  of PG19 and 20. These two slabs are part of a larger database of punching tests on RC slabs. Many slabs with the same dimensions, with or without shear reinforcement and with varying amount of flexural reinforcement have been tested under punching shear by various authors [2.9, 20-22]. Slabs PG19 and 20 have been chosen as being representative. Slab PG19 is the main reference slab because, as the RC sections of the composite slabs, it had a reinforcement ratio of 0.75%. It also had the lowest mechanical reinforcement ratio  $\omega_{tot}$  of all presented slabs. Slab PG20 had a higher reinforcement ratio of 1.50%. It is interesting to compare its behavior to the case of composite slabs as it also had a higher mechanical reinforcement ratio, similar to the one of composite slab PBM4, 13.4% and 12.3% respectively.

### 3.2 Material properties

The RC section of all specimens was fabricated with conventional concrete with a maximum aggregate diameter of 16 mm. The age of the concrete when the specimens were tested is given in Table 2 as well as the average concrete properties at 28 days obtained from standardized tests on three cylinders.

**Table 2 Tested material properties**

<b>Concrete</b>					
Slab	Age at testing [days]	$E_{cm,28}$ [GPa]	$f_{cm,28}$ [MPa]		
SAMD1*	192	33.3	51.4		
SAMD2*	176	34.2	46.7		
PBM1	114	25.5	32.6		
PBM2	101	27.7	36		
PBM3	88	25.5	32.3		
PBM4	76				
PG19 <sup>x</sup>	20	32.7	46.2		
PG20 <sup>x</sup>	33	33.9	51.7		
<b>UHPFRC</b>					
Type	Elastic		Strain Hardening		
	$E_{Um,28}$ [GPa]	$f_{Ute}$ [MPa]	$\epsilon_{Utu}$ [‰]	$f_{Utu}$ [MPa]	
CM22*	47.2	11.2	1.4	13.3	
S3-13	44.5	6.6	1.2	7.5	
<b>Steel</b>					
Type	$\emptyset$ [mm]	$f_{sy}$ [MPa]	$f_{su}$ [MPa]	$f_{su}/f_{sy}$	$\epsilon_{su}$ [%]
<b>High strength</b>	8	772	905	1.17	2.9
	10*	937	959	1.02	Not measured
	8	532	606	1.14	5.7
<b>Standard</b>	10	518	616	1.19	6.7
	14*	526	607	1.15	Not measured
	16	546	621	1.13	11.9
	20 <sup>x</sup>	551	659	1.20	9.4

\*Material properties obtained from [2.19]

<sup>x</sup> Material properties obtained from [2.20]

The UHPFRC layer of SAMD series was made with mix CM22 which contained 10-mm long straight steel fibres and steel wool. This CM22 mix is part of the CEMTECmultiscale© family of UHPFRCs developed by Rossi [2.23, 24] and adapted for rehabilitation. The tensile properties of UHPFRC CM22 given in Table 2 are the average of three tests on individually cast specimens [2.19].

For the PBM series, the UHPFRC layer was fabricated with an industrial premix named S3-13 containing 13-mm long straight steel fibers. This material was submitted to an extensive



characterization campaign. To obtain its tensile properties, 16 dog-bone shaped specimens were cut out from four square plates of 50-mm thick and 1000-mm sides. This fabrication method allowed capturing the variability of tensile behavior in a plate similar to the layers cast on the composite slabs. The tensile properties of UHPFRC S3-13 given in Table 1 are the average of 11 tests on these dog-bone specimens.

The UHPFRC layers were cast on a washed concrete surface with exposed aggregates. The layer was applied from one side of the slab progressing towards the other. It is reasonable to assume that this procedure slightly oriented the fibers in the casting direction.

The RC section of all slabs was fabricated using standard hot rolled steel rebars with nominal yield strength of 500 MPa. The same type of steel was used in the UHPFRC layer of slab PBM2. For slabs SAMD1 and PBM3 however, high strength steel with yield strength higher than 750 MPa was used in the UHPFRC layer. The steel properties in Table 2 are the average values from standardized tensile tests on three random samples.

### 3.3 Test setup and procedure

All specimens were tested in a 9-point system (Figure 3), with the column in the center and 8 loading points located on a circle around it. The tests were displacement controlled at constant rates using hydraulic systems. Loading was stopped at planned force levels during the tests in order to make some observations and manual measurements.

The PBM slabs were tested in the setup developed for RC slabs in [2.9] and also used in [2.20] for the RC slabs PG19 and 20 (Figure 3a). The layer of UHPFRC was placed on top and the concrete face was resting on a square 260-mm side length column. The force was applied downwards in 8 points with a system of rods and hydraulic jacks placed below the laboratory strong floor. The eight steel loading plates were squares of 200-mm side length. These loading points were placed on a circle of 1500-mm radius. For these slabs, the self-weight and the weight of the test setup was added to the measured force.

The SAMD slabs were tested upside down, with the UHPFRC layer at the bottom (Figure 3b). Slabs were resting on eight rollers with square steel plates of 100-mm side length. These supports were placed on a circle of 1000-mm radius. The force was applied downwards with a hydraulic jack on the top concrete face. The square loading plate had 200-mm side length.

In the following, and for simplicity, all slabs will be described as if they had been tested in a normal position for a composite slab, with the UHPFRC layer on top.

Continuous measurements were made during the tests. Load cells were placed at the hydraulic jacks to monitor the acting force. Strain gauges with 100-mm base lengths were placed on the UHPFRC and concrete faces. With reference to the laboratory strong floor, vertical deflections were measured at various points from the top and bottom sides of the slabs.

For the PBM series, rotation was recorded using inclinometers arranged on a 1380-mm radius circle (Figure 3a). Local thickness variation in the slab was also measured. It corresponds to the vertical relative displacements of the top and bottom face of the slab. The device used to record the change in thickness has been described in [2.21, 22].

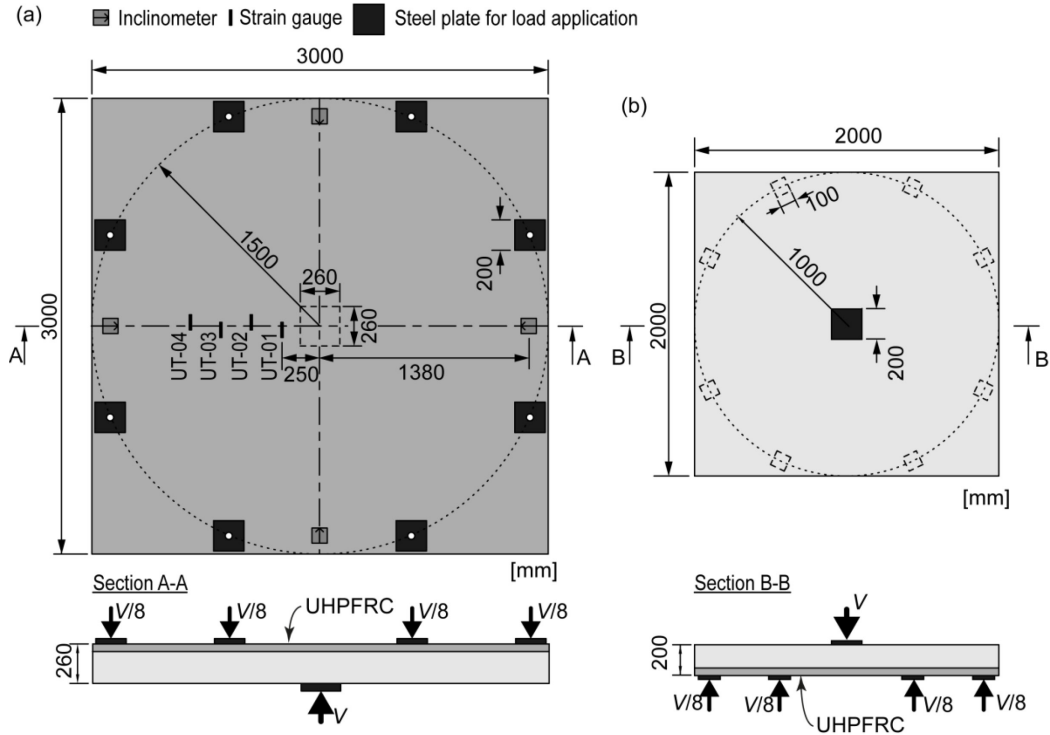


Figure 3 Schematic test setup: (a) PBM series; (b) SAMD series [2.19]

## 4 Experimental results and discussion

### 4.1 Force-rotation response and failure mode

All normalized force-rotation curves are given in Figure 4. The curves are normalized as proposed in [2.10] to neutralize the effects of various concrete compressive strengths and specimen and column sizes. In the case of the SAMD slabs, the rotations were not measured. They were approximated using the deflection measurements made below the loading point and supposing that the center of rotation is at the column face.

All slabs failed in punching mode. The failure is defined by the instant when the resistance drops suddenly after the maximum force is recorded. The plots in Figure 4 show the slab response up to the maximal resistance before this resistance drop. The last reading before this drop is represented by a circle. The small drops in the force-rotation curves are due to the planned pauses in the tests. PBM3 was partially unloaded twice and SAMD1 was completely unloaded twice. The slabs were unloaded to record any stiffness change.

Tests on slabs PBM1 and 2 and PG19 and 20 were ended right after the drop in resistance due to punching shear failure. In the other cases, the displacement increase was continued after the punching shear failure in order to record the post-peak behavior. This post-peak behavior will be discussed later in this paper.

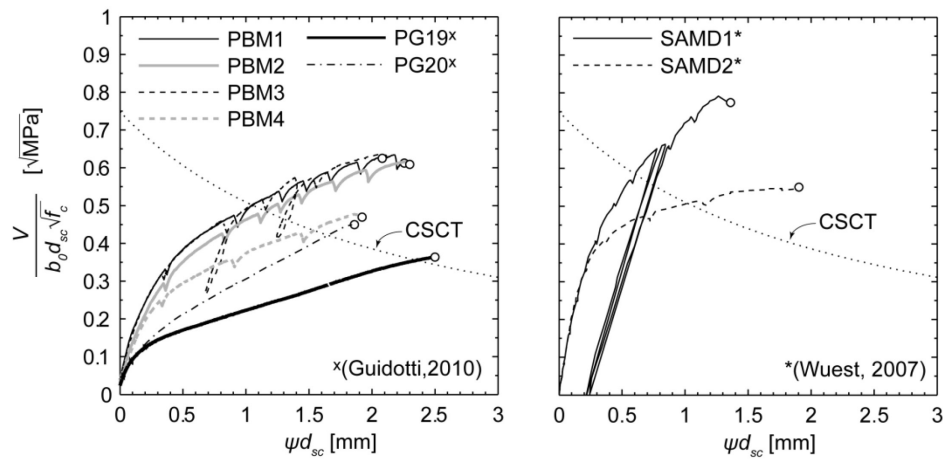

**Figure 4 Normalized force-rotation curves**

Table 3 gives an overview of the main results for each slab: the maximum resistance ( $V_R$ ), the rotation and deflection at  $V_R$  ( $\psi_R$  and  $w_R$ ), the residual resistance ( $V_{res}$ ) after the resistance drop and the minimum angle of the punching cone ( $\alpha_c$ ) measured on the cracking pattern (Figure 5).

**Table 3 Main test results**

Slab	$\alpha_c$ [°]	$V_R$ [kN]	$V_R/V_{PG19}$ [-]	Normalised ratio $V_{Rnom}/V_{PG19nom}$ [-]	$\psi_R$ [‰]	$w_R$ [mm]	$V_{res}$ [kN]	$V_{res}/V_R$ [-]
SAMD1*	20	971	--	--	9.6 <sup>y</sup>	8.6	480	0.49
SAMD2*	23	675	--	--	13.4 <sup>y</sup>	12.1	236	0.35
PBM1	24	1089	1.27	1.74	11.9	14.0	335	0.31
PBM2	28	1223	1.42	1.69	12.2	14.8	365	0.30
PBM3	21	1186	1.38	1.75	11.3	13.2	308	0.26
PBM4	29	1023	1.19	1.31	9.1	10.2	249	0.24
PG19 <sup>x</sup>	22	860	1.00	1.00	12.1	13.7	--	--
PG20 <sup>x</sup>	25	1094	1.27	1.24	9.2	10.9	--	--

<sup>y</sup> Calculated

\*Tested by [2.19]

<sup>x</sup> Tested by [2.20]

The ratio between the normalized maximum resistance of slabs PBM and the reference slab PG19 (Table 3) shows that the increase in resistance is between 69% and 75 % for a slab with a layer of 50 mm of UHPFRC (PBM1-3) while the increase is of 31% for a 25-mm layer (PBM4). In all cases, this increase in resistance is significant.

Although it is expected that the addition of tensile reinforcement would reduce the rotation capacity while increasing the punching shear resistance of the slab, this was not observed for PBM1-3, which all had a 50-mm layer of UHPFRC. These three slabs failed at rotations close to what was measured for PG19, between 11.3‰ and 12.2‰.

The composite slabs PBM1-3 all had approximately the same normalized resistance which indicates that failure occurred before yielding of the tensile reinforcement in the UHPFRC layer of slabs PBM2 and 3. The use of an R-UHPFRC layer for the specific case of punching shear reinforcement is thus not necessary, as a plain layer of UHPFRC with the same thickness brings the same gains in resistance and deformability.

In the case of slab PBM4 which had a UHPFRC layer of 25-mm thick only, the resistance was also increased, but the rotation reduced compared to PG19. Slab PBM4 had a maximum resistance and rotation closer to what was measured for RC slab PG20, which has a higher reinforcement ratio than PG19. However, the force-rotation curves (Figure 4) show that the composite slab PBM4 has a higher rigidity than slab PG20.

Finally, SAMD1, with a 50-mm layer of UHPFRC reinforced with a large amount of high strength steel, failed at a measured deflection lower than what was measured for SAMD2 which was reinforced with only a 25-mm layer of UHPFRC.

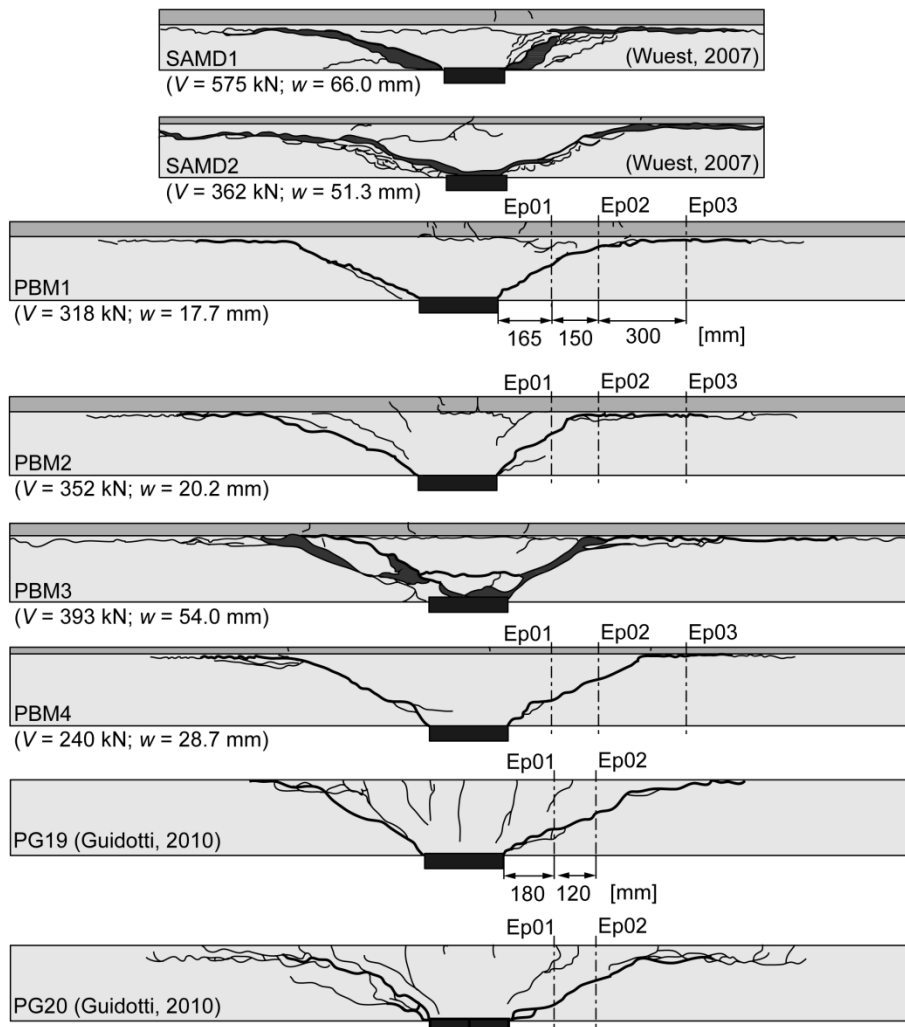


**Figure 5 Fully developed cracking pattern on cut sections of the slabs at the end of the test and position of the thickness measurements**

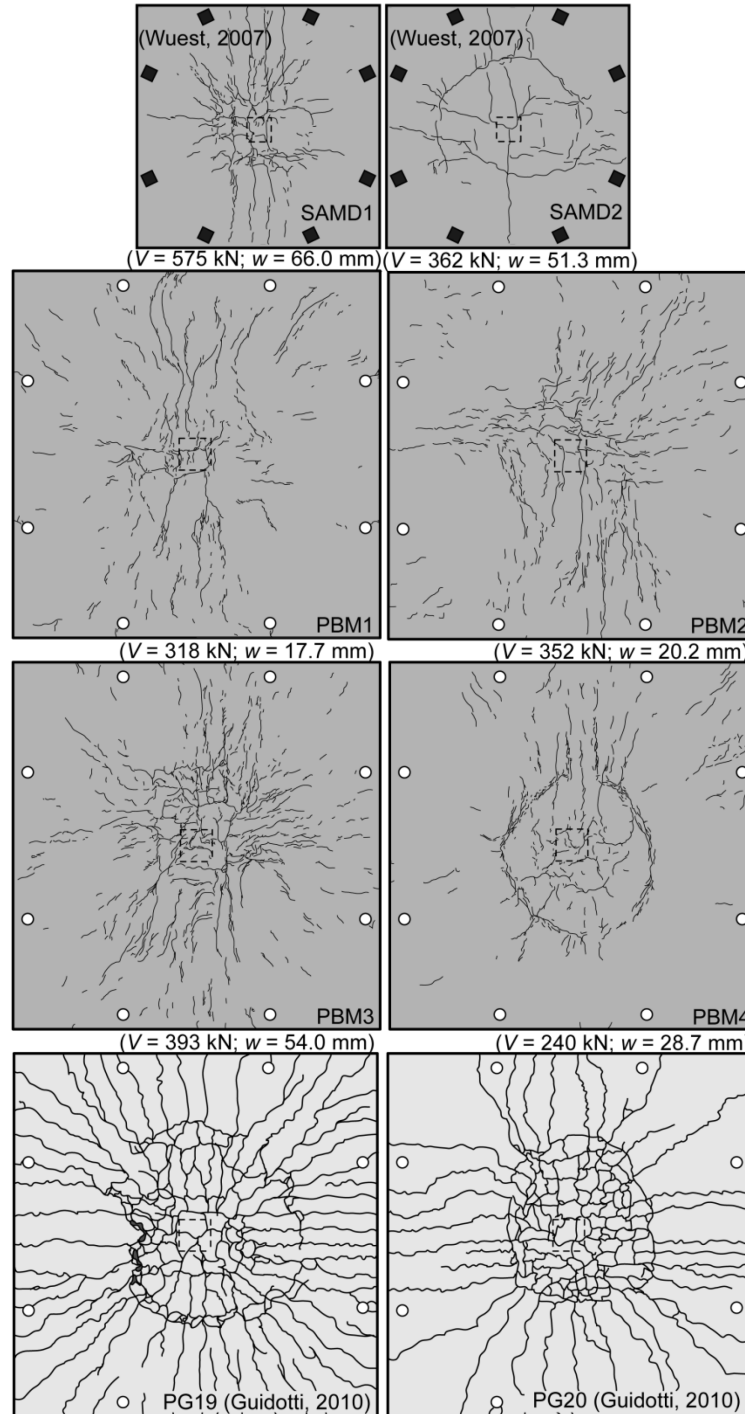


Figure 6 Fully developed cracking pattern of the top tensile faces at the end of the tests

#### 4.2 Cracking patterns

The slabs were cut on their central axis after the tests were ended and the internal cracking patterns could then be observed on the cut sections (Figure 5). Figure 5 and Figure 6 show the fully developed cracking patterns of, respectively, the cut face and the top tensile surface. The figures also indicate, for the composite slabs, at which load and displacement the test was ended. Because all tests were stopped at different levels of deformation, the patterns

show differences in crack opening and extent of cracking. The cracking patterns seen for slabs PBM1 and 2 and PG19 and 20 reflect the cracking state right after the resistance drop due to the punching shear failure.

All punching cones observed on the cut slabs in Figure 5, including the reference RC slabs PG19 and 20, have a similar shape with an angle  $\alpha$  between  $20^\circ$  and  $30^\circ$  with respect to the horizontal (Table 3). The layer of UHPFRC does not appear to significantly modify the inclination of the critical shear crack in the lower part of the concrete. In the composite slabs, this main critical diagonal crack rotates just below the interface between the concrete and the UHPFRC layer, at the level of the upper rebar layer in the concrete. The failure of the concrete and not of the clear interface proves that the bond between the UHPFRC layer and the RC section is sufficient.

No significant vertical bending cracking is observed over the column in the RC sections of the composite slabs contrary to PG19 (Figure 5). However, between one and three vertical cracks are visible in the UHPFRC, developing radially (Figure 6), showing that the UHPFRC layer mainly carries the bending efforts in the tangential direction. Over the column, these cracks have a typical crack mouth opening at maximum resistance of 0.5 to 0.7 mm for slabs PBM1-3, as measured by the strain gauges of 100-mm base length. The UHPFRC is thus softening in this location, meaning that the measured strains are higher than the strain at maximum tensile strength ( $\varepsilon_{Um}$ ). These vertical cracks in the UHPFRC layer are accompanied by limited horizontal cracking in the concrete, near the interface.

### 4.3 Deflections, deformations and strains

#### 4.3.1 Thickness variation and UHPFRC cracking

The thickness variation measurements give indications on how the cracking developed inside the slab. The exact locations of those measurements are shown in Figure 5. Two measurements were taken close to the column (Ep01 and Ep02). These measurements showed that internal cracking for composite slabs started at 50% to 70% of the maximum punching shear force  $V_R$  (Figure 7), which is similar to what had been previously observed for RC slabs [2,9, 11]. Yet, it is clear in Figure 7 that, up to maximum resistance, the layer of UHPFRC of the composite slab allowed the cracking in the concrete to develop much more than what was observed for the RC slab PG19. At maximum resistance, for all the composite slabs, the thickness of the slabs had increased by 1 to 1.5 mm (measured near the column by Ep01). For PG19, this increase was 3 to 5 times less. PBM4, which had a thinner layer of 25 mm of UHPFRC, allowed as much cracking development inside the slab as the slabs with a layer of 50 mm.

The opening of radial cracks on the top surface of the UHPFRC layer was captured by the strain gauges. Strain gauge UT01 (Figure 3) was placed at 250 mm from the center of the slab and measured radial displacements over a 100-mm base length. The measurements of UT01 showed that radial cracks also started localizing approximately at the same instant as the internal cracking started developing (Figure 7). A crack has localized when the measured strain is higher than the strain at the maximum tensile strength of the UHPFRC ( $\varepsilon_{Um}$ ), meaning that the material has started softening at the measured location.

For the composite slabs PBM, a third measurement (Ep03) was taken further away from the column face. At this location, cracking in the concrete near the interface with the UHPFRC layer can be observed in the fully developed crack pattern (Figure 5). However, no change in the thickness was recorded at this location prior to the punching shear failure which reveals that NIC had not yet propagated that far. NIC observed on the cut sections (Figure 5) thus developed after the punching shear failure when the relative displacement between the punching cone and the outside part of the slab became more important. The layer of UHPFRC could not be punched by the top of the concrete cone and the critical shear crack in the concrete had to rotate to become parallel to the interface.

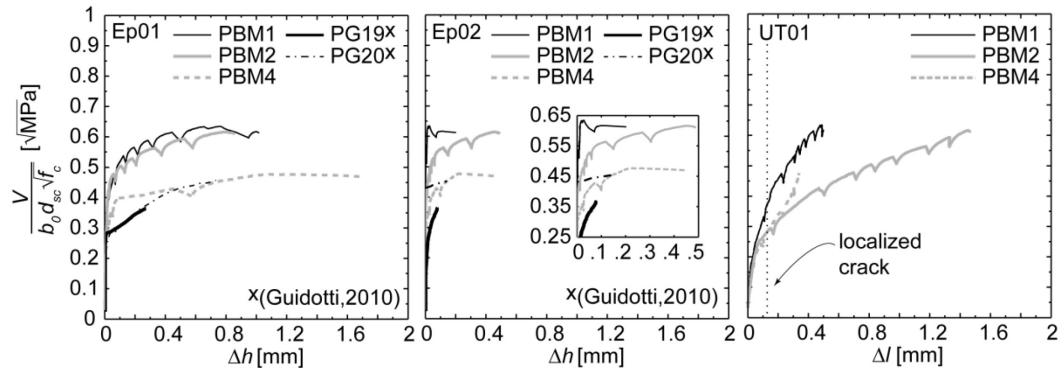


**Figure 7 Change of thickness of the slab in two locations (Ep01 and 02) and radial displacements of the UHPFRC layer (UT01) as a function of the normalized force**

#### 4.3.2 Slab deformation

The top and bottom deformed shape of composite slab PBM1 and reference RC slab PG19 are compared in Figure 8. The two slabs had approximately the same maximum deflection at maximum resistance, which is consistent with what was observed for rotations.

In both cases, the bottom face of the slab rotated around the column face with an increase in the rate of deflections after 60% of the maximum force  $V_R$ , which corresponds to the start of the development of internal cracking (Figure 7). For the RC slab PG19, this increase in the rate of deflections also appeared on the top face at a distance from the column face equal to the flexural depth of the slab ( $d_{sc}$ ). This reflects the rigid body movement of the sector located outside the critical shear crack necessary to activate shear resistance once the concrete is cracked [2.20].

This rigid body movement was also observed in the composite slab PBM1 after internal cracking started to develop but it was accompanied by an upward deflection of the UHPFRC layer. Over the column and up to a distance of  $d_{sc}$  from the column face, the top surface lifted up instead of stabilizing at a constant position as for the RC slab.

This upward movement of the top surface in the composite slab is also illustrated by the plots in Figure 8b showing together, as a function of the normalized force, the top deflections (IS3) and bottom deflections (II3) both located at the same horizontal distance from the column face. The difference between these two measurements is illustrated by the shaded area on the graphs. For both slabs, top and bottom face had the same rate of deflection up to 50 to 70% of the maximum force  $V_R$  when, as showed before, internal

cracking started to develop inside the RC section. Then, in the case of PG19, the rate of deflection of the top surface (IS3) reduced when compared to what was measured on the bottom face (II3). For the composite slab PBM1, the rate of deflection measured on top was reduced and then inverted. From 88% of  $V_R$  the top face of PBM1 had an upward movement, while the bottom face continued its downward movement. At maximum resistance, the difference between top and bottom surface was 1.5 mm. A part of this difference can be attributed to the thickness variation due to the development of internal cracking in the slab but this cannot be more than 0.7 mm for PBM1 (Figure 7). The rest of the difference corresponds to NIC and an upward deflection of the layer.

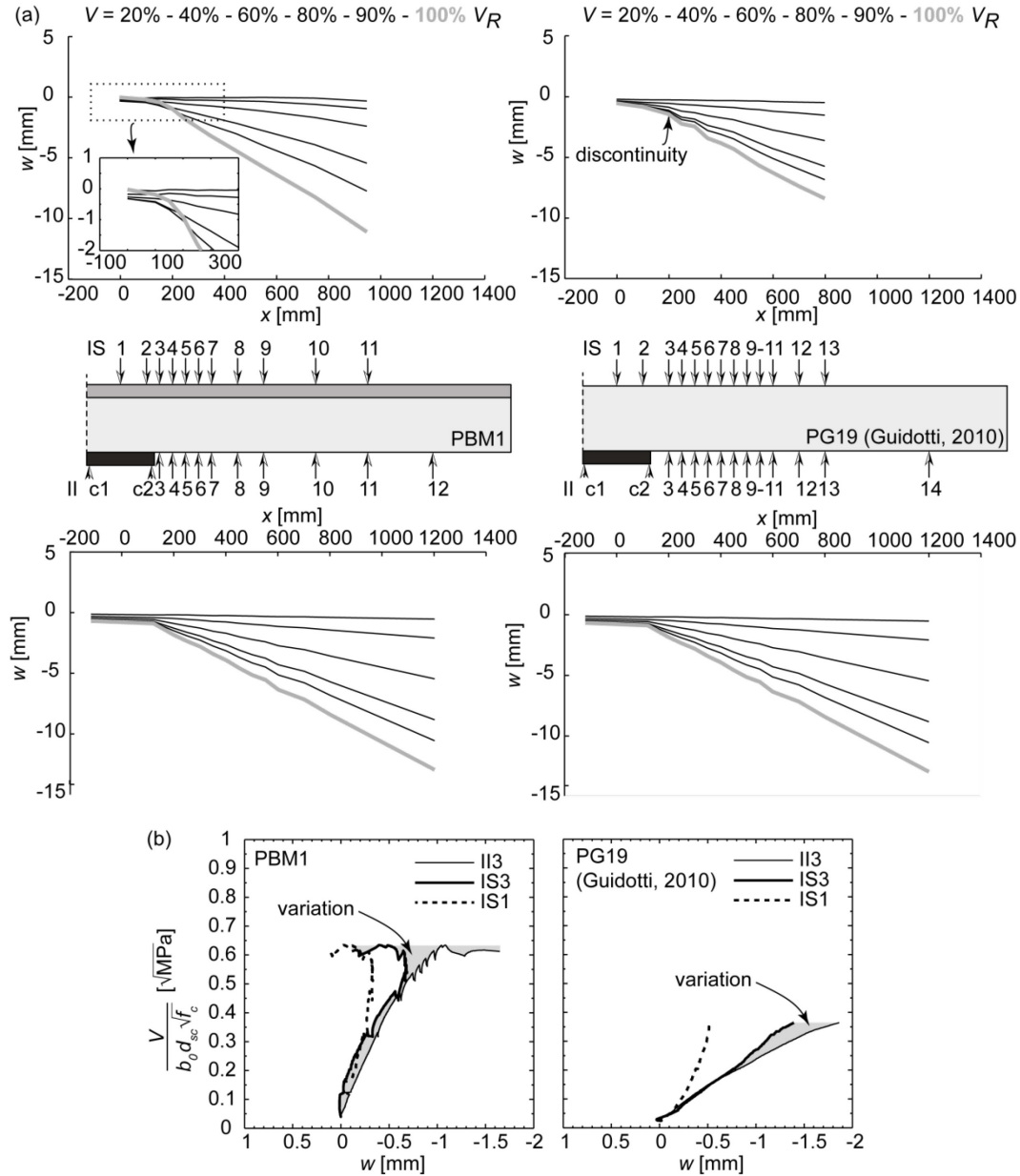


Figure 8 Deflections of PBM1 and PG19: (a) top and bottom deformed shapes; (b) central deflections as a function of the normalized force



The deflection measured on the top surface directly over the column (IS1) also reflects the upward movement, as seen in Figure 8b. If the settlement of the column support plate is taken into account (measured by  $\Pi c1$  and  $c2$ , in Figure 8), the upward deflection of the top face of the slab over the column was of 0.8 mm at maximum resistance.

### 4.3.3 Shear deformation

Shear deformation at the column face  $\Delta w$ , illustrated in Figure 9, is calculated with Equation 3 using the deflection measurements made under the slab [2.21]. It is the relative displacement between the cone and the slab sector located outside the critical shear crack.

$$\Delta w = (w_{12} - w_{c2}) - \frac{(w_{12} - w_3)}{x_0} \cdot x_1 \tag{3}$$

Shear deformation as a function of the normalized force is plotted in Figure 9. The RC slab PG19 had very limited shear deformation prior to maximum resistance, lower than 0.1 mm. In the case of the composite slabs, shear deformation was 3 to 8 times higher depending on the thickness of the layer of UHPFRC.

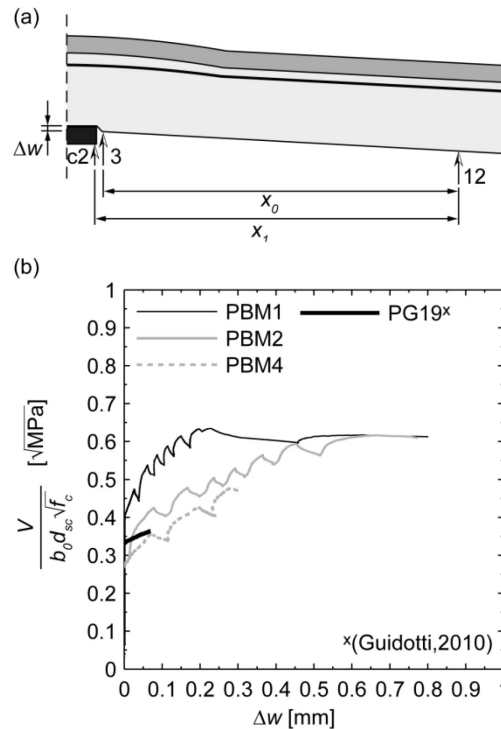


**Figure 9 Shear deformation: (a) definition [2.21]; (b) measurements at column face as a function of the normalized force for selected specimen**

### 4.3.4 Concrete strains

Strains on the concrete bottom face of the slab were measured tangentially at 100 mm from the column for slabs PBM and PG19 and 20. For the RC slabs PG19 and 20, compressive strains reached values of 2‰ just prior to the punching shear failure. For the composite slabs with a 50-mm layer of UHPFRC (PBM1-3), the measured values were two times

bigger, reaching compressive strains of 4%. This is just another demonstration of the increase in deformability of the RC section provided by the addition of the UHPFRC layer.

#### 4.4 Contribution of the UHPFRC layer to punching shear resistance

From the previous observations made with the experimental results, it is clear that the layer of UHPFRC increases rigidity and maximum punching shear resistance of a RC slab while keeping the rotation capacity equivalent. The UHPFRC layer primarily contributes to the bending resistance of the composite slabs by carrying tensile stress in tangential directions. Cracks are observed on the surface of the layer, progressing radially from the center of the slab. The RC section cannot follow the upward deflection of the UHPFRC layer due to these bending efforts and limited NIC develops over the column to ensure geometrical compatibility.

Very limited NIC is also assumed to develop in the concrete at the mouth of the critical shear crack. This inclined critical crack cannot propagate through the layer of UHPFRC. Instead, bending efforts are introduced in the UHPFRC layer by the relative movement between the two lips of the critical shear crack, creating this second zone of NIC. Figure 10 illustrates the assumed cracking state in the composite slab at maximum resistance.

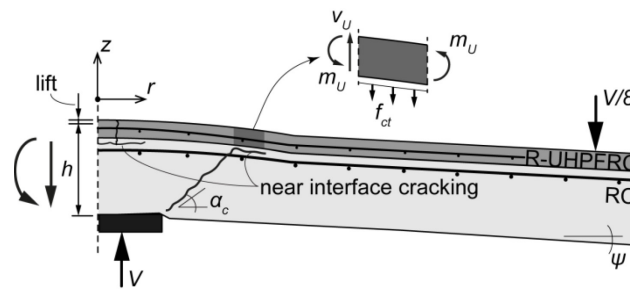


**Figure 10 Bending of the UHPFRC layer and shear deformations at column face**

Thus, the layer of UHPFRC carries part of the shear force by bending. By doing so, it allows more deformation to take place in the RC section before punching shear failure. This has been demonstrated by various measurements taken around the column: thickness variation, which reflects the development of cracking in the RC section, shear deformation at the column face and compressive strain at the soffit of the slab. This increased deformation of the RC section explains why the rotation capacity of the composite slab is larger than what is expected for a slab with an added flexural reinforcement. The development of cracking and the opening of the critical crack also have an influence on the punching shear resistance of the RC section.

In the case of slab SAMD1, the layer of UHPFRC was heavily reinforced. This made the layer stiffer and reduced its deformation capacity in bending. As a result, the global rotation of this slab was lower at maximum resistance than what was measured for SAMD2 with a thinner layer of UHPFRC.

A thinner layer of 25 mm of UHPFRC can also increase the maximum resistance of a slab by over 30%, depending on the ratio between the thickness of the UHPFRC layer and the thickness of the RC section. It will also carry shear by bending and allow more deformation to take place in the RC section. However, the bending resistance of the layer being smaller,

less shear can be carried and the failure will finally happen for a smaller rotation than for the RC reference slab.

#### 4.5 Post-peak remaining resistance

The residual resistance of the composite slabs right after the punching shear failure was between 49 and 24% of the maximum resistance (Table 3). It corresponds to the carrying capacity of the UHPFRC layer and the top reinforcement in the RC section. These elements provide shear support by bending of the UHPFRC layer and dowel action of the rebars. SAMD1 has a larger post-peak resistance due to the high amount of reinforcement in the UHPFRC layer.

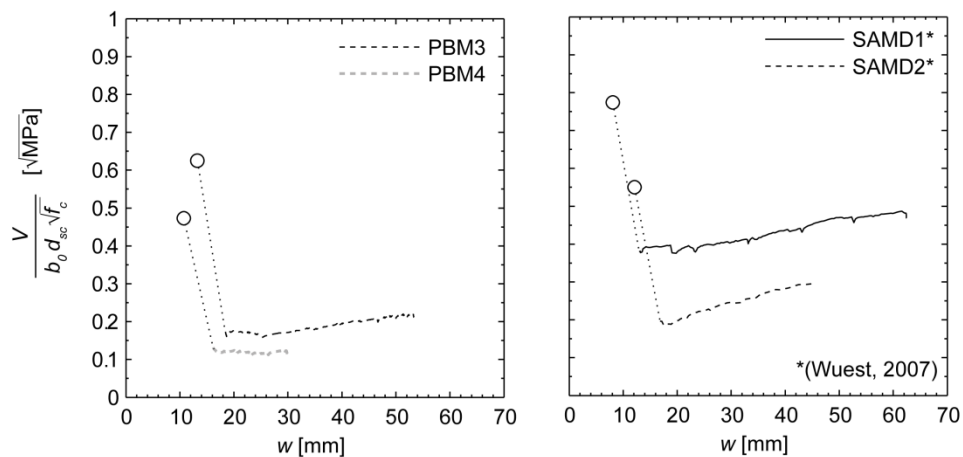


**Figure 11 Post-peak behaviour of selected slabs as a function of the normalized force**

The post-peak behavior was only measured for selected slabs and is shown in Figure 11. In the case of slabs PBM, the deflection measurements in post-peak is recorded with II12 located at 1200 mm from the center of the slab (see position in Figure 8). For slabs SAMD, the deflection is measured right below the loading point, in the center of the slab.

As was shown in [2.25], post-peak resistance due to flexural reinforcement, such as the UHPFRC layer and the top tensile rebars, is activated right after punching shear failure and remains stable when the displacement is increased. The increase in post-peak resistance in Figure 11 is due to the bottom compression rebars passing above the column, as also observed by the aforementioned work and in [2.26]. Due to this, when the tests were ended, post-peak resistance had reached values up to 60% of the maximum resistance.

NIC in the concrete also continues progressing in the post-peak regime as the relative displacement between the punching cone and the outside sector of the slab increases. This horizontal cracking is expected to stop in the regions where clamping is provided such as support areas or at the point of zero moments in the case of a continuous slab.

This residual post-peak resistance is not of interest for resistance based design; however it enhances the robustness of structures by avoiding progressive collapse of flat slabs [2.25, 26].

## 5 Comparison with resistance models for RC Slabs

### 5.1 Overview

In the following, resistance models for RC slabs are used to emphasize the contribution of the UHPFRC layer to the punching shear resistance of a RC section. The yield-line method is used to calculate the bending resistance and the critical shear crack theory (CSCT) [2.10] is used to calculate the punching shear resistance of the RC section of the composite slabs.

### 5.2 Yield-line method

The bending resistance ( $V_{flex}$ ) of each slab, given in Table 4, is estimated using the yield-line method, as was proposed in [2.9]. As expected, punching shear failure always happens before the slab reaches its maximum bending resistance. For the slabs with more reinforcement, such as the composite slabs with a 50-mm layer (SAMD1, PBM1-3), the punching shear failure happened at forces between 56% and 66% of the estimated bending resistance, close to what is calculated for RC slab PG20. The composite slabs with only a 25-mm layer of UHPFRC (SAMD2 and PBM2) reached a higher ratio of their respective bending resistance, between 72 and 85% of  $V_{flex}$ , which is similar to what is observed for the reference RC slab PG19.

**Table 4 Comparison to flexural capacity**

Slab	$V_R$ [kN]	$\psi_R$ [%]	$V_{flex}$ [kN]	$V_R/V_{flex}$ [-]	$V_{csct}$ [kN]	$V_R/V_{csct}$ [-]	$\psi_{csct}$ [%]
SAMD1*	971	9.6 <sup>y</sup>	1597	0.61	454	2.14	16.1
SAMD2*	675	13.4 <sup>y</sup>	798	0.85	448	1.51	16.6
PBM1	1089	11.9	1654	0.66	644	1.69	11.3
PBM2	1223	12.2	1948	0.63	701	1.74	12.7
PBM3	1186	11.3	2099	0.56	662	1.79	12.8
PBM4	1023	9.1	1417	0.72	771	1.33	11.0
PG19 <sup>x</sup>	860	12.1	1196	0.72	805	1.07	12.4
PG20 <sup>x</sup>	1094	9.2	2225	0.49	1076	1.02	7.3

<sup>y</sup> Calculated

\*Tested by [2.19]

<sup>x</sup> Tested by [2.20]

### 5.3 Critical shear crack theory

The resistance to punching shear of the RC section of each composite slab was estimated using the CSCT proposed in [2.10]. As seen in Table 4, for a 50-mm UHPFRC layer, the resistance of the composite slabs was at least 69% higher than the calculated resistance of the RC section alone using the following analytical expression [2.10]:

$$\frac{V_{csct}}{b_0 d_{sc} \sqrt{f_c}} = \frac{3/4}{1 + 15 \frac{\psi_{csct} d_{sc}}{d_{g0} + d_g}} \quad (4)$$

Since the layers of UHPFRC are kept thin relatively to the concrete thickness, it can be supposed that a major part of the shear stress is carried by the RC section, as proposed in [2.7] for composite beams. The punching shear resistance of the RC section depends on its deformation which can be measured by its rotation, as proposed by the CSCT. The layer of UHPFRC, as was shown, allows the RC section to withstand higher deformation before failing.

Existing models to calculate the punching shear resistance of a RC slab that account for the deformation of the slab, such as the CSCT, can thus be used to predict the concrete contribution to the resistance of a composite slab. The failure criterion as proposed by the CSCT is plotted with the force-rotation curves, in Figure 4. It intersects the curves at forces over 75% and over 90% of  $V_R$  for a 50-mm and 25-mm layer of UHPFRC respectively. The resistance beyond the criterion is due to the contribution of the UHPFRC.

## 6 Conclusions

The following conclusions can be drawn on the basis of the experimental investigation presented herein:

1. The layer of UHPFRC increases the normalized punching shear resistance of the RC section by at least 69% for a layer of 50 mm. At maximum resistance, the rotation capacity of the composite slab is comparable to that of the reference RC slab.
2. The use of reinforcement in the UHPFRC layer does not have an important influence on the resistance or deformation of the composite slab because punching shear failure happens before yielding of the reinforcement in the layer. Yet, it could significantly make a difference in the bending resistance and should be considered in the design of composite sections [2.5].
3. The layer of UHPFRC provides shear resistance to the cracked RC section by out-of-plane bending. At the mouth of the critical shear crack, bending efforts are introduced in the layer due to the relative movement of the lips of the crack.
4. Over the column, the layer deflects upward due to the high bending efforts in the slab. Because of geometrical compatibility, limited horizontal cracking is created in the concrete underneath the interface.
5. The layer of UHPFRC increases the rigidity of the slab, as an added flexural reinforcement is expected to do. However, the deformability of UHPFRC in bending allows the RC section to deform more. Shear deformation and crack opening of the RC section are larger than for the reference RC slab. This results in rotations and deflections at maximum resistance similar to what is observed for the reference RC slab.
6. A thinner UHPFRC layer of 25 mm also increases the punching shear resistance and rigidity of a slab. However, this thinner layer evidently has less bending resistance

than a layer of 50 mm and the rotation at maximum resistance is smaller than for the reference RC slab.

7. The CSCT model for RC slabs cannot be used to directly calculate the maximum resistance and deformability of composite slabs. This model may be used to determine the contribution of the RC section of the composite slabs and a new term has to be developed to account for the contribution of the UHPFRC layer.

## 7 References

- [2.1] Broms CE. Elimination of flat plate punching failure mode. *ACI Structural Journal*. 2000;97(1):94-101.
- [2.2] Habel K, Denarie E, Brühwiler E. Structural Response of Elements Combining Ultrahigh-Performance Fiber-Reinforced Concretes and Reinforced Concrete. *Journal of Structural Engineering*. 2006;132(11):1793-800.
- [2.3] Denarié E, Brühwiler E. Strain Hardening of Ultra-high Performance Fibre Reinforced Concrete: Deformability versus Strength Optimization. *International Journal of Restoration of Buildings and Monuments*. 2012;17(6):397-410.
- [2.4] Brühwiler E, Denarie E. Rehabilitation and Strengthening of Concrete Structures Using Ultra-High Performance Fibre Reinforced Concrete. *Structural Engineering International*. 2013;23(4):450-7.
- [2.5] Oesterlee C. Structural Response of Reinforced UHPFRC and RC Composite Members. Doctoral thesis EPFL no. 4848. Lausanne: Ecole Polytechnique Fédérale de Lausanne; 2010; 136 p.
- [2.6] Habel K, Denarie E, Brühwiler E. Experimental investigation of composite ultra-high-performance fiber-reinforced concrete and conventional concrete members. *ACI Structural Journal*. 2007;104(1):93-101.
- [2.7] Noshiravani T, Brühwiler E. Experimental investigation on reinforced ultra-high-performance fiber-reinforced concrete composite beams subjected to combined bending and shear. *ACI Structural Journal*. 2013;110(2):251-61.
- [2.8] Bastien-Masse M. Punching test on R-UHPFRC - RC composite slabs without shear reinforcement. Test report. Lausanne: Ecole Polytechnique Fédérale de Lausanne; ENAC-MCS;2014.
- [2.9] Guandalini S, Burdet OL, Muttoni A. Punching tests of slabs with low reinforcement ratios. *ACI Structural Journal*. 2009;106(1):87-95.
- [2.10] Muttoni A. Punching Shear Strength of Reinforced Concrete Slabs without Transverse Reinforcement. *ACI Structural Journal*. 2008;105(4):440-50.
- [2.11] Theodorakopoulos DD, Swamy RN. Ultimate punching shear strength analysis of slab-column connections. *Cement and Concrete Composites*. 2002;24(6):509-21.
- [2.12] Menetrey P. Synthesis of punching failure in reinforced concrete. *Cement and Concrete Composites*. 2002;24(6):497-507.
- [2.13] Koppitz R, Kenel A, Keller T. Punching shear of RC flat slabs - Review of analytical models for new and strengthening of existing slabs. *Engineering Structures*. 2013;52:123-30.
- [2.14] Amsler M, Thoma K, Heinzmann D. Punching slab strengthened with an additional concrete layer - Test and recalculations. *Beton und Stahlbetonbau*. 2014;109(6):394-402.
- [2.15] Chen C-C, Li C-Y. Punching shear strength of reinforced concrete slabs strengthened with glass fiber-reinforced polymer laminates. *ACI Structural Journal*. 2005;102(4):535-42.

- [2.16] Esfahani MR, Kianoush MR, Moradi AR. Punching shear strength of interior slab-column connections strengthened with carbon fiber reinforced polymer sheets. *Engineering Structures*. 2009;31(7):1535-42.
- [2.17] Harajli MH, Soudki KA. Shear strengthening of interior slab-column connections using carbon fiber-reinforced polymer sheets. *Journal of Composites for Construction*. 2003;7(2):145-53.
- [2.18] Sharaf MH, Soudki KA, Van Dusen M. CFRP strengthening for punching shear of interior slab-column connections. *Journal of Composites for Construction*. 2006;10(5):410-8.
- [2.19] Wuest J. Comportement structural des bétons de fibres ultra performants en traction dans des éléments composés. Doctoral thesis EPFL no. 3987. Lausanne: Ecole Polytechnique Fédérale de Lausanne; 2007; 244 p.
- [2.20] Guidotti R. Poinçonnement des planchers-dalles avec colonnes superposées fortement sollicitées. Doctoral thesis EPFL no. 4812. Lausanne: Ecole Polytechnique Fédérale de Lausanne; 2010; 189 p.
- [2.21] Lips S, Fernandez Ruiz M, Muttoni A. Experimental Investigation on Punching Strength and Deformation Capacity of Shear-Reinforced Slabs. *ACI Structural Journal*. 2012;109(6):889-900.
- [2.22] Clement T, Pinho Ramos A, Fernandez Ruiz M, Muttoni A. Influence of prestressing on the punching strength of post-tensioned slabs. *Engineering Structures*. 2014;72:56-69.
- [2.23] Rossi P. High Performance Multimodal Fiber Reinforced Cement Composites (HPMFRCC): the LCPC Experience. *ACI Materials Journal*. 1997;94(6):478-83.
- [2.24] Rossi P, Arca A, Parant E, Fakhri P. Bending and compressive behaviours of a new cement composite. *Cement and Concrete Research*. 2005;35(1):27-33.
- [2.25] Fernandez Ruiz M, Mirzaei Y, Muttoni A. Post-punching Behavior of Flat Slabs. *ACI Structural Journal*. 2013;110(5):801-11.
- [2.26] Habibi F, Cook WD, Mitchell D. Predicting Post-Punching Shear Response of Slab-Column Connections. *ACI Structural Journal*. 2014;111(1):123-34.





## Paper III

### Composite Model for Predicting the Punching Resistance of R-UHPFRC – RC Composite Slabs

---

**Reference:** Bastien-Masse M, Brühwiler E. Composite Model for Predicting the Punching Resistance of R-UHPFRC – RC Composite Slabs. *Submitted to Engineering Structures on August 27<sup>th</sup> 2015.*

#### Abstract

Adding a thin layer of Ultra-High Performance Fiber Reinforced cement-based Composite (UHPFRC), with or without steel rebars, over a Reinforced Concrete (RC) slab is an efficient reinforcement method for existing structures. The thin layer of UHPFRC serves as a tensile reinforcement for the RC slab, creating a composite element. A recent experimental campaign showed that the layer of UHPFRC significantly increases the rigidity and the punching shear resistance of a RC slab submitted to a point force. An analytical composite model is developed herein to predict the global bending behavior of the composite slab and the punching shear resistance. A multilinear moment-curvature relation for composite sections is proposed to calculate the global force-rotation behavior of a slab which can then be used in combination with a composite failure criterion to predict the punching shear resistance. The contribution of the concrete section to the punching shear resistance is obtained with existing models from the literature. The UHPFRC layer resists to punching shear by out-of-plane bending over a limited length equal to its height. This mechanism induces tensile stresses perpendicularly to the interface with the concrete. The contribution of the UHPFRC layer to the punching shear resistance thus depends on the tensile strength of concrete. The results of this analytical composite model are in good agreement with the experimental result. A method is also proposed to consider pre-existing deformation of the RC section for a post-installed UHPFRC layer.

**Keywords:** Composite slab, Flat slabs, Punching shear resistance, Ultra-High Performance Fiber Reinforced cement-based Composite (UHPFRC), Strengthening, Sector model, Composite model, Near interface cracking.

## List of Symbols

### Subscripts

$R$	Resistance
$RU$	Reinforced UHPFRC
$RC$	Reinforced Concrete
$U$	UHPFRC
$Ut_u$	UHPFRC tensile strength
$c$	concrete
$cc$	concrete in compression
$cr$	cracking of concrete
$el$	elastic state
$i$	steel, UHPFRC or concrete
$r$	radial
$s$	steel
$sc$	top steel reinforcement layer in RC section
$sb$	UHPFRC strain hardening
$sU$	steel reinforcement in the R-UHPFRC layer
$sy$	yielding of steel
$t$	tangential
$x$	related to the calculation of the height of the compression zone

### Latin upper case

$A$	Area
$B$	side length of slab specimen
$E$	modulus of elasticity
$EI_0$	elastic flexural rigidity
$EI_1$	flexural rigidity after concrete cracking
$EI_2$	flexural rigidity after tensile strength of UHPFRC is reached
$EI_3$	flexural rigidity when the composite section is softening
$F$	force in cross section
$F_{RU}$	force in the R-UHPFRC tension chord
$F_T$	force in the composite R-UHPFRC – RC tension chord
$M$	moment
$M_{br}$	resisting moment of composite beam calculated with the layered analytical model
$M_{ml}$	resisting moment of composite beam calculated with the multilinear moment-curvature relation
$M_{test}$	resisting moment of composite beam obtained from a bending test
$S$	parameter related to the calculation of the height of the compression zone
$V$	punching shear force
$V_c$	concrete contribution to punching shear resistance
$V_{calc}$	calculated shear force
$V_{exp}$	measured shear force
$V_U$	UHPFRC layer contribution to punching shear resistance

### Latin lower case

$b$	beam width
$b_0$	critical perimeter for punching shear set at $d_{sc}/2$ from the column face
$b_1$	distance between two force introduction points in the square test slab
$b_2$	distance between force introduction point and nearest slab side
$c$	side length of column

$d$	flexural depth for a tensile reinforcement: distance from the bottom compression face of the slab to the centroid of the tensile reinforcement
$d_g$	maximum diameter of aggregate
$d_{g0}$	reference aggregate size set at 16 mm
$f$	strength of a material
$f_c$	concrete compressive strength
$f_{ct}$	concrete tensile strength
$f_{sy}$	yield strength of steel reinforcement
$f_{Uc}$	UHPFRC compressive strength
$f_{Ute}$	elastic tensile strength of UHPFRC
$f_{Um}$	tensile strength of UHPFRC
$f_{Uts}$	softening tensile strength of UHPFRC
$h$	height
$l_{cb}$	UHPFRC characteristic length for the softening behavior
$l_{NIC}$	near interface cracking length at the UHPFRC – concrete interface
$m$	bending moment per unit width
$r$	radius measured from the center of the slab
$r_0$	radius of inclined crack at the top reinforcement layer located at $d_{ic}$ from the column side
$r_c$	radius of circular column
$r_q$	radius of force introduction at perimeter
$r_s$	radius of circular slab
$r_U$	radius of inclined crack at the top of the slab located at $h_c+h_U$ from the column side
$w_{Uf}$	crack opening in UHPFRC
$x$	height of the compression zone
<b>Greek lower case</b>	
$\alpha_c$	minimum angle of the inclined shear crack
$\beta$	efficiency factor to take into account the reduced torsional rigidity of orthogonal reinforcement
$\varepsilon$	strain
$\varepsilon_{sy}$	yielding strain in steel reinforcement
$\varepsilon_{ct}$	strain in concrete at maximum compressive strength
$\varepsilon_{Uc}$	strain in UHPFRC at maximum compressive strength
$\varepsilon_{Ute}$	strain in UHPFRC at tensile elastic limit strength
$\varepsilon_{Um}$	strain in UHPFRC at maximum tensile strength
$\theta_U$	angle of rotation in the UHPFRC hinge
$\varkappa$	curvature in a cross-section
$\varkappa_1$	curvature when cracking has stabilized in a RC cross-section
$\varkappa_{add}$	curvature when the layer of UHPFRC is added to a RC section
$\varkappa_{TS}$	reduction in the curvature due to tension stiffening
$\lambda$	remaining ratio of $f_{Um}$
$\rho$	reinforcement ratio
$\rho_{TC}$	reinforcement ratio in the tension chord
$\sigma$	stress
$\psi$	rotation
$\psi_{add}$	rotation when the layer of UHPFRC is added to a RC slab



## 1 Introduction

The use of a thin layer of Ultra-High Performance Fiber Reinforced cement-based Composite (UHPFRC) as an external tensile reinforcement for Reinforced Concrete (RC) slabs is a spreading technique for strengthening existing structures [3.1]. UHPFRC layers reinforced (or non-reinforced) with small diameter steel rebars (R-UHPFRC) have a typical thickness of between 25 and 50 mm and are cast in place over RC slabs, creating a composite RU-RC section (Figure 1a).

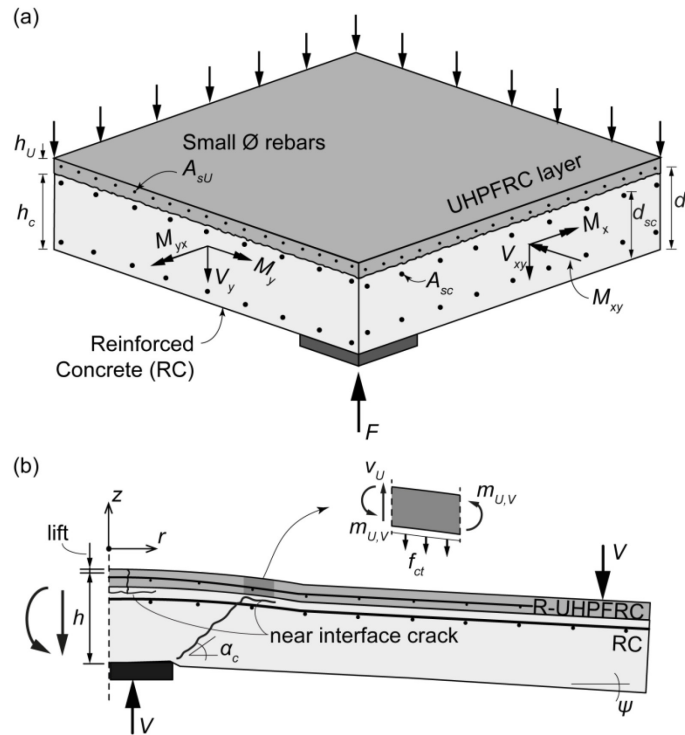


**Figure 1 (a) Typical RU-RC composite slab element; (b) Resisting mechanisms for composite slabs [3.2]**

This reinforcement method was proven effective to strengthen one-way elements in bending and in shear [3.3, 4]. With its high tensile properties, the UHPFRC layer contributes to the resistance of the element by its in-plane tensile resistance and deformability as well as its out-of-plane bending resistance and rotation capacity [3.5, 6].

In a previous paper by the authors [3.2], an experimental campaign on the punching shear resistance of composite RU-RC slabs submitted to a point force was presented. The tests showed that the layer of UHPFRC can increase the punching shear resistance of a RC slab by at least 69% without modifying its rotation capacity as it would be expected for a slab with added flexural reinforcement. As for one-way shear, the layer of UHPFRC resists to punching shear by out-of-plane bending (Figure 1b), meaning that it activates a bending mechanism perpendicular to the plane of the deflected shape of the composite slab.

Over the last century, punching shear resistance of RC slabs has been the object of extensive research [3.7]. Various analytical models were developed to predict the punching shear

resistance of RC slabs using elasticity and plasticity theories. A full review of the existing models can be found in [3.8].

A sector model was developed in 1960 by Kinnunen and Nylander [3.9]. Their model allowed simulating the behavior of an axisymmetric slab by assuming that slab sectors rotate around the edge of the column. With the assumed kinematic, the force-rotation curve of the slab is obtained and combined to a failure criterion to predict the punching shear resistance (Figure 2). The proposed failure criterion is expressed as the ultimate tangential strain in the concrete near the column. The punching shear resistance is thus related to the state of deformation in the slab due to bending.

The sector model served as a basis for further model developments [3.10-12]. Hallgren [3.10] modified the failure criterion using fracture mechanics. Muttoni [3.12] used the sector model to develop the critical shear crack theory (CSCT) in which the failure criterion is a function of the slab rotation. The CSCT is now the basis for the punching shear resistance calculation in the *fib* Model Code 2010 [3.13] as well as the Swiss standards for the design of concrete structures [3.14].

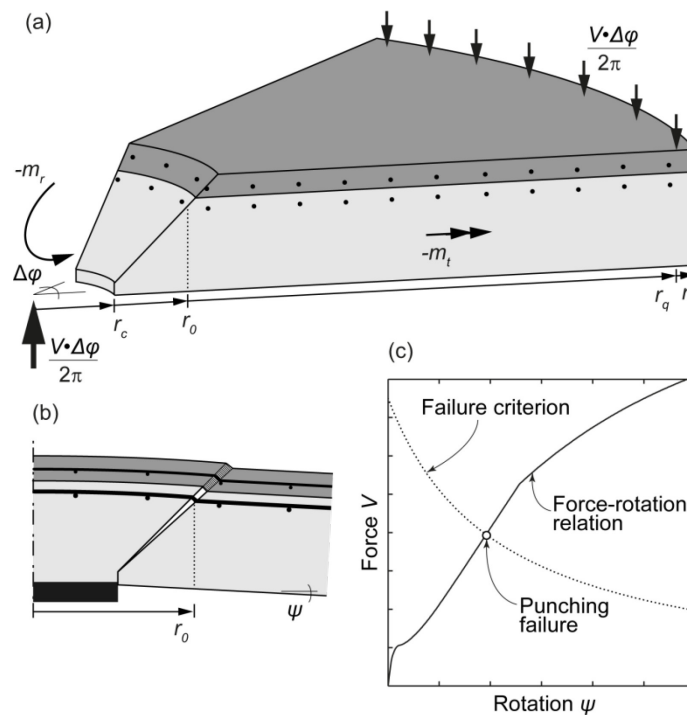


**Figure 2 (a) Efforts in slab sector; (b) assumed behavior of slab; (c) calculation of punching shear resistance with a failure criterion, adapted from [3.12]**

The objective of the presented work is to develop analytical models to include the contribution of the UHPFRC layer to the punching shear resistance calculation of a composite slab. First, a multilinear moment-curvature relation is proposed to predict the composite bending behavior and calculate the force-rotation curve of a composite slab. Second, an expression to consider the contribution of the UHPFRC layer to the punching shear resistance is proposed. This new expression is then added to existing failure criteria for RC slabs, such as the CSCT failure criterion. The development of the new term is based on the observed failure mode of the composite slabs during the experimental campaign (Figure

1b) [3.2] and on previously developed shear resistance models for composite beams [3.6]. The intersection between the composite failure criterion and the force-rotation curve gives the theoretical punching shear resistance of the composite slab (Figure 2c). This new composite model is validated with the experimental results. Finally, a method to take into account pre-existing deformations in a slab for the case of a post-installed UHPFRC layer is proposed.

## 2 Model parameters

### 2.1 Material constitutive laws

#### 2.1.1 Concrete

The stress-strain relations for concrete in tension and compression are based on the proposals of the *fib* Model Code 2010 [3.13]. In tension, concrete has a linear-elastic behavior. Once the tensile strength of concrete  $f_{ct}$  is reached the concrete cracks. Concrete then has a softening behaviour expressed by a stress-crack opening relation [3.13]. In the models presented here, the softening behavior of concrete was however neglected and it is supposed that no stress is transferred through the cracks.

In compression, the stress-strain relation of concrete is linear up to a stress of  $0.4 \cdot f_c$  (compressive strength of concrete). According to the *fib* Model Code 2010, once this limit is reached, the stress strain relation can be estimated by a parabola, as illustrated in Figure 3b.

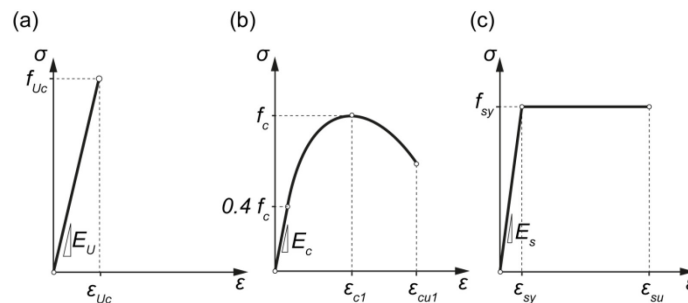


**Figure 3 Constitutive laws: (a) UHPFRC in compression; (b) concrete in compression [3.13]; (c) steel**

#### 2.1.2 Steel

Actual stress-strain diagrams of steel rebars in tension show a hardening behavior and tensile limit strength higher than the yield strength. When examining existing structures, this strength reserve should be taken into account. In the following models, however an elastic-plastic stress-strain relation is used with the yield strength as maximum strength for the rebars (Figure 3c).

### 2.1.3 UHPFRC

For design purpose, the behavior of UHPFRC in compression is supposed to be linear elastic until maximum compressive strength  $f_{Uc}$  is reached (Figure 3a) [3.15]. Then, it is assumed that no more stress is transferred by the material.

In tension, UHPFRC has a hardening-softening behavior. Once the material reaches its elastic limit strength  $f_{Ute}$ , distributed microcracking starts to develop and the material enters its hardening phase until it reaches tensile strength  $f_{Utu}$ . This phase is normally expressed with a stress-strain relation and can be defined with a reduced modulus:

$$E_{Ush} = \frac{f_{Utu} - f_{Ute}}{\epsilon_{Utu} - \epsilon_{Ute}} \quad (1)$$

The softening phase begins when all deformation localizes at one crack. Softening behavior is described as a stress-crack-opening relation. It is approximated with a bilinear relation (Figure 4) where the maximum crack opening at the end of the softening phase is equal to half the fiber length. When designing with UHPFRC, crack opening are converted to strains using a characteristic length  $l_{cb}$ . In the French recommendations for UHPFRCs [3.16]  $l_{cb}$  is taken equal to two thirds of the thickness of the element in bending. For composite elements this corresponds to two thirds of the total height of the section.

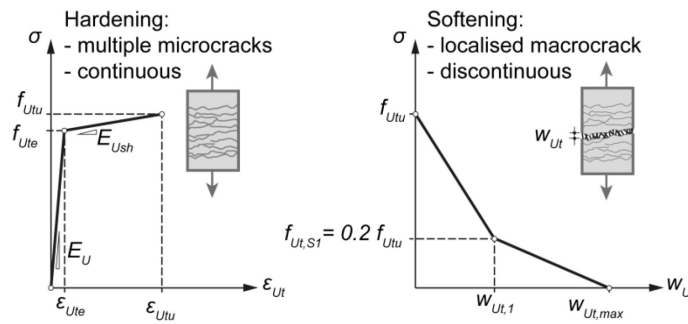


**Figure 4 UHPFRC tensile law**

The effect of fiber orientation must be considered when defining the tensile properties of UHPFRC for the design of a tensile reinforcement layer. A complete procedure was developed in [3.17] to identify the average fiber orientation factor in the two orthogonal direction of a UHPFRC layer and scale the tensile properties accordingly. This procedure will be used herein to choose the tensile properties for the prediction of the force-rotation behavior and punching shear resistance of composite slabs.

## 2.2 Tension chords

### 2.2.1 Overview

In a composite section submitted to hogging moments, tensile stresses are carried by the UHPFRC layer, the steel rebars in it and the top steel rebars in the concrete, creating a composite RU-RC tension chord. The interaction between all the materials in the tension chord depends on cracking, deformations and bond behavior.



### 2.2.2 RC tension chord

A model is presented in [3.18] to predict the behavior of a tension chord formed by concrete and reinforcement bars. It allows calculating the tension stiffening of the chord happening after the concrete has cracked. Tension stiffening is a decrease in the strains expected for the naked rebars due to the concrete between the cracks still bonded to it. To calculate this tension stiffening effect, a stepped rigid-plastic bond-slip behavior between the concrete and the ribbed rebars was proposed in [3.19]. Prior to yielding of the steel rebar, the bond is equal to twice the tensile strength of concrete  $f_{ct}$ . It decreases to  $f_{ct}$  at the onset of yielding of the rebar.

With this relation, a simplified resolution of the differential equation describing the equilibrium and compatibility of the tension chord is possible. After concrete cracking and prior to yielding of the steel rebar, the strain in the tension chord is reduced by the following constant factor [3.18]:

$$\Delta\varepsilon = \frac{f_{ct}}{2E_s} \cdot \frac{1-\rho_{TC}}{\rho_{TC}} \quad (2)$$

where  $\rho_{TC}$  is the reinforcement ratio of the tension chord.

Tension stiffening has an effect on the flexural rigidity of a RC section. This effect should also be taken into account when calculating the moment-curvature relation of a composite RU-RC section.

### 2.2.3 RU tension chord

Adding steel rebars in UHPFRC, to create R-UHPFRC, enhances its performance in tension. Tensile tests on R-UHPFRC specimens [3.20-24] showed that steel rebars extend the hardening domain of UHPFRC and that the maximum force is achieved at the onset of yielding of the rebars.

Various models were developed to predict the behavior of an R-UHPFRC tension chord [3.20-25]. Two strategies are adopted in these models. The first strategy consists of considering UHPFRC as a homogenous material combined with steel rebars. In this case, the response of the tension chord is obtained by superposing the tensile behavior of both materials, i.e. UHPFRC and steel. In the second strategy, the matrix, the fibers and the steel rebars are considered as three constituents. The interaction between each of them is described by bond laws. This second modelling strategy gives a better insight on the actual behavior of a R-UHPFRC tension chord.

Based on the experimental observations and on the bond assumptions of the second type of models, the effect of the steel rebars on the tensile behavior of UHPFRC can be explained. Steel rebars in UHPFRC act like long continuous fibers. Once the matrix has cracked, hardening starts with distributed microcracking along the tension specimen (Figure 4a). Both types of reinforcement (fibers and rebars) then enter into an activation phase during which they are gradually debonded from the matrix. A crack localizes when the fibres are being pulled out from the matrix and the steel rebar starts to yield. Hardening phase of a RU tension chord can thus extend until steel yields. The maximum strain of UHPFRC at the end

of hardening in a reinforced tension chord ( $\varepsilon_{Utu,RU}$ ) is considered equal or larger than the yield strain of the steel rebars:

$$\varepsilon_{Utu,RU} = \max \left[ \varepsilon_{Utu}, \min \left( \varepsilon_{sy} = \frac{f_{sy}}{E_s}, 2 \cdot \varepsilon_{Utu} \right) \right] \quad (3)$$

The hardening domain of the plain UHPFRC ( $\varepsilon_{Utu}$ ) may be longer than the yield strain of steel due to favourable fiber orientation in the R-UHPFRC specimen or high fiber volume in the UHPFRC mix. However, it can also be shorter when high performance steel is used, as these steels have larger yield strain. The extended hardening domain is thus limited to twice the value measured for plain UHPFRC, as experimentally observed in [3.24].

#### 2.2.4 RU-RC tension chord

The behavior of the composite RU-RC tension chord depends on the behavior of the two tension chord previously presented. Their interaction is governed by the bond between the UHPFRC and the concrete. The bond between UHPFRC and normal-strength concrete was assessed with pull-out tests, indirect tensile tests and slant shear tests in [3.26]. The results showed that the bond strength is higher than the tensile strength of the concrete. Bending tests on composite RU-RC beams also showed that prior to maximum resistance the section behaves monolithically [3.3]. When debonding does occur, it rather takes the form of near interface cracking (NIC) in the concrete near the top rebars in the RC section. It thus depends on the tensile strength of concrete. When calculating the moment-curvature behavior of the composite section, perfect bond is thus assumed between the UHPFRC and the concrete.

### 3 Force-rotation behavior

#### 3.1 Assumed bending behavior

An axisymmetric circular slab of radius  $r_s$  is considered, with reinforcement placed in radial and tangential directions. The column has a radius  $r_c$  and the force is introduced on the edge of this isolated specimen, at radius  $r_q$  (Figure 2). As was proposed by Kinnunen and Nylander [3.9] and adapted by Muttoni [3.12], it is supposed that rigid slab sectors rotate around the column edge with a constant rotation  $\psi$  in radial direction (Figure 2) while the radial curvature is zero. This gives a conical shape to the outer part of the slabs. Over the column, the truncated conical part of the slab deforms in a spherical shape. This deformed shape was also confirmed for composite slabs by experimental observations [3.2].

Based on the previous considerations, the distributions of curvatures in tangential and radial directions are given. The inclined plane separating the outer sectors from the central part crosses the top layer of rebars in the RC section at radius  $r_0$  from the center of the slab. Radius  $r_0$  is assumed to be at a distance  $d_{sc}$  of the column side (Figure 1).

The central part of the slab has a constant curvature both in tangential and radial direction. The radial curvature of the outer sectors is approximated to zero while the tangential curvature is inversely proportional to the radius  $r$ .

$$\kappa_r = \kappa_t = -\frac{\psi}{r_0} \text{ for } r \leq r_0 \quad (4)$$

$$\kappa_t = -\frac{\psi}{r} \text{ for } r > r_0 \quad (5)$$

The exact distribution of tangential and curvatures along radius  $r$  can be found in [3.12]. With the assumed simplified curvature distribution, the moment distribution can be deduced using the moment-curvature relation of the section. The equilibrium of the outer slab sector illustrated in Figure 2a is then verified with the following equation where  $m_r$  is the radial moment at  $r$ :

$$V \frac{\Delta\varphi}{2\pi} \cdot (r_q - r_c) = -m_r \Delta\varphi r_0 - \Delta\varphi \cdot \int_{r_0}^{r_s} m_t dr \quad (6)$$

### 3.2 Moment-curvature relations

#### 3.2.1 RC section

The moment-curvature relation of an RC section is estimated with a quadrilinear relation in [3.12]. This relation is illustrated in Figure 5a and the expressions of the limit moments, curvatures and flexural rigidities are given in Table 1. The four characteristic phases of the moment-curvature relation of a RC section are:

1. Elastic phase (from point O to A): Ends when the cracking moment  $m_{cr}$  is reached.
2. Cracking phase (from point A to B): Cracking develops until it reaches a fully cracked state. The moment stays constant at  $m_{cr}$  while the curvature increases until  $\kappa_I$ .
3. Fully cracked phase (from point B to C): A linear elastic behaviour is assumed for concrete in compression and steel in tension.

Due to tension stiffening in the RC tension chord (see paragraph 2.2.2), a constant decrease in curvature  $\kappa_{TS}$  is taken into account from cracking moment. It is obtained by considering the constant strain reduction in the tension chord (equation 2) and is expressed by the following equation in [3.12]:

$$\kappa_{TS} = \frac{\Delta\varepsilon}{d_{sc} - x_{cr}} \approx \frac{f_{ct}}{\rho_{sc} \cdot \beta \cdot E_s} \cdot \frac{1}{6 \cdot h_c} \quad (7)$$

4. Yielded phase (beyond point C): The resisting moment  $m_R$  of the section has been reached and steel is yielding.

Using the equilibrium of the slab sector (equation 6) and the quadrilinear relation, the force  $V$  on the slabs can be calculated as a function of the slab rotation  $\psi$ . Equation 6 is valid for an axisymmetric slab, as described in paragraph 3.1. However, it is more common to have slabs with orthogonal reinforcement where the principal moments can differ from the direction of the rebars causing a softening of the section after cracking and reducing the torsional stiffness. To take this phenomenon into account, the flexural rigidity of the section is reduced by the efficiency factor  $\beta$  after cracking of the concrete. Proposed values vary between 0.6 and 0.75 [3.12, 27, 28]. In the present work, the value of 0.75, proposed in [3.28]

and adjusted to the results of numerical calculations, was adopted as the most suitable for a slab without shear reinforcement.

**Table 1 Expressions for the quadrilinear moment-curvature relation for an RC section [3.12]**

Points	Moments $m$	Curvature $\kappa$	Flexural rigidity $EI$	Height of compression zone $x$
O	0	0	$EI_0 = \frac{E_c h_c^3}{12}$	$x_{el} = \frac{d_{sc}}{2}$
A		$\kappa_{cr} = \frac{m_{cr}}{EI_0}$		
B	$m_{cr} = \frac{f_{ct} h_c^2}{6}$	$\kappa_1 = \frac{m_{cr}}{EI_1} - \kappa_{ts}$	$EI_1 = \rho_{sc} \beta E_s d_{sc}^3 \cdot \left(1 - \frac{x_{cr}}{d_{sc}}\right)$	$x_{cr} = \rho_{sc} \beta \frac{E_s}{E_c} d_{sc}$
C	$m_R = \rho_{sc} f_{sy} d_{sc}^2 \cdot \left(1 - \frac{\rho_{sc} \cdot f_{sy}}{2f_c}\right)$	$\kappa_R = \frac{m_R}{EI_1} - \kappa_{ts}$	$EI_1 = \rho_{sc} \beta E_s d_{sc}^3 \cdot \left(1 - \frac{x_{cr}}{3d_{sc}}\right)$	$\cdot \left(\sqrt{1 + \frac{2E_c}{\rho_{sc} \cdot \beta \cdot E_s}} - 1\right)$
Beyond C		$> \kappa_R$	0	

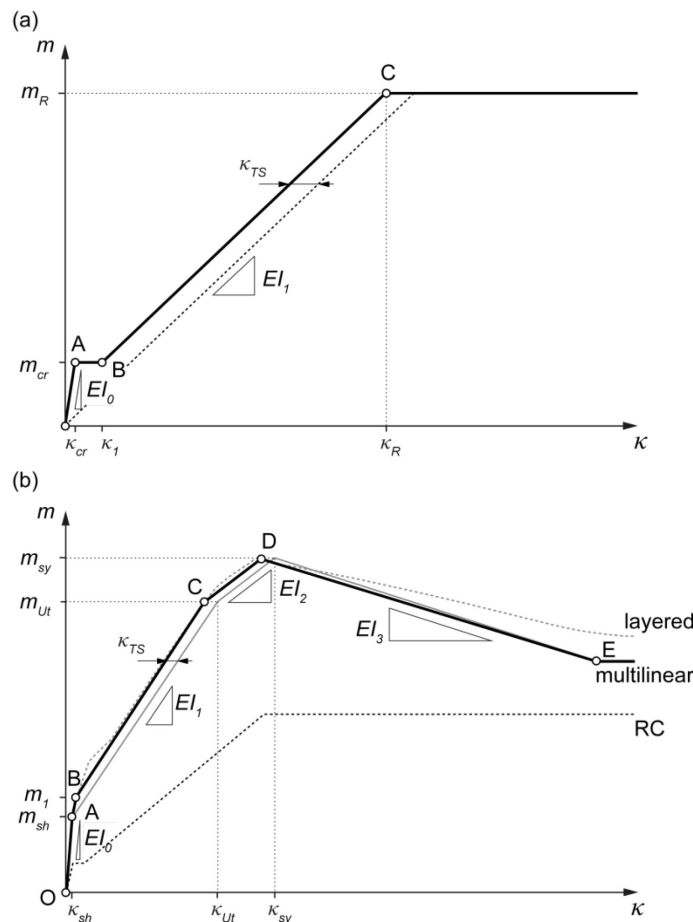


**Figure 5 Moment-curvature relations: (a) RC section [3.12]; (b) RU-RC section**

### 3.2.2 RU-RC composite section

Extensive experimental work has been carried out on the behavior of composite RU-RC beams submitted to bending efforts [3.3, 4, 24]. A detailed analytical cross-sectional layered model was developed in [3.5] to obtain the full moment-curvature relation of a composite RU-RC section. The main hypotheses of this layered model are: (1) plane sections remain plane and the composite section is monolithic; (2) stresses in each layer of the cross-section can be found with non-linear material laws; and (3) the equilibrium of forces and moments is assured on the cross-section.

Based on the conclusions of this work and on the experimental observations, a multilinear relation of the moment-curvature relation is proposed here to speed up the calculation of the force-rotation curve of a composite slab (Figure 5b). The hypotheses of this model are the same as for the layered model. The materials behavior presented in section 2.1 are used and the stress distribution over the height of the UHPFRC layer is approximated to a constant value. For typical thickness of UHPFRC layers (between 25 and 50 mm) considered here, the position of the steel rebars is approximated to the center of the layer.

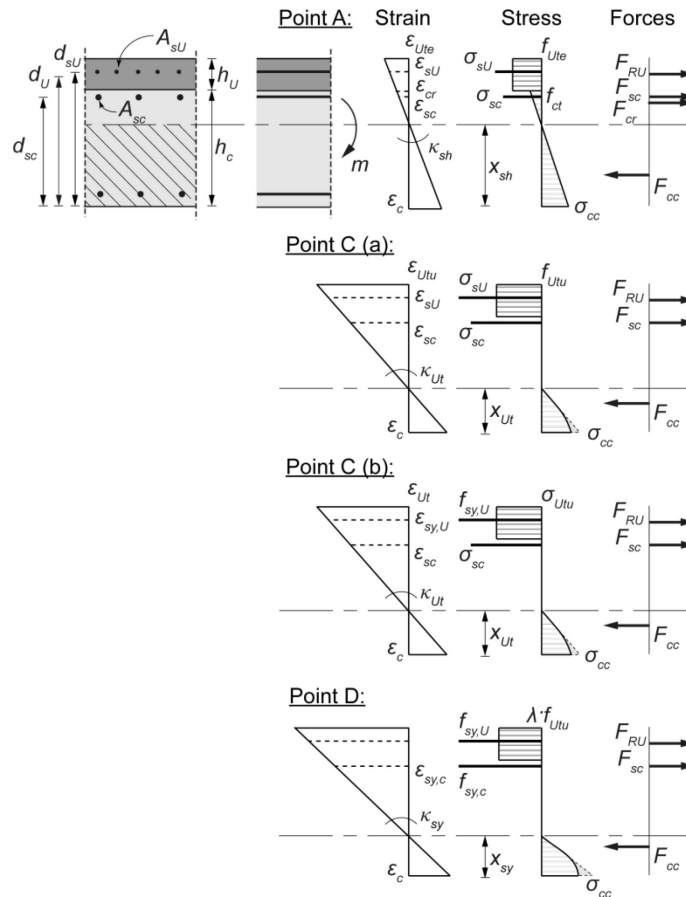


**Figure 6 Sectional distributions of strains, stress and forces**

All expressions related to the different points seen in Figure 5b are given in Table 2 and Table 3. These expressions are obtained by imposing the equilibrium of forces over the cross-section at each point (hypothesis 3). The behavior of a composite section is defined by the following phases:

1. Elastic phase (from point O to A): All materials are behaving in a linear elastic way. Both concrete and UHPFRC are uncracked. The height of the compression zone  $x_{el}$  and the flexural rigidity  $EI_0$  can thus be obtained by considering the rigidity of all materials. With the flexural rigidity  $EI_0$ , the moment can be deduced for any curvature in the elastic phase:

$$m = EI_0\kappa \quad (8)$$

The elastic phase ends when the concrete has reached its tensile strength  $f_{ct}$  near the interface with the UHPFRC layer (point A in Figure 5b and Figure 6). At this point, most of the thickness of the UHPFRC layer has reached its elastic tensile limit  $f_{Ute}$ . The curvature at point A is obtained with the tensile strength of concrete and the height of the compression zone  $x_{sb}$ , calculated as for the elastic phase, but using the strain hardening rigidity of UHPFRC  $E_{Ush}$  (equation 1) to take into account the reduced stiffness of the layer.

2. Hardening phase 1 (from point A to C): The UHPFRC layer is in hardening and all layers of steel are still elastic. The concrete in tension is cracked and, as stated in paragraph 2.1.1, does not transfer anymore stress. Its contribution is limited to the stiffening of the RC tension chord. The effect of tension stiffening is taken into account by considering the same decrease in curvature  $\kappa_{TS}$  considered for a RC section and expressed by equation 7. This decrease in curvature is applied from point B.

The hardening phase ends at point C (Figure 5b and Figure 6) when one of the following conditions is reached:

- (a) The layer of UHPFRC has reached its tensile strength  $f_{Ut}$  (point C in Figure 5b and Figure 6). The curvature is obtained by supposing that the strain at the center of the layer is equal to the strain at the end of the hardening domain of the UHPFRC layer,  $\varepsilon_{Utm}$ . This condition is reached when UHPFRC has a hardening domain  $\varepsilon_{Utm}$  smaller or equal to the yielding strain of the steel rebars in it (see 2.2.3). In the latter case, the steel in the layer is also yielding.
- (b) The steel in the UHPFRC layer yields, but UHPFRC has not yet reached the end of its hardening. This happens when the hardening domain of UHPFRC  $\varepsilon_{Utm}$  is larger than the yield strain of the steel placed in it. The curvature is then obtained with the yielding strain of the steel.

With the flexural rigidity  $EI_1$  and the moment at the end of the elastic phase  $m_{sb}$ , the moment is obtained for any curvature of the hardening phase 1:

$$m = EI_1(\kappa - \kappa_{sh}) + m_{sh} \quad (9)$$

3. Hardening phase 2 (from point C to D): At least one of the layers of tensile reinforcement has reached its maximum strength: either the UHPFRC layer or the steel in it. Depending on the condition that was applied in the previous phase the UHPFRC layer is softening or is still in its hardening domain.

This phase ends when all the tensile reinforcement layers have reached or exceeded their maximum strength (UHPFRC) or yielding strength (steel rebars), which corresponds to point D in Figure 5b and Figure 6. Depending on the different mechanical ratios of tensile reinforcements (UHPFRC layer, steel rebars in the layer and in the concrete), point D can be higher or lower than point C.

If UHPFRC is already softening at point D, its contribution is a fraction  $\lambda$  of its tensile strength  $f_{Ut}$ . Using the curvature calculated for point D,  $\kappa_y$ , the deformation in the softening UHPFRC layer  $\varepsilon_{Ut,S}$  is obtained. With the softening law described in section 2.1.3, the value of  $\lambda$  can be calculated.

$$\varepsilon_{Ut,S} = \max \left[ \frac{f_{sy,c}}{E_s} \cdot \frac{(d_{sU} - x_{Ut})}{(d_{sc} - x_{Ut})}, \frac{f_{sy,U}}{E_s} \right] \quad (10)$$

$$\lambda = 1 - 0.8 \cdot \frac{(\varepsilon_{Ut,S} - \varepsilon_{Ut}) l_{ch}}{w_{Ut,1}} \leq 1 \quad (11)$$

As for the previous phases, with the flexural rigidity  $EI_2$ , the moment is obtained for any curvature in the hardening phase:

$$m = EI_2(\kappa - \kappa_{Ut}) + m_{Ut} \quad (12)$$

4. Yielded phase (beyond point D): All steel rebars are yielding and the UHPFRC is ending its softening. In pure bending, final fracture occurs when the rebars reach their ultimate strains or when the concrete compression zone fails in compression.

In the proposed multilinear relation, the stress distribution of concrete in compression at point C and D is supposed to be linear. This slightly overestimates height of the compression zone and the strain in the concrete. The compressive strain at the bottom fiber of the concrete,  $\varepsilon_c$ , should be verified for those 2 points:

$$\varepsilon_c = \kappa_i x_i \quad (13)$$

If this strain is larger than 1.75‰ (value proposed in [3.13]), the contribution of concrete at the corresponding point should be approximated using an equivalent stress block distribution. The height of the compression zone for this point is then obtained with the following equation:

$$x_i = \frac{F_{Ti}}{0.8f_c} \quad (14)$$

If the compressive strain at the bottom fiber of concrete calculated with a stress block distribution is larger than 3.5‰, which is the deformation at failure of concrete in compression [3.13], the tensile reinforcement mechanical ratios should be reduced. Thus, the amount of tensile reinforcement (here UHPFRC with or without rebars) that can be added on a RC section is limited by the strength of the concrete.

As was specified before, in phase 3 (between points C and D), the resisting moment can be increasing or decreasing depending on the amount of each tensile reinforcement. The maximum bending moment of the composite section,  $m_R$ , is thus the maximum value between  $m_{Ut}$  and  $m_y$  and curvature  $\kappa_R$  is the curvature related to this maximum moment.

This multilinear behavior was used to predict the bending resistance of composite RU-RC beams found in [3.4, 5, 24]. The model predictions are compared to the experimental results as well as to the predictions of the layered model. Table 4 gives the geometry and material properties used in the calculations as well as the ratios between multilinear relation predictions and experimental results or layered model predictions. It shows that the multilinear relation predicts the resistance of a composite beam within a bandwidth of  $\pm 5\%$  which is considered as sufficiently precise.

As for the RC section, by verifying the equilibrium of the outer slab sector (equation 6) and using the multilinear moment-curvature relation for the composite section described here, the force  $V$  on the slabs can be obtained for any rotation  $\psi$ . Again, when using equation 6 to predict the force-rotation behavior of a composite slab with orthogonal reinforcement, the flexural rigidity must be reduced by the efficiency factor  $\beta$ . This is to account for the reduced torsional stiffness where the principal moments differ from the direction of orthogonal reinforcement. The efficiency factor  $\beta$  is applied after point B of the multilinear moment-curvature relation, once the concrete is cracked and UHPFRC is hardening and thus has a lower rigidity. The same value of 0.75 as for the RC section is used.

### 3.3 Direct method

To predict the force-rotation behavior of a slab, the moment distribution must be defined along the radius and then integrated to obtain the force (equation 6). To directly obtain the rotation of the slab for a given force, Muttoni [3.12] proposed to estimate the force-rotation with a parabola and a cap at the theoretical bending resistance of the slab,  $V_{flex}$ . It is supposed that the bending resistance of the slab is reached when three quarter of the slab radius  $r_s$  has reached or exceeded the maximum bending resistance of the slab  $m_R$ .

$$\psi = 1.5r_s\kappa_R \left( \frac{V}{V_{flex}} \right)^{3/2} \quad (15)$$

The bending resistance of the slab can be estimated using yield-line method, as proposed in [3.29] (see Figure 9 for notations):

$$V_{flex} = \frac{4m_R}{r_q \left( \cos \frac{\pi}{8} + \sin \frac{\pi}{8} \right) - c} \cdot \frac{B^2 - Bc - c^2/4}{B - c} \quad (16)$$



**Table 2 Expressions for the multilinear moment-curvature relation for an RU-RC composite section**

Pts	Moments $m$	Curvature $\kappa$	Flexural rigidity $EI$	Height of compression zone $x$
O	0	0	$EI_0 = \frac{E_c h_c^3}{12} + \frac{E_u h_u^3}{12} + E_c h_c \cdot (x_{el} - d_c)^2 + E_u h_u \cdot (x_{el} - d_u)^2$	$x_{el} = \frac{\sum E_i A_i d_i}{\sum E_i A_i}$
A	$m_{sh} = EI_0 \kappa_{sh}$	$\kappa_{sh} = \frac{f_{ct}}{E_c \cdot (h_c - x_{sh})} = \kappa_A$	$EI_{0,1} = \frac{m_1 - m_{sh}}{\kappa_1 - \kappa_{sh}}$	$x_{sh} = \frac{\sum E_i A_i d_i}{\sum E_i A_i}$ with $E_{i \neq 0}$ for UHPFRC
B	$m_1 = EI_1 \kappa_{ts} + m_{sh}$	$\kappa_1 = \frac{\kappa_{sh}}{\beta} + \kappa_{ts}$ $\kappa_B = \frac{\kappa_{sh}}{\beta}$		
C (a)	$m_{Ut} = F_{sc2} (d_{sc} - x_{Ut}/3) + (F_{su} + F_u) \cdot (d_{su} - x_{Ut}/3)$	$\kappa_{Ut} = \frac{\varepsilon_{Utu}}{\beta (d_{su} - x_{Ut})}$ $\kappa_C = \kappa_{Ut} - \kappa_{ts}$	$EI_1 = \frac{m_{Ut} - m_{sh}}{\kappa_{Ut} - \kappa_{sh}}$	$x_{Ut} = \frac{-F_{x,T} + \sqrt{F_{x,T}^2 + 2S_1 (F_{x,sc} d_{sc} + (F_{x,su} + F_u) d_{su})}}{S_1}$
C (b)	$m_{sy} = F_{sc2} (d_{sc} - x_{sy}/3) + (F_{su2} + F_u) \cdot (d_{su} - x_{sy}/3)$	$\kappa_{Ut} = \frac{f_{syu}}{\beta E_s (d_{su} - x_{Ut})}$ $\kappa_C = \kappa_{Ut} - \kappa_{ts}$	$EI_2 = \frac{m_{sy} - m_{Ut}}{\kappa_{sy} - \kappa_{Ut}}$	$x_{sy} = \frac{-F_{x,T} + \sqrt{F_{x,T}^2 + 2S_1 (F_{x,sc} d_{sc} + (F_{sc} + F_{ute} + F_{x,u}) d_{su})}}{S_1}$ $x_{sy} = \frac{-F_{T2} + \sqrt{F_{T2}^2 + 2S_2 F_{T2} d_{sc}}}{S_2}$
D	$m_{Ut, end} = F_{sc2} (d_{sc} - 0.4 \cdot x_{Ut, end}) + F_{su2} (d_{su} - 0.4 \cdot x_{Ut, end})$	$\kappa_{Ut, end} = \frac{w_{Ut, max}}{\beta L_R (d_{su} - x_{Ut, end})} = \kappa_E$		
E				$x_{Ut, end} = \frac{F_{T3}}{0.8 f_c}$

**Table 3 Equation of forces on the composite section at different stages of the moment-curvature relation**

Points	Forces F	Other parameters
	$F_{x,T} = F_{x,sc} + F_{x,sU} + F_U$ $F_T = F_{sc} + F_{sU} + F_U$	
C (a)	$F_{x,sc} = \varepsilon_{Utu} E_s \rho_{sc} d_{sc}$ $F_{sc} = \kappa_{Utu} E_s \rho_{sc} d_{sc} (d_{sc} - x_{Ut}) \leq F_{sc2}$ $F_{x,sU} = \varepsilon_{Utu} E_s \rho_{sU} h_U$ $F_{sU} = \kappa_{Utu} E_s \rho_{sU} h_U (d_{sU} - x_{Ut}) \leq F_{sU2}$	$S_1 = E_c \varepsilon_{Utu}$
	$F_U = f_{Utu} h_U$	
	$F_{x,T} = F_{x,sc} + F_{sU} + F_{x,U} + F_{Ute}$ $F_T = F_{sc} + F_{sU} + F_U + F_{Ute}$	
C (b)	$F_{x,sc} = \frac{f_{sy,U}}{E_s} E_s \rho_{sc} d_{sc}$ $F_{sc} = \kappa_{Utu} E_s \rho_{sc} d_{sc} (d_{sc} - x_{Ut}) \leq F_{sc2}$ $F_{sU} = f_{sy,U} \rho_{sU} h_U$	$S_1 = \frac{E_c}{E_s} f_{sy,U}$
	$F_{x,U} = \frac{f_{sy,U}}{E_s} E_s h_U$ $F_U = \kappa_{Utu} E_s h_U (d_{sU} - x_{Ut}) \leq F_{U2} - F_{Ute}$ $F_{Ute} = f_{Ute} h_U$	
D	$F_{T2} = F_{sc2} + F_{sU2} + F_U$ $F_{sc2} = f_{sy,c} \rho_{sc} d_{sc}$ $F_{sU2} = f_{sy,U} \rho_{sU} h_U$ $F_{U2} = \lambda f_{Utu} h_U$	$S_2 = \max \begin{bmatrix} \frac{E_c}{E_s} f_{sy,c} \\ \frac{E_c}{E_s} f_{sy,U} \\ E_c \varepsilon_{Utu} \end{bmatrix}$
E	$F_{T3} = F_{sc2} + F_{sU2}$	

**Table 4 Comparison between test results or layered model predictions to multilinear model predictions**

Ref.	Beam	$b$ [mm]	$h_c$ [mm]	$d_{ec}$ [mm]	$\rho_{ec}$ [%]	$h_U$ [mm]	$d_{eU}$ [mm]	$\rho_{eU}$ [%]	$\bar{\epsilon}_{tk}$ [MPa]	$\epsilon_{tk}^{lim}$ [%]	$w_{ult}$ [mm]	$E_s$ [GPa]	$\epsilon_{prc}$ [MPa]	$\epsilon_{prU}$ [MPa]	$M_{test}$ [kN.m]	$M_{pr}$ [kN.m]	$M_{est}/M_{est}$	$M_{pr}/M_{est}$	
[3.5]	R	1000	150	135	0.9	50	175	0.57	8	2.0	2	205	500	500	--	192.0	200.1	--	0.96
[3.4]	L1							0	1.5					--	43.4	42.1	42.6	1.02	0.98
[3.24]	11B3x70R	150	250	237	0.66	50	275	0.37	8	$\epsilon_y$	2	210	594	710	70.2	68.9	69.9	1.00	0.99

## 4 Punching shear resistance

### 4.1 Composite failure criterion

Experimental campaigns on composite elements (beams and slabs) submitted to combined bending and shear [3.2, 4] demonstrated that the layer of UHPFRC hinders the opening of the shear crack by carrying part of the shear force. This allows more global bending deformation to occur in the RC section prior to failure. The layer of UHPFRC contributes to the shear resistance by out-of-plane bending resistance.

Based on the assumptions of the sector model (Figure 2) which describes the bending behavior of the slab, it is supposed that over the column the reinforcement layers (steel rebars and UHPFRC layer) are mobilized both in tangential and radial direction for the bending resistance of the slab. The UHPFRC shear resistance will thus develop outside the inclined shear crack where radial moments rapidly decrease and the bending efforts are mainly carried in the tangential direction.

As explained in [3.30], the shear crack does not propagate through the layer of UHPFRC. Therefore, the UHPFRC layer follows the rotational movement of the RC rigid body by bending out-of-plane in double curvature. This activates radial moment resistance in the layer (Figure 7). This out-of-plane bending mechanism creates tensile stresses in the concrete, perpendicularly to the layer, which can lead to the horizontal development of limited NIC in the concrete volume between the UHPFRC and the top rebar layers. This double-curvature bending mechanism in the layer is analogous to dowel action of rebars along a shear crack. The bar bends to follow the shear movement of the crack. This bending is accompanied by a debonding process between the bar and the concrete.

At a given rotation  $\psi$ , the total resistance of the slab to punching shear  $V_R$  is the superposition of the concrete contribution  $V_c$  and the UHPFRC layer contribution  $V_U$ :

$$V_R(\psi) = V_c(\psi) + V_U \quad (17)$$

The punching shear resistance of the composite slab is found at the intersection between the composite failure criterion  $V_R(\psi)$  and the force-rotation curve. The contribution of each component of this composite criterion is described in the following sections.

### 4.2 Concrete contribution

Many models exist to describe the punching shear resistance of a RC slab [3.8] and could be used with the proposed formulation for the UHPFRC contribution. As it is the basis of the punching shear resistance calculation in the *fib* Model Code 2010 [3.13], the CSCT failure criterion is used here [3.12]. According to this theory, the punching shear resistance of the RC section depends on its state of deformation due to bending [3.12] which is characterized by the global rotation of the slab  $\psi$ . The failure criterion is semi-empirical and calculates the punching shear resistance of a RC slab as a function of its rotation.

$$\frac{V_c}{b_0 d_{sc} \sqrt{f_c}} = \frac{3/4}{1 + 15 \frac{\psi d_{sc}}{a_{g0} + a_g}} \quad (18)$$

In the CSCT failure criterion, it is assumed that the punching shear resistance of a RC slab decreases with increasing rotations. It is also supposed that the deformations in the slab are directly proportional to its rotation. The size effect of the slab is implicitly taken into account by this criterion.

**4.3 UHPFRC layer contribution**

The out-of-plane bending resistance mechanism of the UHPFRC layer activates at the mouth of the inclined shear crack, at radius  $r_U$ , measured at the top of the slab and assumed to be at a distance  $h_c+h_U$  of the column side. Due to this bending mechanism, tensile stresses develop perpendicularly to the interface between the UHPFRC layer and the concrete. These tensile stresses must reach the tensile strength of concrete  $f_{ct}$  before NIC starts developing. As experimental observations showed that NIC close to the mouth of the inclined shear crack is very limited prior to failure [3.2], the maximum contribution of the UHPFRC layer to the global shear resistance  $V_U$  thus depends on  $f_{ct}$  (Figure 7) which controls the development of NIC.

To activate the out-of-plane bending resistance, a minimum length equal to the height of the UHPFRC layer  $h_U$  is needed [3.30]. With this assumption, the contribution of UHPFRC to punching shear resistance is obtained by equilibrating the efforts on the small UHPFRC sector element (Figure 7):

$$V_U = 2\pi \cdot f_{ct} \cdot h_U \cdot \left( r_U + \frac{h_U}{2} \right) \tag{19}$$

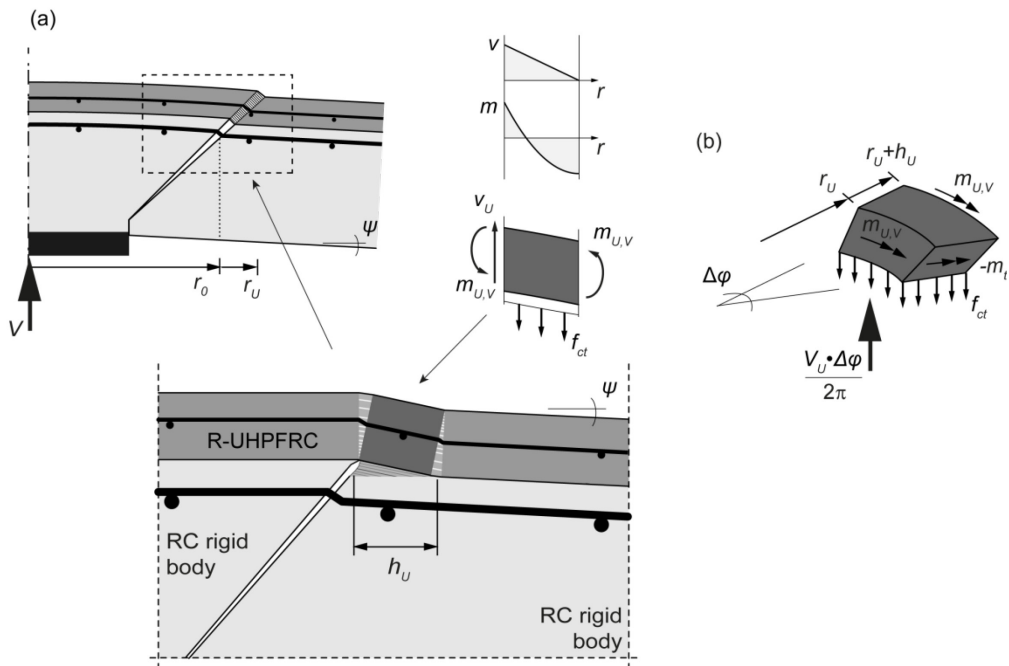


**Figure 7 UHPFRC resisting mechanism**

It must then be verified that the bending efforts  $m_{U,V}$  created in the layers by this resisting mechanism do not exceed the maximum bending resistance of the layer  $m_{UR}$ . These bending efforts in the layer are also obtained by equilibrium of the forces and moment over the small UHPFRC sector element. To simplify this equation, the conservative assumption that the

tangential moments  $m_i$  do not significantly contribute to the punching shear resistance is made.

$$m_{U,V} = \frac{h_U^2 f_{ct}}{4} \leq m_{UR} \quad (20)$$

The bending resistance of the layer  $m_{UR}$  is obtained with a plane section analysis. For typical thickness of the UHPFRC layer and concrete tensile strength, this bending resistance is rarely reached for punching shear resistance. Thus, the steel rebars in the layer do not yield and, as was observed experimentally [3.2], the amount of steel rebars does not influence the maximum punching shear resistance of the composite slab. However, the moment induced in the layer by the out-of-plane bending efforts is higher than the elastic limit of the top fiber of the UHPFRC layer. Its hardening capacity is thus activated even if the maximum bending resistance is not reached as illustrated in Figure 8.

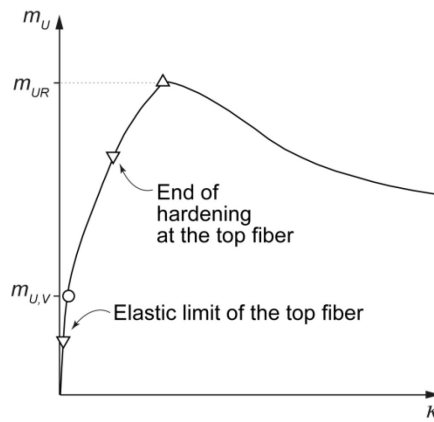


**Figure 8 Moment-curvature behavior of an R-UHPFRC layer**

#### 4.4 Validity of the model

The final equation used to obtain the UHPFRC contribution (equation 19) does not directly consider its material properties or the effect of the global slab rotation on the proposed mechanism. In the following, the conditions for the validity of the proposed model are given.

The material properties of UHPFRC are needed for the proposed bending mechanism to develop. The following conditions in particular need to be fulfilled, which is the case for a standard UHPFRC:

1. A good bond between the new layer and the concrete is ensured. NIC thus develops in the concrete itself and depends on the tensile strength of the latter.
2. The new layer must have rigidity higher than the rigidity of the existing concrete. This will prevent the inclined shear crack from propagating through the layer.
3. The new layer must have a hardening behavior in tension. This ensures that rigidity of the layer is preserved even once it has reached its elastic tensile limit.

Moreover, it should be noted that, as shown in paragraph 3.2.2, the tensile properties of UHPFRC also have a strong influence on the bending deformations of the composite slab and on the global force-rotation behavior of the slab. The UHPFRC tensile properties thus also influence the concrete contribution to punching shear resistance.

Equation 19 calculates a constant contribution of the UHPFRC layer regardless of the state of bending deformation of the composite slab as it is done for the concrete contribution (equation 18). It is assumed that the displacements to activate the out-of-plane bending mechanism and thus the tensile strength of concrete are very small and that the proposed relation is also valid for very rigid slabs.

This model was developed based on observations made on composite slabs with a ratio between the height of the UHPFRC layer and that of the RC section is between 0.1 and 0.3 and a thickness of the layer between 23 and 50 mm. For thickness ratios higher than 0.3, other shear carrying mechanism can activate, but the relation presented here should present a conservative first estimation.

#### **4.5 Punching shear failure and post-peak resistance**

Prior to failure, experimental observations showed that the UHPFRC layer had an upward movement over the column [3.2]. On the slab cuts done after the punching shear failure, it could be seen that this movement was accompanied by limited NIC over the column. This is mainly due to the bending efforts in the slab which are maximal over the column.

Final failure is triggered by the failure of the RC section. The compression strut that carries the shear is weakened by the transversal tensile strains due to bending. The failure of the RC section happens when the state of strains reaches a critical value [3.31]. Once the RC section fails, the UHPFRC layer cannot carry the entire shear force alone and the whole slab fails.

After failure, the tensile strength of concrete at the interface with the UHPFRC layer is exceeded and NIC will be free to propagate, as was observed on the slab cuts done after failure [3.2]. The post-peak carrying capacity is provided by the UHPFRC layer and the top and bottom reinforcement in the RC section. These elements provide shear support by bending of the UHPFRC layer and dowel action of the rebars.

## **5 Model validation**

### **5.1 Slab specimens**

#### **5.1.1 Geometry**

In a previous experimental campaign, six composite slabs were tested under point forces [3.2]. The SAMD slab series was originally tested by Wuest [3.32] and consist of 2×2 m slabs with a total thickness of 200 mm. The PBM series were larger 3×3 m slabs with a total thickness of 260 mm. The parameters of these two test series, other than the slab size, were the thickness of the UHPFRC layer and the reinforcement ratio in it. The RC section of all

slabs had a longitudinal reinforcement ratio of 0.75% and no transverse reinforcement. The main parameters for each slab are detailed in Table 5.

The sector model used to calculate the force-rotation behavior and the failure criterion are derived for an axisymmetric slab. The geometry of the square test slab has to be converted from a square to a circle (Figure 9). In order to have the same shear stresses for both column shape (round or circle), an equivalent perimeter is used for both type of columns [3.27]. The radius of the slab  $r_s$  and the radius of the force introduction points  $r_q$  are calculated so that the flexural resistance of the slab is the same for both cases, as proposed in [3.28].

**Table 5 Parameters of composite slab test series [3.2]**

Slab	Geometry				Steel in RC		Steel in UHPFRC			
	$B$ [mm]	$c$ [mm]	$h_c$ [mm]	$h_U$ [mm]	$d_{sc}$ [mm]	Layout [mm]	Type	Layout [mm]		
SAMD1*	2000	200	150	50	136	Ø14@150	High strength	Ø10@150		
SAMD2*			172	23						
PBM1							--	--		
PBM2	3000	260	210	50	180	Ø16@150	Standard	Ø8@150		
PBM3									High strength	Ø8@150
PBM4							235	25	210	Ø16@125

\*Tested by [3.32]

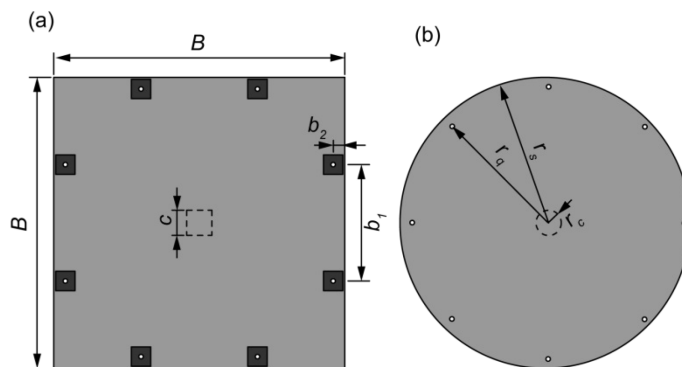


**Figure 9 Geometry for (a) square test slab; (b) axisymmetric circle slab.**

### 5.1.2 Material properties

The material properties used in the models are given in Table 6. All specimens were fabricated with conventional concrete with a maximum aggregate size of 16 mm. The average modulus of elasticity and compressive strength are given by slab series. For the exact values measured from standardized tests for the concrete of each slab, refer to [3.2]. The tensile strength of concrete was estimated using the equations proposed in the *fib* Model Code 2010 [3.13].



The RC section of all slabs was fabricated using standard hot rolled steel rebars with nominal yield strength of 500 MPa, which was also used in the UHPFRC layer of slab PBM2. The UHPFRC layers of slabs SAMD1 and PBM3 were reinforced with high strength steel with yield strength higher than 750 MPa. The exact steel properties used in the models are given in Table 6.

The UHPFRC layer of SAMD series was made with mix CM22 which contained 10-mm long straight steel fibres and steel wool. This CM22 mix is part of the CEMTEC<sub>multiscale</sub>© family of UHPFRCs [3.33]. The tensile properties of UHPFRC CM22 were measured with individually cast specimens [3.32].

For the PBM series, the UHPFRC layer was fabricated with an industrial premix named S3-13 and containing 13-mm long straight steel fibers. This material was submitted to an extensive characterization campaign described in details in [3.17]. Specimens were either cast individually or cut from larger plates. The latter tests were done to capture the variability of fiber orientations and related tensile properties in a plate or layer of UHPFRC. With these test results and some theoretical consideration, it was possible to deduce the average orientation factors in the two orthogonal directions for plates with thicknesses of between 25 and 50 mm.

**Table 6 Average material properties [3.2]**

Concrete								
Slab	$E_c$ [GPa]	$f_c$ [MPa]	$f_{ct}$ [MPa]					
SAMD1-2*	33.7	49.0	3.6 <sup>y</sup>					
PBM1-4	27.4	36.7	2.8 <sup>y</sup>					
Steel								
Type	$E_s$ [GPa]	$\emptyset$ [mm]	$f_{sy}$ [MPa]					
High strength	210	8	772					
		10	937					
Standard	210	8	532					
		14	526					
		16	546					
UHPFRC								
Type	Slab	Elastic		Hardening		Softening		
		$E_U$ [GPa]	$f_{Uie}$ [MPa]	$\varepsilon_{Uiu}$ [%]	$f_{Uiu}$ [MPa]	$w_{U,i}$ [mm]	$f_{U,i,S1}$ [MPa]	$w_{U,i,max}$ [mm]
CM22*	SAMD1	50.0	8.0	1.4	11.5	1.4	2.3	5
	SAMD2		9.5	1.3	12.8	1.4	2.6	5
S3-13	PBM1-3		5.7	2.1	8.7	1.9	1.7	6.5
	PBM4		6.9	2.6	10.1	1.9	2.0	6.5

<sup>y</sup> Calculated according to the *fib* Model Code 2010 [3.13]

\* Material properties obtained from [3.32]

The tensile behaviours of the UHPFRC mix CM22 and S3-13 were scaled according to the fiber orientation expected for a layer of UHPFRC. Table 6 gives the estimated average

tensile properties for each mix and layer thickness. The maximum tensile strength  $f_{Utu}$  varies by 14 to 17% between the two orthogonal directions, the strongest direction being the direction of casting. The influence of varying tensile properties in the 2 main directions is discussed later.

### 5.2 Results

The previously described sector model with the multilinear moment-curvature relation for composite slabs was used to predict the force-rotation curve of the tested slabs. It is then combined with the composite failure criterion, as shown in Figure 10. These calculations were done with the average UHPFRC tensile properties. There is a good agreement between the predicted and the measured force-rotation curves for all slabs. The average ratio between the predicted punching shear resistance  $V_R$  and the measured one  $V_{R,test}$  is 1.01 for the 6 slabs (Table 7). The prediction is always within a range of  $\pm 5\%$  of the measured force. The UHPFRC layer accounts for 18% of the punching shear resistance for a 25 mm layer and for at least 34% of the resistance for a 50 mm layer.

The direct method to estimate the force-rotation curve of the slabs presented in paragraph 3.3 was also used in combination with the composite failure criterion to predict the punching shear resistance of the slabs ( $V_{R,dir}$ ). The predictions were still in a range of  $\pm 9\%$  of the measured force.

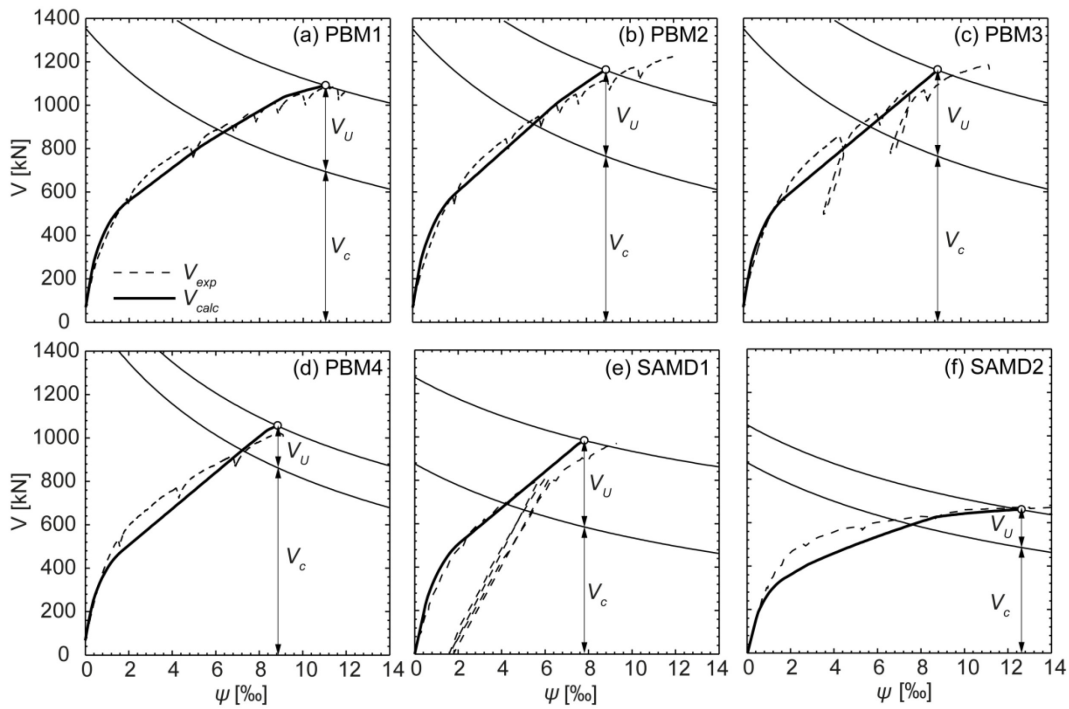


**Figure 10 Experimental force-rotation curves versus model predictions**

The force-rotation behavior as well as the corresponding punching shear resistance was calculated with the UHPFRC tensile properties expected for each orthogonal direction. The difference in the final punching shear resistance calculated with the strongest and the weakest properties was under 6%. Thus, the use of the average properties is the most

suitable solution as it also takes into account the capacity of stress and deformation redistribution of UHPFRC [3.34].

**Table 7 Experimental test results versus model predictions**

Slab	$V_{R, test}$ [kN]	$V_R$ [kN]	$V_{R, test}/V_R$	$V_{R, dir}$ [kN]	$V_{R, test}/V_{R, dir}$	$V_c$ [kN]	$V_c/V_R$	$V_U$ [kN]	$V_U/V_R$	$m_{U,V}$ [kN.m/m]	$m_{U,R}$ [kN.m/m]	$m_{U,V}/m_{U,R}$
<b>SAMD1</b>	971	984	0.99	969	1.00	585	0.59	398	0.41	2.3	17.3	0.13
<b>SAMD2</b>	675	661	1.02	719	0.94	487	0.74	174	0.26	0.5	2.4	0.20
<b>PBM1</b>	1089	1090	1.00	1117	0.97	694	0.64		0.36		8.1	0.22
<b>PBM2</b>	1223	1163	1.05	1165	1.05	767	0.66	396	0.34	1.8	12.3	0.14
<b>PBM3</b>	1186	1160	1.02	1186	1.00	764	0.66		0.34		14.2	0.12
<b>PBM4</b>	1023	1056	0.97	1126	0.91	864	0.82	193	0.18	0.4	2.3	0.19

Table 7 also gives the moment induced in the UHPFRC layer by the out-of-plane bending efforts  $m_{U,V}$  as well as the maximum bending resistance of the layer  $m_{UR}$ . For the thinner layers of 25 mm (slabs PBM4 and SAMD2) as well as the 50-mm layer without reinforcement (PBM1), the moment needed in the layer to contribute to the punching shear resistance corresponds to over 37% of its maximum bending moment resistance. For the slabs with R-UHPFRC layers, this moment corresponds to less the 28% of the maximum bending moment resistance.

## 6 Post-installed UHPFRC layer

### 6.1 Overview

When placing post-installed shear reinforcement in an existing slab, it can be justified to partially unload the structure (for example by propping up) to activate the new shear reinforcement [3.35, 36]. Placing a layer of UHPFRC over an existing slab can however be done with the slab still supporting its self-weight, since the UHPFRC does not need to be pre-deformed to activate its shear resistance.

Under its self-weight, the existing slab is already deformed and the concrete may be partially cracked. These pre-existing deformations should be taken into account when designing the UHPFRC reinforcement as they can modify the force-rotation behavior of the slab [3.36, 37] and affect the concrete contribution to the punching shear resistance.

### 6.2 Moment-curvature relations

The simplified moment-curvatures of a RC section and a RU-RC composite section (Figure 5, paragraph 3.2) can be combined as it was done for a reinforcement using fiber reinforced polymers [3.37]. It is supposed that the layer of UHPFRC is installed once the concrete has already cracked. As illustrated in Figure 11, two cases can thus occur: (1) the layer is installed prior to the yielding of the top reinforcement in the concrete section; (2) the layer is installed after the yielding of the rebars in the concrete section. This first case is the common case that can be found in current reinforcement case. In the second case, it is possible that the rebars in the concrete section reach their ultimate failure strain before the maximum bending moment. If not, the maximum bending moment of the new composite RU-RC section,  $m_{R,RU-RC}$ , is the same for both cases. Only the rigidity of the section is modified. It is the resistance of the UHPFRC layer that governs the maximum bending moment, which is reached when all the layers of tensile reinforcement have yielded (point D in Figure 5b and Figure 11).

Prior to the casting of the new UHPFRC layer, the behavior of the section can be described using the quadrilinear moment-curvature relation [3.12] (paragraph 3.2.1). When the layer of UHPFRC is installed, the rebars in the concrete section are already stressed ( $\sigma_{sc}$ ) and the curvature of the section,  $\kappa_{add}$  is:

$$\kappa_{add} = \frac{\sigma_{sc}}{E_s(d_{sc} - x_{cr})} \quad (24)$$

Due to this pre-existing curvature, there is a strain difference ( $\Delta\varepsilon_U$ ) between the top fiber of concrete and the UHPFRC layer which is taken into account when calculating the behavior of a composite section with a post-installed layer (Figure 11):

$$\Delta\varepsilon_U = \kappa_{add}(h_c - x_{cr}) \tag{25}$$

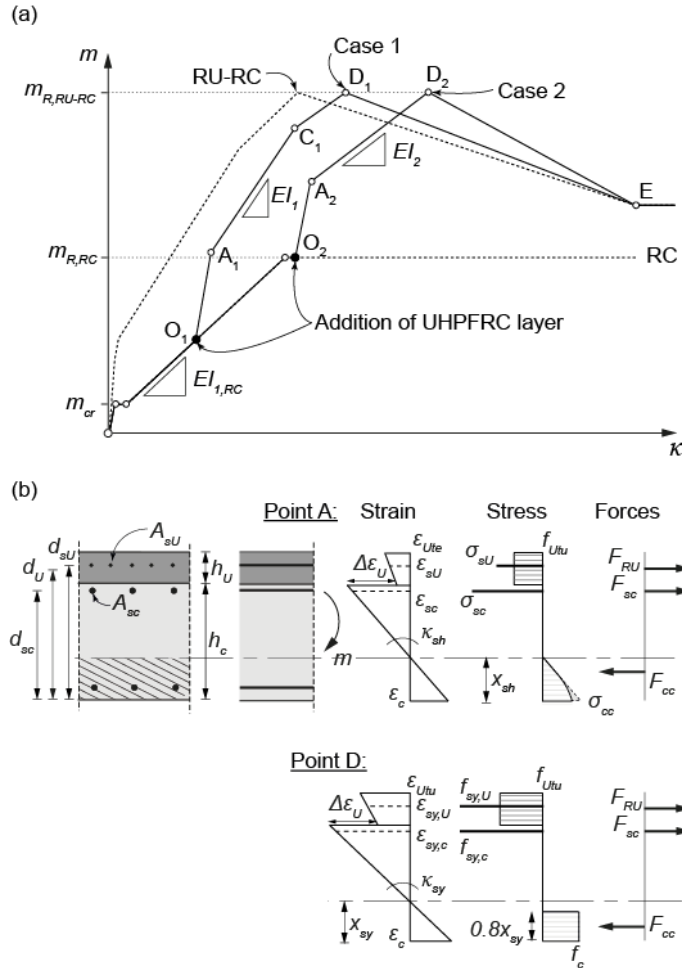


**Figure 11 (a) Moment-curvature relation for a composite section with a post-installed UHPFRC layer; (b) Related sectional distributions of strains, stress and forces**

Once the layer of UHPFRC installed, the behavior of the composite section goes through phases similar to the ones described in paragraph 3.2.2. The modified expressions for the moment-curvature relation are given in Table 8 and Table 9 and are described here:

1. Elastic phase (from point O to A): The UHPFRC layer is elastic. This phase ends at point A when the layer reaches its elastic tensile limit  $f_{Ute}$ . For case 1, the steel in the concrete section has not yet yielded.
2. Hardening phase (from point A to D): The UHPFRC layer is in hardening. For case 1, the steel in the concrete section yields at point  $C_1$ .

Point D for both cases is calculated with the equations given in Table 2 and Table 3. However, since the steel in the RC section has already yielded, the curvature  $\kappa_{sy}$  is

calculated with  $f_{ys,U}$  or  $\varepsilon_{Ut}$ . The height of the compression zone  $x_{cy}$  is obtained with equation 14, considering an equivalent stress block distribution. It should also be verified that the compressive strain at the bottom fiber of the concrete section does not exceed 3.5‰.

### 6.3 Force-rotation behavior and punching shear failure

The force-rotation relation is obtained with equation 6. The first part of the curve is calculated using the RC moment-curvature relation. With the rotation at the instant of addition of the UHPFRC layer,  $\psi_{add}$ , the stress in the rebars over the column  $\sigma_{sc}$  and the curvature at radius  $r_0$ ,  $\kappa_{add}$ , is known:

$$\kappa_{add} = -\frac{\psi_{add}}{r_0} \quad (26)$$

The rest of the force-rotation curve is calculated using the moment-curvature relation for composite sections with a post installed UHPFRC layer.

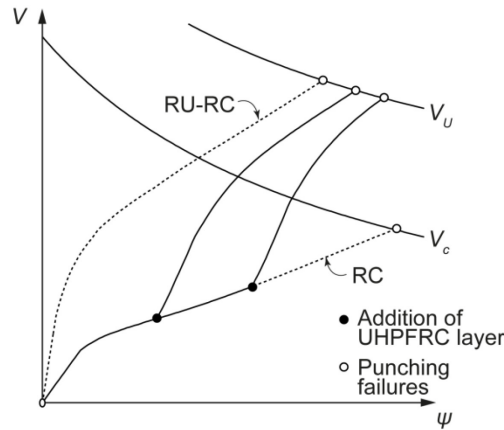


**Figure 12 Force-rotation behavior for a composite section with a post-installed UHPFRC layer**

Figure 12 shows that, as expected, the addition of a layer of UHPFRC increases the rigidity and the punching shear resistance of a RC slab. Regardless of the pre-existing state of deformation in the RC slab, the increase in punching shear resistance due to the shear carrying capacity of the UHPFRC layer ( $V_U$ ) is constant. However, these pre-existing deformations can slightly reduce the contribution of the concrete section ( $V_c$ ) which depends on the state of bending deformation in the slab. These pre-existing deformations can be taken into account with the combined multilinear moment relation curvature (Figure 11) however, for most cases the effect on the final punching shear resistance is small. Moreover, unloading-reloading cycles prior to the addition of the layer can create a rotation increase which also affects the concrete contribution to the punching shear resistance. These cycles can be taken into account with the procedure proposed in [3.36].

**Table 8 Modified expressions for the multilinear moment-curvature relation of composite section with a post-installed UHPFRC layer**

Pts	Moments $m$	Curvature $\kappa$	Height of compression zone $x$
$A_1$	$m_{sh} = F_{sc}(d_{sc} - x_{sh}/3) + (F_{su} + F_{ute}) \cdot (d_{su} - x_{sh}/3)$	$\kappa_{sh} = \left( \frac{f_{ute}}{E_U} + \Delta\varepsilon_U \right) \cdot \frac{1}{\beta(h_c - x_{sh})}$ $\kappa_A = \kappa_{sh} - \kappa_{ts}$	$x_{sh} = \frac{-F_{x,T} + \sqrt{F_{x,T}^2 + 2S_0(F_{x,sc}d_{sc} + (F_{su} + F_{ute})h_c)}}{S_0}$
$A_2$			$x_{sh} = \frac{-F_T + \sqrt{F_T^2 + 2S_0F_T h_c}}{S_0}$
C	$m_{sy,c} = F_{sc2} \left( d_{sc} - \frac{x_{sy}}{3} \right) + (F_{su2} + F_{2U}) \cdot \left( d_{su} - \frac{x_{sy}}{3} \right)$	$\kappa_{sy,c} = \frac{f_{sy,c}}{\beta E_s (d_{sc} - x_{sy})}$ $\kappa_C = \kappa_{sy,c} - \kappa_{ts}$	$x_{sy,c} \approx x_{sh}$

**Table 9 Equation of forces on the composite section with a post-installed UHPFRC layer**

Points	Forces F	Other parameters
A1	$F_{x,T} = F_{x,sc} + F_{sU} + F_{Ute}$	
	$F_T = F_{sc} + F_{sU} + F_{Ute}$	
	$F_{x,sc} = \left(\frac{f_{ute}}{E_U} + \Delta\varepsilon_U\right) E_s \rho_{sc} d_{sc}$	
	$F_{sc} = \kappa_{sh} E_s \rho_{sc} d_{sc} (d_{sc} - x_{Ut})$	
	$F_{sU} = \frac{f_{Ute}}{E_U} E_s \rho_{sU} d_{sU}$	$S_0 = E_c \left(\frac{f_{ute}}{E_U} + \Delta\varepsilon_U\right)$
	$F_{Ute} = f_{Ute} h_U$	
A2	$F_T = F_{sc} + F_{sU} + F_{Ute}$	
	$F_{sc} = f_{sy,c} \rho_{sc} d_{sc}$	
	$F_{sU} = \frac{f_{ute}}{E_U} E_s \rho_{sU} d_{sU}$	
	$F_{Ute} = f_{Ute} h_U$	
C	$F_{T2} = F_{sc2} + F_{sU2} + F_{U2}$	
	$F_{sc2} = f_{sy,c} \rho_{sc} d_{sc}$	
	$F_{sU2} = (\kappa_{sy,c} (h_c - x_{sy,c}) - \Delta\varepsilon_U) E_s \rho_{sU} d_{sU}$	
	$F_{U2} = (\kappa_{sy,c} (h_c - x_{sy,c}) - \Delta\varepsilon_U) E_{Ush} h_U + F_{Ute}$	

## 7 Conclusions

Using well known models for RC slabs as a basis, it was possible to develop a composite model to predict the force-rotation behavior and the punching shear resistance of a composite R-UHPFRC – RC slab. The proposed composite model is in good agreement with test results. The following points can be highlighted:

1. A multilinear moment-curvature relation is used with the sector model to predict with sufficient precision the force-rotation behavior of a slab submitted to a point force. This relation can also be used for the resistance calculation of members submitted to bending.
2. The UHPFRC layer contributes to the punching shear resistance by bending out-of-plane in double curvature which mobilizes the radial bending resistance of the layer. This mechanism creates tensile stresses perpendicularly to the interface with the concrete. The effectiveness of this resisting mechanism thus depends on the tensile strength of the concrete. As only limited NIC was observed in the tested slabs prior to punching failure, it is assumed that this mechanism is activated over a very short length.
3. The contribution of a UHPFRC layer to the punching shear resistance is expressed by a simple relation which depends on the thickness of the layer and on the tensile strength of the concrete. The tensile properties of UHPFRC are considered implicitly. The new layer must provide a good bond with the concrete substrate, have a high rigidity and a tensile hardening behavior.



4. A composite section has the same maximum bending resistance regardless of pre-existing deformation of the concrete slab to be strengthened by a UHPFRC layer. The maximum bending resistance is reached when all the layers of tensile reinforcement have yielded in the section. The punching shear resistance of a composite slab will be slightly decreased by pre-existing deformations in the concrete slab. However, the effect is considered to be small.

## 8 References

- [3.1] Brühwiler E, Denarie E. Rehabilitation and Strengthening of Concrete Structures Using Ultra-High Performance Fibre Reinforced Concrete. *Structural Engineering International*. 2013;23(4):450-7.
- [3.2] Bastien-Masse M, Brühwiler E. Experimental Investigation on Punching Resistance of R-UHPFRC – RC Composite Slabs. *Materials and Structures*. 2015: doi:10.1617/s11527-015-0596-4.
- [3.3] Habel K, Denarie E, Brühwiler E. Experimental investigation of composite ultra-high-performance fiber-reinforced concrete and conventional concrete members. *ACI Structural Journal*. 2007;104(1):93-101.
- [3.4] Noshiravani T, Brühwiler E. Experimental investigation on reinforced ultra-high-performance fiber-reinforced concrete composite beams subjected to combined bending and shear. *ACI Structural Journal*. 2013;110(2):251-61.
- [3.5] Habel K, Denarie E, Brühwiler E. Structural Response of Elements Combining Ultrahigh-Performance Fiber-Reinforced Concretes and Reinforced Concrete. *Journal of Structural Engineering*. 2006;132(11):1793-800.
- [3.6] Noshiravani T, Brühwiler E. Analytical Model for Predicting Response and Flexure-Shear Resistance of Composite Beams Combining Reinforced Ultrahigh Performance Fiber-Reinforced Concrete and Reinforced Concrete. *Journal of Structural Engineering*. 2014;140(6):04014012 (10 pp.).
- [3.7] fib. Punching of structural concrete slabs. *fib Bulletin No. 12*. Lausanne: Fédération Internationale du Béton; 2001; 314 p.
- [3.8] Koppitz R, Kenel A, Keller T. Punching shear of RC flat slabs - Review of analytical models for new and strengthening of existing slabs. *Engineering Structures*. 2013;52:123-30.
- [3.9] Kinnunen S, Nylander H. Punching of concrete slabs without shear reinforcement. *Transactions of the Royal Institute of Technology No.158*. Stockholm:1960; 112 p.
- [3.10] Hallgren M. Punching shear capacity of reinforced high strength concrete slabs. *Doctoral thesis Trita-BKN Bull. No. 23*. Stockholm: Royal Institute of Technology; 1996; 206 p.
- [3.11] Broms CE. Concrete flat slabs and footings - design method for punching and detailing for ductility. *Doctoral thesis Trita-BKN Bull. No. 80*. Stockholm: Royal Institute of Technology; 2005; 114 p.
- [3.12] Muttoni A. Punching Shear Strength of Reinforced Concrete Slabs without Transverse Reinforcement. *ACI Structural Journal*. 2008;105(4):440-50.
- [3.13] fib. *Model Code for Concrete Structures 2010*. Fédération Internationale du Béton ed. Lausanne: Ernst & Sohn; 2013; 434 p.
- [3.14] SIA. SN 505 262 : Construction en béton. Zurich: Société suisse des Ingénieurs et Architectes; 2013.

- [3.15] Graybeal BA. Compressive Behavior of Ultra-High-Performance Fiber-Reinforced Concrete. *ACI Materials Journal*. 2007;104(2):146-52.
- [3.16] AFGC. Ultra High Performance Fibre-reinforced Concretes – Recommendations. Paris: Association Française de Génie Civil; 2013; 358 p.
- [3.17] Bastien-Masse M, Denarié E, Brühwiler E. Effect of fiber orientation on the in-plane tensile response of UHPFRC reinforcement layers. Submitted to *Cement and Concrete Composites*. [Research paper]. 2015.
- [3.18] Marti P, Alvarez M, Kaufmann W, Sigrist V. Tension Chord Model for Structural Concrete. *Structural Engineering International*. 1998;8(4):287-98.
- [3.19] Sigrist V. Zum Verformungsvermögen von Stahlbetonträgern. Doctoral thesis ETHZ no. 11169. Zürich, Switzerland: ETH Zürich; 1995; 160 p.
- [3.20] Pfyl T. Tragverhalten von Stahlfaserbeton. Doctoral thesis ETHZ no. 15005. Zürich: ETH Zürich; 2003; 139 p.
- [3.21] Jungwirth J. Zum Tragverhalten von zugbeanspruchten Bauteilen aus Ultra-Hochleistungs-Faserbeton. Doctoral thesis EPFL no. 3429. Lausanne: Ecole Polytechnique Fédérale de Lausanne; 2006; 158 p.
- [3.22] Redaelli D. Comportement et modélisation des éléments de structure en Béton Fibré à Ultra-Hautes Performances avec armatures passives. Doctoral thesis EPFL no. 4298. Lausanne: Ecole Polytechnique Fédérale de Lausanne; 2009; 290 p.
- [3.23] Leutbecher T, Fehling E. Tensile behavior of ultra-high-performance concrete reinforced with reinforcing bars and fibers: minimizing fiber content. *ACI Structural Journal*. 2012;109(2):253-63.
- [3.24] Oesterlee C. Structural Response of Reinforced UHPFRC and RC Composite Members. Doctoral thesis EPFL no. 4848. Lausanne: Ecole Polytechnique Fédérale de Lausanne; 2010; 136 p.
- [3.25] Rauch M, Sigrist V. Reinforced UHPFRC Tension Chords. 17th IABSE Congress; Septembre 2008; Chicago 2008. p. 352-3.
- [3.26] Carbonell Munoz MA, Harris DK, Ahlborn TM, Froster DC. Bond Performance between Ultrahigh-Performance Concrete and Normal-Strength Concrete. *Journal of Materials in Civil Engineering*. 2014;26(8):04014031 (9 pp.).
- [3.27] Guandalini S. Poinçonnement symétrique des dalles en béton armé. Doctoral thesis EPFL no. 3380. Lausanne: Ecole Polytechnique Fédérale de Lausanne; 2005; 289 p.
- [3.28] Lips S. Punching of flat slabs with large amounts of shear reinforcement. Doctoral thesis EPFL no. 5409. Lausanne: Ecole Polytechnique Fédérale de Lausanne; 2012; 217 p.
- [3.29] Guandalini S, Burdet OL, Muttoni A. Punching tests of slabs with low reinforcement ratios. *ACI Structural Journal*. 2009;106(1):87-95.
- [3.30] Noshiravani T. Structural Response of R-UHPFRC - RC Composite Members Subjected to Combined Bending and Shear. Doctoral Thesis EPFL no. 5246. Lausanne: Ecole Polytechnique Federale de Lausanne; 2012; 188 p.
- [3.31] Vecchio FJ, Collins MP. The Modified Compression-Field Theory for Reinforced Concrete Elements Subjected to Shear. *ACI Journal Proceedings*. 1986;83(2):219-31.
- [3.32] Wuest J. Comportement structural des bétons de fibres ultra performants en traction dans des éléments composés. Doctoral thesis EPFL no. 3987. Lausanne: Ecole Polytechnique Fédérale de Lausanne; 2007; 244 p.

- [3.33] Rossi P. High Performance Multimodal Fiber Reinforced Cement Composites (HPMFRCC): the LCPC Experience. *ACI Materials Journal*. 1997;94(6):478-83.
- [3.34] Makita T, Brühwiler E. Tensile fatigue behaviour of ultra-high performance fibre reinforced concrete (UHPFRC). *Materials and Structures*. 2014;47(3):475-91.
- [3.35] Ruiz MF, Muttoni A, Kunz J. Strengthening of flat slabs against punching shear using post-installed shear reinforcement. *ACI Structural Journal*. 2011;108(3):382-3.
- [3.36] Koppitz R, Kenel A, Keller T. Effect of load history on punching shear resistance of flat slabs. *Engineering Structures*. 2015;90:130-42.
- [3.37] V. Faria DM, Einpaul J, P. Ramos AM, Fernandez Ruiz M, Muttoni A. On the efficiency of flat slabs strengthening against punching using externally bonded fibre reinforced polymers. *Construction and Building Materials*. 2014;73:366-77.



# Paper IV

## Contribution of R-UHPFRC Strengthening Layers to the Shear Resistance of RC Elements

---

**Reference:** Bastien-Masse M, Brühwiler E. Contribution of R-UHPFRC Strengthening Layers to the Shear Resistance of RC Elements. *Submitted to Structural Engineering International on September 30<sup>th</sup> 2015.*

### Abstract

To strengthen a Reinforced Concrete (RC) slab with deficient shear resistance, it has been proposed to add to the top of the slab a layer of 25 to 50 mm thick of Ultra-High Performance Fiber Reinforced cement-based Composite (UHPFRC) with small diameter rebars (R-UHPFRC). This creates a monolithic composite element where the new UHPFRC layer acts as an external tensile reinforcement. The present work will focus on the parameters influencing the shear resistance of R-UHPFRC – RC composite elements and how the layer influences the shear transfer mechanism involved in the RC section. This will be done by presenting the analytical models available to predict the shear and punching shear resistance of a composite section. The test results database on composite elements subjected to shear will be used to verify these models. A parametric study will also be realized to show how the layer of UHPFRC can influence shear resistance. Finally, design examples will be given through examples of slab strengthening using a UHPFRC layer.

**Keywords:** Composite section, Shear resistance, Punching shear resistance, Ultra-High Performance Fiber Reinforced cement-based Composite (UHPFRC), Strengthening, Near interface crack.

## List of Symbols

### Subscripts

$E$	Action effect
$R$	Resistance
$U$	UHPFRC
$c$	concrete
$d$	design value
$e$	effective
$i$	steel or UHPFRC tensile reinforcement
$p$	pin support
$r$	roller support
$s$	steel
$sc$	top steel reinforcement layer in RC section
$sU$	steel reinforcement in the R-UHPFRC layer
$sy$	yielding of steel
$w$	transverse steel reinforcement in the RC section

### Latin upper case

$A$	Area
$B$	side length of slab specimen
$E$	modulus of elasticity
$L$	Floor span
$M$	Moment
$M_{supp}$	Moment at the support of the continuous beam
$Q$	applied force
$T$	Tensile force
$V$	Shear force
$V_{flex}$	Flexural resistance
$V_{test}$	Applied force during a test
$V_{pred}$	Predicted force

### Latin lower case

$a_v$	shear span
$b$	beam width
$b_0$	critical perimeter for punching shear set at $d_{sc}/2$ from the column face
$c$	side length of column
$d$	flexural depth for a tensile reinforcement: distance from the bottom compression face of the slab to the centroid of the tensile reinforcement
$d_{eff}$	effective flexural depth calculated with the mechanical ratio of each tensile reinforcement
$d_g$	maximum diameter of aggregate
$d_{g0}$	reference aggregate size set at 16 mm
$f$	strength of a material
$f_c$	concrete compressive strength
$f_{ct}$	concrete tensile strength
$f_{sy}$	yield strength of steel reinforcement
$f_{Uc}$	UHPFRC compressive strength
$f_{Ute}$	elastic tensile strength of UHPFRC
$f_{Utu}$	tensile strength of UHPFRC
$h$	height
$k_{Ut}$	interaction factor between bending and tensile forces in a UHPFRC element
$l_{NIC}$	Near Interface Cracking length at the UHPFRC – concrete interface

$m$	bending moment per unit width
$q$	uniformly distributed force
$r_0$	radius of inclined crack located at $d_{sc}$ from the column side
$r_s$	radius of circular slab
$r_q$	radius of force introduction at perimeter
$s_w$	spacing of the transverse reinforcement in a member
$v$	shear force per unit width
$w_{c\kappa}$	crack opening in concrete
$w_{Ut}$	crack opening in UHPFRC
$x$	height of the compression zone
<b>Greek lower case</b>	
$\alpha_c$	minimum angle of the inclined shear crack
$\beta$	efficiency factor to take into account the reduced torsional rigidity of orthogonal reinforcement
$\varepsilon$	strain
$\varepsilon_{Ut}$	strain in UHPFRC in tension
$\varepsilon_{Um}$	strain in UHPFRC at maximum tensile strength
$\kappa$	curvature in a cross-section
$\kappa_{TS}$	reduction in the curvature due to tension stiffening
$\rho$	reinforcement ratio
$\sigma$	stress
$\psi$	rotation





## 1 Introduction

Many structural elements are submitted to high shear forces combined with bending moments, such as structural systems with hogging moments (Figure 1). To increase the ultimate resistance of Reinforced Concrete (RC) elements which do not comply with code requirements without increasing significantly the self-weight of the structure, it is possible to add a layer of 25 to 50 mm of Ultra-High Performance Fiber Reinforced cement-based Composite (UHPFRC) with or without small diameter steel reinforcement bars, thus creating a composite section [4.1, 2] (Figure 2a). The layer of UHPFRC serves as a tensile reinforcement for the RC section.

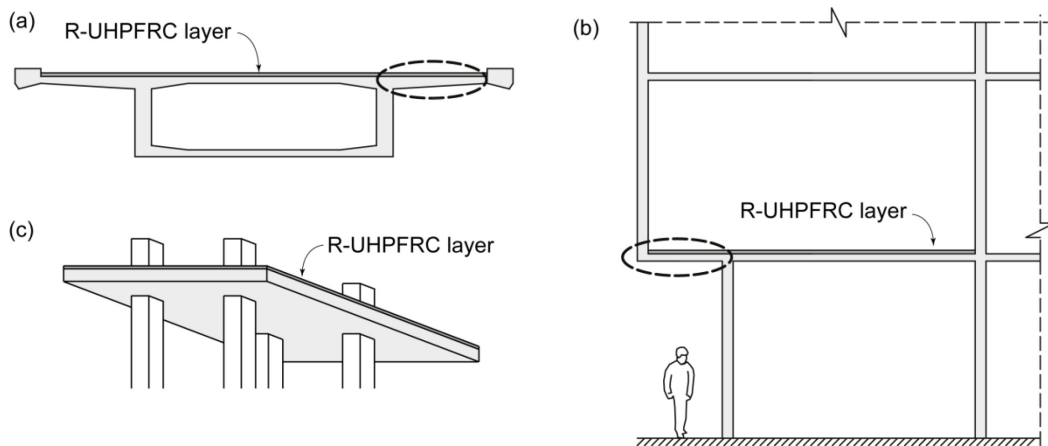


**Figure 1** Example of structures submitted to combined bending and shear: (a) cantilevers on a box girder bridge; (b) cantilever floor in a building; (c) flat slabs on columns

Adding longitudinal tensile reinforcement to a RC section increases as expected its bending resistance. A layer of UHPFRC, thanks to its hardening-softening behavior in tension (Figure 2b) can increase it significantly [4.3, 4]. However, it is less obvious to understand how this added reinforcement can contribute to the shear resistance of the section. A vast experimental investigation was thus undertaken in recent years to study the behavior of composite sections submitted to combined bending and shear [4.5, 6]. Experiments showed that a layer of reinforced UHPFRC (R-UHPFRC or RU) contributes to shear resistance in two ways. First, as a tensile reinforcement, it modifies the shear carrying mechanism of the concrete section. Second, it resists to part of the shear by bending out-of-plane.

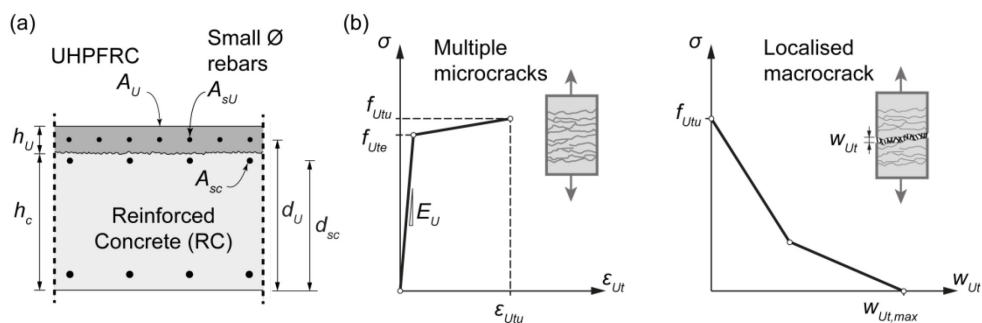


**Figure 2** (a) Typical RU-RC composite cross-section [4.2]; (b) Schematic tensile behavior of UHPFRC [4.7]

Using experimental evidence, analytical models were developed to predict the shear and punching shear resistances of composite members and slabs [4.8, 9] and are presented herein. Based on these models, the influence of material properties and element geometry on the shear resistance of composite slabs and beams is studied and design examples are given. Finally, the similarities and differences between the shear failure mode of a composite beam and the punching shear failure mode of a composite slab are outlined.

## 2 Background

### 2.1 Shear transfer mechanism in RC elements

RC members without shear reinforcement submitted to combined bending and shear first develop vertical bending cracks initiating at the tensile face of the section. The cracked RC section then carries shear through well-known beam shear mechanisms [4.10-12]: (1) friction (or aggregate interlock) and residual tensile strength along the crack; (2) dowel action of the longitudinal reinforcement; and (3) cantilever action of the RC concrete tooth created by two adjacent bending cracks. To these mechanisms is added the shear resistance of the uncracked concrete compression chord also known as direct strut or arching action. As was observed in [4.13], the contribution of each of these mechanisms varies as the shear force increases.

The shear resistance and the mechanisms involved strongly depend on the slenderness of the member defined by the span-to-depth ratio  $a_v/d$ . According to Kani [4.10], for values of  $a_v/d$  below 2.5, shear resistance is governed by arching or direct strut action. For larger values, beam action takes over until the point where bending resistance governs again the behavior of the member.

Beams with higher longitudinal reinforcement ratios have a higher neutral axis in bending and lower longitudinal strains at mid-depth of the section [4.14]. The uncracked concrete compression chord can thus carry more shear and these beams thus have a higher shear resistance but a lower bending deformation capacity [4.12].

In the case of two-way spanning slabs submitted to point forces, shear forces are carried in the radial direction and decrease rapidly along the radius centered at the force introduction point [4.15]. The effective shear span for this loading case is thus rather short and direct strut action governs the punching shear resistance [4.16]. Due to the contribution of the tangential compressive strains to the resistance of the compression zone, larger deformations are observed prior to failure.

### 2.2 Bending behaviour of a composite section

Experimental work carried on composite RU-RC beams showed that the layer of R-UHPFRC contributes to the bending behavior by mobilizing its hardening and softening tensile behavior [4.3, 4]. Based on the experimental observations and analytical work, a multilinear moment-curvature relation is established for composite section [4.9], shown in Figure 3. This model assumes that plane sections remain plane, the composite section is monolithic and the equilibrium of forces and moments is assured on the cross-section. All

expressions to calculate the moment, the curvature and the height of the compression zone related to the different points in Figure 3 can be found in [4.9].

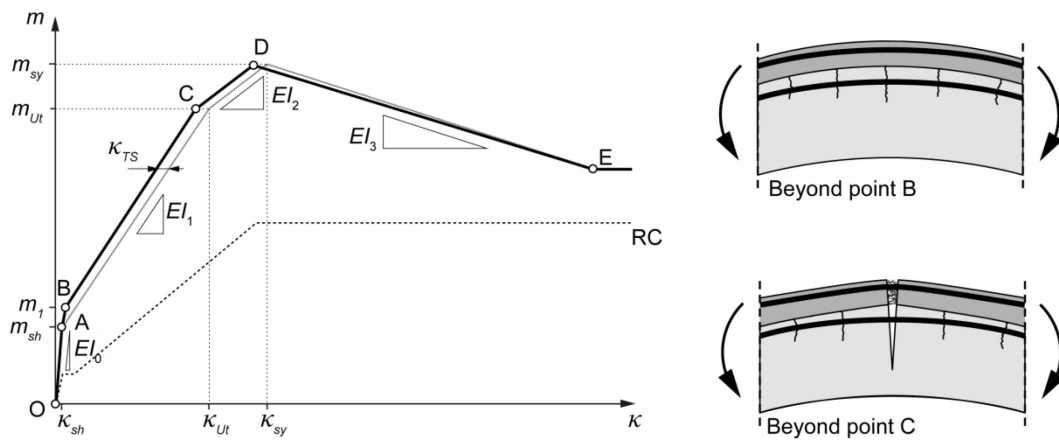


**Figure 3 Multilinear moment-curvature relation for composite RU-RC sections**

Beyond point B in Figure 3, the concrete is cracked and the UHPFRC layer has exceeded its tensile limit strength  $f_{Ute}$  and is hardening (see Figure 2b). Over the vertical macrocracks in the concrete, distributed microcracks develop in the UHPFRC layer. Beyond point C, a macrocrack localizes in the UHPFRC layer in the region of maximal moments. At point D, all the layers of tensile reinforcement in the composite section (UHPFRC, steel rebars in the RC and RU section) have yielded. Maximum bending resistance,  $m_R$ , can be reached at point C or D depending on the ratios of tensile reinforcement.

After point D, the resistance of the section slowly decreases as the UHPFRC layer softens, allowing the stresses to redistribute in redundant continuous structures. The residual bending resistance corresponds to the contribution of the yielded steel rebars. Final ruin happens either by crushing of the concrete in compression or by fractures of the rebars.

### 3 Shear resistance of RU-RC composite members

#### 3.1 Shear transfer mechanism in RU-RC composite members

The contribution of an R-UHPFRC layer to the shear resistance of a composite section was studied through a vast experimental campaign on composite beams tested in a cantilever test setup [4.5]. These tests showed that an R-UHPFRC layer carries part of the shear but also, as a longitudinal tensile reinforcement, improves the efficiency of the shear transfer mechanism in the RC section. As for members with high longitudinal reinforcement ratios, the position of the neutral axis in a composite member is higher than the reference RC beam and the uncracked compression strut can carry more shear.

The development of the critical inclined flexure-shear crack in the RC section of a composite member is delayed when compared to a reference RC beam. The widening of this inclined crack in the RC section creates a prying action on the R-UHPFRC layer which then resists by bending out-of-plane in double curvature, similarly to the dowel action of a rebar. This

induces Near Interface Cracking (NIC) or softening of the concrete below the layer, at the level of the top reinforcement rebars (Figure 4a). The collapse of the composite beam happens with a vertical translational movement and the crushing of the compression zone ahead of the crack tip (Figure 4b). NIC has then completely developed from the mouth of the inclined crack to the force point and plastic hinges have formed in the UHPFRC layer.

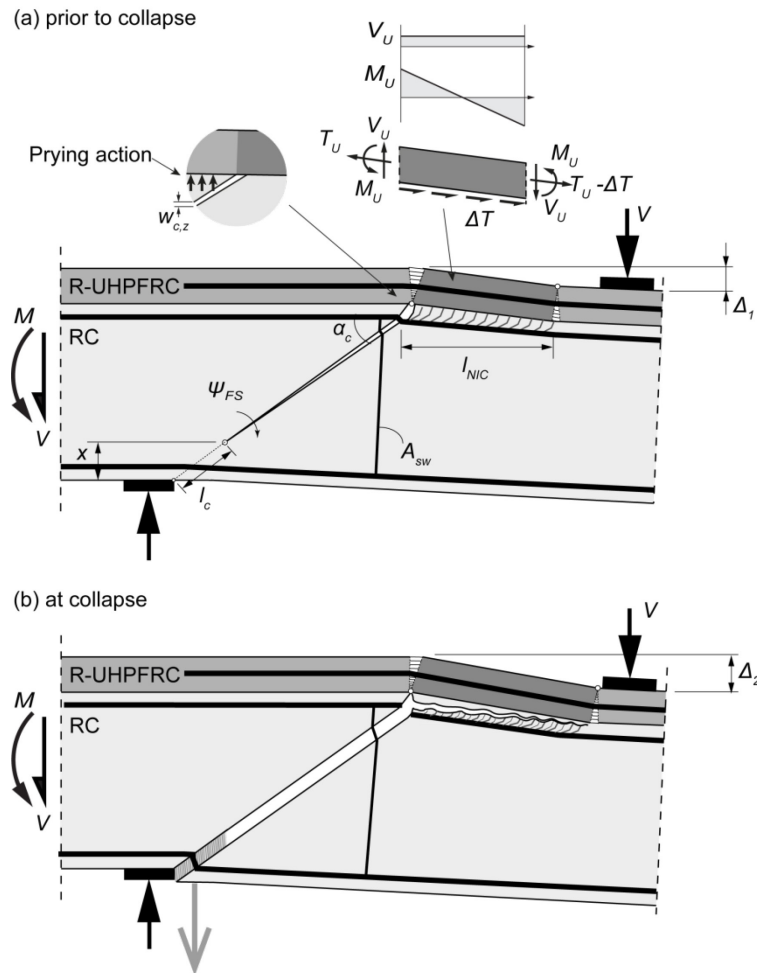


Figure 4 Flexure-shear failure mechanisms of composite RU-RC member, adapted from [4.8]

### 3.2 Analytical model

#### 3.2.1 Overview

Based on the mechanism previously described and the theory of plasticity, Noshiravani [4.8] developed an upper-bound solution to predict the contribution of each component to the shear resistance of a composite member. The shear resistance of a composite beam  $V_R$  is calculated as the sum of contribution of concrete ( $V_c$ ), stirrups in steel ( $V_s$ ) and UHPFRC layer ( $V_U$ ):

$$V_R = V_c + V_s + V_U \quad (1)$$

### 3.2.2 Concrete contribution

The contribution of the concrete  $V_c$  is due to the web crushing mechanism [4.17]. The concrete ahead of the crack tip is crushing along line  $l_c$ . This is accompanied by a vertical downwards translation of the member. Due to the extensive flexural cracking of the member, compressive stresses are mainly carried by the compression zone. The height of the latter reduces until a point when strength of concrete is exceeded and failure occurs [4.8]. The contribution of the concrete is thus obtained with the following equation [4.18]:

$$V_c = \frac{f_{ce}b}{2} \left[ \frac{x}{\sin \alpha_c} (1 - \cos \alpha_c) \right] \quad (2)$$

In this equation, the variables are estimated as follow:

- Effective compressive strength of concrete  $f_{ce}$ : The strength of concrete is reduced by bending cracks in the RC section and  $f_{ce}$  is thus taken equal to  $0.8f_c$ .
- Height of the compression zone  $x$ : In a first approximation,  $x$  is taken equal to the height of the compression zone when maximum bending resistance is reached,  $x_R$ , found with the multilinear moment-curvature relation [4.9]. In the case of the verification of an element where the exact moment distribution is known from a structural analysis, the height of the compression zone over the support corresponding to the applied moment can be considered.
- Angle of the inclined crack  $\alpha_c$  (Figure 4): The angle of the crack corresponds to the angle of the compression strut in the strut and tie analysis. Based on experimental observation [4.5], for most cases, it can be taken equal to  $30^\circ$ .

### 3.2.3 Shear reinforcement contribution

Shear reinforcement crossing the inclined crack contribute to the shear resistance of the member. It is reasonable to consider that the stirrups will yield at failure. The contribution of this reinforcement is calculated with the equation given by the *fib* Model Code 2010 [4.19] and adapted to the case of composite structures:

$$V_s = f_{sy,w} \frac{A_{sw}}{s_w} (d_{sc} - x/3) \cot \alpha_c \quad (3)$$

In this equation,  $A_{sw}$  is the cross-sectional area of the shear reinforcement,  $f_{sy,w}$  is its yield strength and  $s_w$  is the spacing of the shear reinforcement along the member.

### 3.2.4 R-UHPFRC layer contribution

The layer of UHPFRC carries shear by bending out-of-plane and plastic hinges develop in it. Its contribution to shear resistance  $V_U$  is thus a function of its bending resistance  $m_{UR}$ . The maximum contribution of the layer is given by the equilibrium of the efforts on the element over the NIC length  $l_{NIC}$  (Figure 4):

$$V_U = \frac{2m_{UR}b}{l_{NIC}} \quad (4)$$

As NIC is fully developed at the moment of collapse, the NIC length  $l_{NIC}$  is equal to the distance between the mouth of the inclined crack and the point of counter-flexion. To estimate this length, the angle of the inclined crack  $a_c$  has to be known.

The maximum bending resistance of the layer,  $m_{UR}$  is calculated as proposed in [4.8] by supposing that the bottom compressed fiber of the UHPFRC section reaches half its maximum compressive strength  $f_{Uc}$  when the tensile strength of UHPFRC  $f_{Utu}$  has been reached.

$$m_{UR} = f_{sy,U} \rho_{sU} h_U \left( \frac{h_U}{2} - \frac{x_U}{2} \right) + f_{Utu} (h_U - x_U) \left( \frac{h_U}{2} - x_U \right) \quad (5)$$

The height of the compression zone in the layer  $x_U$  is calculated as follow:

$$x_U = \frac{h_U f_{Utu}}{0.5 f_{Uc} + f_{Utu}} \text{ if } \rho_{sU} = 0 \quad (6a)$$

$$x_U = \frac{\rho_{sU} h_U f_{sy,U}}{0.5 f_{Uc}} \text{ if } \rho_{sU} > 0 \quad (6b)$$

### 3.3 Validation with test results

#### 3.3.1 Overview and specimens

A total of 17 composite beams were tested in a cantilever configuration [4.5, 21] and 2 composite beams in a continuous configuration [4.22] (Figure 5). The moment distribution for these tests is known and the multilinear moment-curvature relation can be used to evaluate the state of strains and stresses in various cross-sections of these beams as well as the bending resistance. The shear resistance of these beams is calculated with equations 2, 3 and 4.

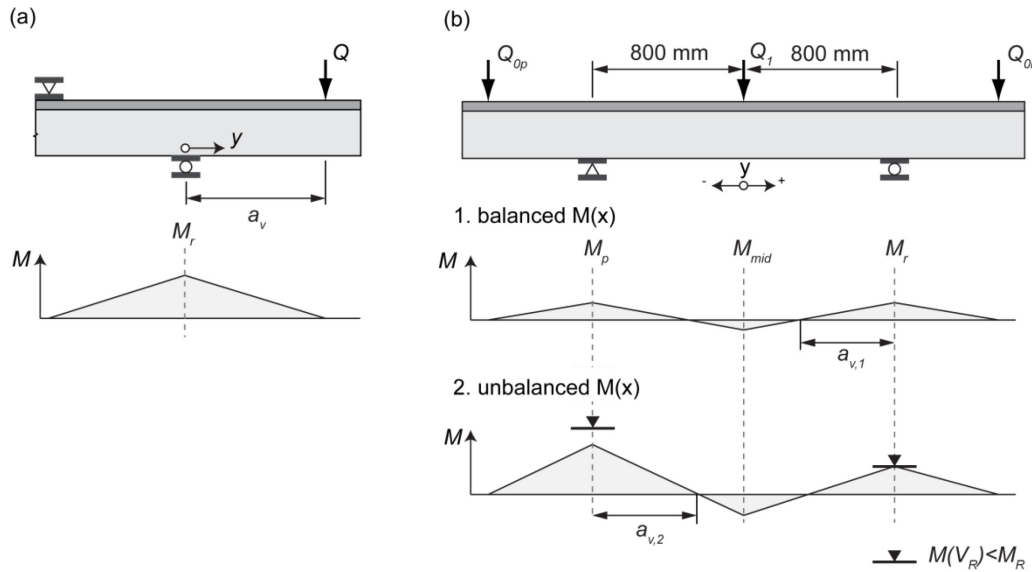


Figure 5 Moment distribution for the two test setups, adapted from [4.5, 22]: (a) cantilever beams; (b) continuous beams

The geometry and steel reinforcement ratios of each specimen (cantilever and continuous) are presented in Table 1. Other than the shear spans, the amount and type of longitudinal reinforcement in the UHPFRC layer was varied as well as the amount of shear reinforcement  $A_w$ . Table 1 gives the total area of shear reinforcement crossing the inclined crack as observed experimentally. The material properties are given in Table 2. The concrete properties were updated to take into account the age at which the beams were tested using the equation proposed in the *fib* Model Code 2010 [4.19]. The steel properties correspond to the tested values. Finally, the UHPFRC properties were also scaled to take into account the effect of fiber orientation as proposed in [4.23]. The UHPFRC layer of the cantilever beams described in [4.5] was cast as a continuous layer on several beams positioned next to each other. By using this casting method, the fiber orientation and the tensile properties are lower than for layers cast individually on each beam, as it is the case for the beams presented in [4.21] and for the continuous beams [4.22].

**Table 1 Geometry and steel ratios of the tested composite beams**

Ref.	Beam	$b$ [mm]	$h_c$ [mm]	$d_{sc}$ [mm]	$\rho_{sc}$ [%]	Steel type RC	$h_U$ [mm]	$d_{sU}$ [mm]	$\rho_{sU}$ [%]	Steel type UHPFRC	$A_{sw}$ [mm <sup>2</sup> ]	$a_v$ [mm]
	L1								0	--	101	
	L2									High, Ø8	1000	
	L3				0.66	Std, Ø10					202	
	MN1								2.68	SmStd, Ø8		
	MN2									SmHigh, Ø8	101	
	MN3				1.33	Std, Ø14				High, Ø8		
	MW1								0	--		
[4.5]	MW2	150	250	237			50	275	2.68	SmStd, Ø8		800
	MW3				0.66	Std, Ø10			2.01	High, Ø8		
	MW4									Std, Ø8	0	
	MW5									SmHigh, Ø8		
	MW6				1.33	Std, Ø14			2.7	High, Ø8		
	SN1									SmStd, Ø8	101	
	SW1				0.66	Std, Ø10				SmStd, Ø8	0	600
	S_L1										101	1000
[4.21]	S_M1	400	170	155	1.30	Std, Ø16	50	195	1.57	Std, Ø10	0	700
	S_S1										450	
	C1r								0	--	0	
[4.22]	C1p	150	250	237	1.33	Std, Ø14	50	275			57	--
	C2r										0	
	C2p								2.68	High, Ø8	57	

Definition of steel types:

- Sm: Rebar with a smooth surface (no ribs)
- Rib: Rebar with a ribbed surface
- Std: Standard strength steel ( $f_{sy} \approx 500$  MPa)
- High: High strength steel ( $f_{sy} \geq 700$  MPa)

### 3.3.2 Cantilever beams

Composite beams were tested in a cantilever test setup with a varying shear length,  $a_v$  (Figure 5). The distance between the roller and the pin support was reinforced with external prestressing to prevent a shear failure outside the cantilever span. Two types of failures were observed during these tests: either a bending failure (F) or a flexure-shear failure (FS). The latter is accompanied by a sudden loss in the resistance of the member. Based on the experimental observation, it is supposed that, even for a flexure shear failure, the maximum bending resistance of the composite section is reached over the supports prior to failure [4.5].

**Table 2 Updated material properties of the tested composite beams**

Concrete				
Beam	$E_c$ [GPa]	$f_c$ [MPa]	$f_{ct}$ [MPa]	
L1-3, MN1, MW1, MW4, SW1	31.5	50	3.8	
MN2-3, MW2-3, MW5-6, SN1	28.2	47	3.8	
S_L1, S_M1 & S_S1	31.5	65	4.0	
C1 – C2	31.6	41.5	4.2	
Steel				
Type	$E_s$ [GPa]	$\emptyset$ [mm]	$f_{sy}$ [MPa]	
SmHigh	210	8	703	
RibHigh	210	8	710	
SmStd	210	8	566	
		8	516	
		10	594	
		14	565	
RibStd	210	16	546	
		8	516	
		6	626	
$A_{ms}$ , cantilever beams	210	8	516	
$A_{ms}$ , continuous beams	210	6	626	
UHPRC				
Beam	$E_U$ [GPa]	$f_{ute}$ [MPa]	$\epsilon_{Um}$ [‰]	$f_{Um}$ [MPa]
L1-3, MN1-3, MW1,-6, SN1,SW1	48.8	6	1.5 or $\epsilon_{sy}$	8
C1-2	48.0	10	3.0 or $\epsilon_{sy}$	12.5
S_L1, S_M1 & S_S1	43.8	8	$\epsilon_{sy}$	10

Definition of steel types:

- Sm: Rebar with a smooth surface (no ribs)
- Rib: Rebar with a ribbed surface
- Std: Standard strength steel ( $f_{sy} \approx 500$  MPa)
- High: High strength steel ( $f_{sy} \geq 700$  MPa)

The predicted failure force is the minimum value between the shear resistance  $V_R$  and the bending resistance, expressed as the force applied at the end of the cantilever:



$$V_{flex} = m_{sy} \cdot b \cdot a_v \cdot \quad (7)$$

The comparison between the predicted and measured failure forces for the cantilever beams is given in Table 3. For all beams the angle of the inclined crack  $a_c$  was fixed at  $30^\circ$  for simplicity, which already gave good results. However, a better accuracy can be obtained using the actual angle of the inclined crack measured during testing.

In all but two cases, the failure mode was predicted correctly with satisfactory precisions. For the beams MW2 and SW1, a flexure-shear failure was predicted while a bending failure was experimentally observed. This is due to the test configuration for which the bending resistance  $V_{flex}$  is very close to the shear resistance  $V_R$ .

**Table 3 Comparison between test results and predictions for composites beams in a cantilever configuration**

Ref.	Beam	$a_v/d_{eff}$	Failure	$V_{test}$ [kN]	$V_c$ [kN]	$V_s$ [kN]	$V_U$ [kN]	$V_R$ [kN]	$V_{flex}$ [kN]	Predicted failure	$V_{test}/V_{pred}$
	L1	3.78	F	43.4	56.8	51.9	4.4	113.1	47.2	F	0.92
	L2	3.62	F	96.5	70.7	51.9	13.1	135.7	83.7	F	1.15
	L3	3.62	F	92.9	70.7	103.7	13.1	187.6	83.7	F	1.11
	MN1	2.87	F	96.84	68.1	51.9	19.9	139.9	96.0	F	1.01
	MN2	2.85	F	92.7	66.4	51.9	21.5	139.8	92.7	F	0.88
	MN3	2.94	FS	134.7	74.7	35.4	21.6	131.7	135.8	FS	1.02
[4.5]	MW1	2.98	F	58.9	56.8	0	7.3	64.1	60.0	F	0.98
	MW2	2.87	F	104.7	64.0	0	19.9	83.9	96.0	FS	1.25
	MW3	2.87	FS	91.7	63.7	0	19.5	83.2	95.0	FS	1.10
	MW4	2.87	FS	90.7	67.1	0	18.8	85.9	92.5	FS	1.06
	MW5	2.85	FS	99.6	66.4	0	21.5	87.9	105.8	FS	1.13
	MW6	2.96	FS	90.9	74.7	0	21.6	96.3	135.8	FS	0.94
	SN1	2.09	F	115.0	64.0	51.9	57.2	173.1	131.6	F	0.87
	SW1	2.09	F	124.4	68.1	0	57.2	125.3	131.6	FS	0.99
	S_L1	5.77	F	108.8	184.8	51.9	21.3	258.0	124.9	F	0.87
[4.21]	S_M1	4.04	F	178.0	184.8	0	37.0	221.8	178.4	F	1.00
	S_S1	2.60	F	272.3	184.8	0	96.5	281.4	277.5	F	0.98
<b>Mean</b>											1.02
<b>Std. Dev.</b>											0.10

### 3.3.3 Continuous beams

In the case of the continuous beams [4.22], the two cantilever spans were also externally prestressed to prevent a shear failure in these regions. The tests were then done in two stages. First, two downward displacements (inducing forces  $Q_{0p}$  and  $Q_{0r}$ ) are applied at the two cantilever ends to induce a constant negative moment in the central span. Second, a downward displacement is applied in the central span. For both beams, two flexure-shear failures were observed consecutively: first in the span between the roller support and the central force  $Q_1$ , where less shear reinforcement is placed; second, in the span between the pin

support and the central force  $Q_j$ . Prior to the first failure, the moment distribution along the beam is symmetric. Afterwards, the moment over the roller support is limited to the residual resistance of the composite section and the moment distribution is unbalanced (Figure 5). When calculating the shear resistance of the roller (r) span and the pin (p) span, the moment distribution is taken from the experimental observations and the shear span  $a_v$  is calculated between the support and the point of counter-flexion (Figure 5).

Table 4 compares the predicted to the measured shear resistance of each span of the continuous beams. For these beams the angle of the inclined crack  $\alpha_c$  was fixed in order to obtain the minimum value of shear resistance which gives good results.

**Table 4 Comparison between test results and predictions for continuous composite beams**

Ref.	Beam	$M_{supp}$ [kN.m]	$a_v$ [mm]	$a_v/d_{eff}$	$V_{test}$ [kN]	$V_c$ [kN]	$V_s$ [kN]	$V_U$ [kN]	$V_R$ [kN]	$V_{test}/V_{pred}$
	C1r	60.0	584	2.41	96.6	71.7	0	19.6	91.3	1.06
[4.22]	C1p	67.0	484	1.99	138.5	83.7	35.4	23.3	142.4	0.97
	C2r	57.5	542	2.15	103.5	79.6	0	39.5	119.1	0.87
	C2p	78.4	524	2.08	150.8	84.4	35.4	38.0	157.9	0.96

### 3.4 Parametric study

As for RC beams, the shear resistance of a composite beam is very dependent on the span-to-depth ratio  $a_v/d_{eff}$ . The depth of the section is defined as its effective flexural depth calculated with equation 12 where  $i$  stands for each layer of tensile reinforcement: the top steel rebars in the RC section (subscript  $s$ ), the layer of UHPFRC (subscript  $U$ ) and the steel rebars in the UHPFRC layer (subscript  $sU$ ).

$$d_{eff} = \frac{\sum d_i A_i f_i}{\sum A_i f_i} \quad (12)$$

The shear resistance of the composite section also depends on the material properties and section geometry. In some cases, it might even be impossible to fail a given section in shear, as the bending resistance will always be lower than the shear resistance.

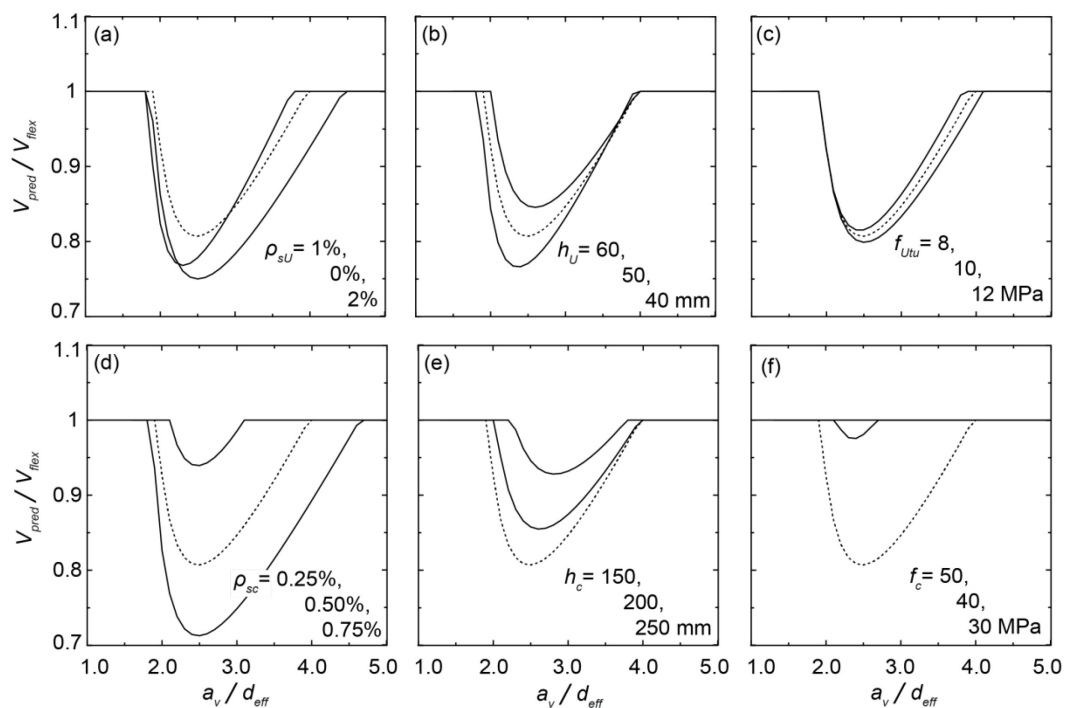
A parametric study is realized for the case of cantilever with a point force at the end of the span, such as the ones tested in [4.5]. For varying parameters, the shear and bending resistances were calculated using the methods and equations previously presented. For all cases, the angle of the inclined compressive strut  $\alpha_c$  is kept constant at  $30^\circ$  and it is supposed that maximum bending resistance is acting over the support. These are reasonable and conservative assumptions based on the experimental evidences.

The following parameter are varied: the reinforcement ratio in the layer  $\rho_{sU}$ , the height of the layer  $h_U$ , the tensile strength of UHPFRC  $f_{Um}$ , the reinforcement ratio in the RC section  $\rho_s$ , the height of the RC section  $h_U$  and the compressive strength of concrete  $f_c$ . Parameters were varied one at the time while the others were kept constant at their reference values. The reference values are given in Table 5.

**Table 5 Reference values for parametric study on shear resistance of composite beams**

UHPFRC layer		Concrete section		Steel reinforcement	
Parameters	Reference value	Parameters	Reference value	Parameters	Reference value
$b_U$	50 mm	$b_c$	250 mm	$\rho_{sU}$	1%
$E_U$	50 GPa	$E_c$	30 GPa	$\rho_{sc}$	0.5%
$f_{UtU}$	10 MPa	$f_c$	30 MPa	$E_s$	210 GPa
$f_{Ute}$	$f_{UtU} - 2$ MPa	$f_{ct}$	$0.3 \cdot f_c^{2/3}$ [4.19]	$f_{sy}$	500 MPa
$\varepsilon_{UtU}$	2.5‰				
$f_{Uc}$	150 MPa				

In Figure 6, the ratio between the predicted failure force (minimum value between the shear resistance and the bending resistance), and the bending resistance is given in relation to the span-to-depth ratio. These graphs show that, as for concrete elements [4.10], shear failure is strongly related to the geometry and configuration of the element. In the cases verified here, the shear failures happened only for span-to-depth ratios between 2.0 and 4.5. For cases where the concrete is strong enough, a shear failure can even be avoided ( $f_c = 50$  MPa in Figure 6f).


**Figure 6 Relation between span-to-depth ratio and shear strength**

### 3.5 Design example

Chillon viaducts are two parallel highway RC bridges, each carrying one direction, opened to traffic in 1969 and located on the shores of Lake Geneva near Montreux in Switzerland. They consist of variable height box girders (Figure 7a) built by posttensioned segmental construction with epoxy-glued joints, and spanning between 92 m and 104 m over a total

length of 2120 m. Recently, early signs of the alkali-aggregate reaction (AAR) were discovered in the concrete. In later stages, this reaction could lead to the deterioration of the concrete compressive strength. In prevision of a weaker concrete strength, it was decided to reinforce the deck slab with a 40-mm thick layer of R-UHPFRC [4.24].

In the following, the transversal shear resistance is calculated using the equations presented in section 3.2. The factored design properties as well as the geometry and steel layout of the slab are given in are given in Table 6. The concrete strength is reduced to take into account future degradation due to AAR. From an elastic analysis, the maximum acting shear force at the support  $v_{Ed}$  is 198 kN/m.

**Table 6 Main parameters for the shear design example on the Chillon viaduct cross-section**

UHPFRC layer		Concrete section		Steel reinforcement	
Para.	Ref. value	Para.	Ref. value	Para.	Ref. value
$b_U$	40 mm	$b_c$	180 mm	$\rho_{sU}$	Ø12@125mm: 2.5%
$d_{sU}$	196 mm	$d_{sc}$	152 mm	$\rho_{sc}$	Ø16@125mm: 1.2%
$E_U$	50 GPa	$E_c$	35 GPa	$E_s$	205 GPa
$f_{Utd}$	8 MPa	$f_{cd}$	20 MPa	$f_{sd}$	435 MPa
$f_{Utd}$	6 MPa	$f_{td}$	1.7 MPa		
$\varepsilon_{Um}$	$\varepsilon_{gy} = 2.1\text{‰}$				
$f_{Utd}$	106 MPa				

For shear resistance verification, the critical wheel load position is shown in Figure 7b. The shear span  $a_v$  corresponds to the distance between the side of the wheel load and the wide part of the web of the box-girder, right under the slab.

$$d_{eff} = \frac{\sum d_i A_i f_i}{\sum A_i f_i} = 166 \text{ mm}$$

$$a_v = 2 \cdot d_{eff} = 332 \text{ mm}$$

It is supposed that the maximum bending resistance of the section will be acting over the webs when the shear resistance is reached. The height of the compression zone  $x$ , calculated with the multilinear moment-curvature relation, is thus 54 mm. Supposing an angle of the compression strut of  $35^\circ$ , the concrete contribution to the shear resistance is calculated as follows:

$$v_c = \frac{f_{cd}}{2} \left[ \frac{x}{\sin \alpha_c} (1 - \cos \alpha_c) \right] = 170 \text{ kN/m} < v_{Ed}$$

The design strength of concrete is used in the previous calculation as this value was already reduced to take into account the effects of AAR. It is thus not needed to reduce it again to the effective value as cracking in the concrete has already been considered.

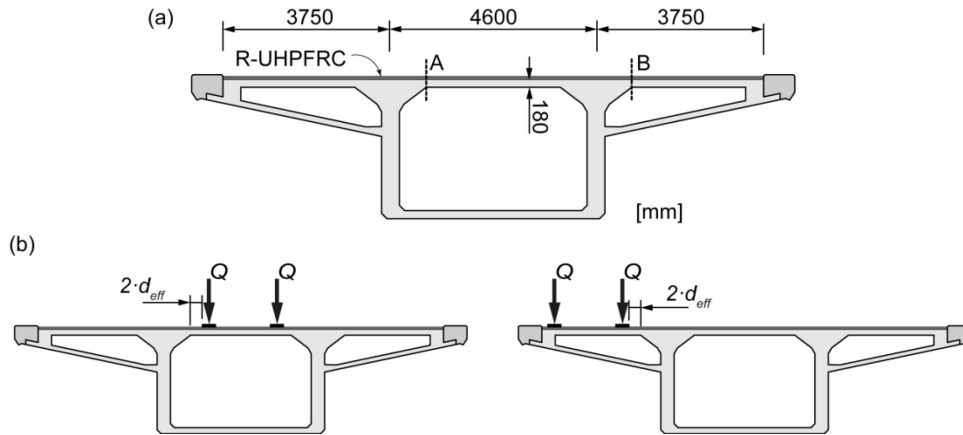


**Figure 7 Design example: Chillon viaducts box girders cross-section, adapted from [4.24]**

The maximum bending resistance of the R-UHPFRC layer is calculated with equations 5 and 6.

$$x_U = \frac{\rho_{sU} h_U f_{sd,U}}{0.5 f_{Ucd}} = \frac{2.5\% \cdot 40 \text{ mm} \cdot 435 \text{ MPa}}{0.5 \cdot 106 \text{ MPa}} = 8.4 \text{ mm}$$

$$m_{UR} = f_{sd,U} \rho_{sU} h_U \left( \frac{h_U}{2} - \frac{x_U}{2} \right) + f_{Utud} (h_U - x_U) \left( \frac{h_U}{2} - x_U \right) = 9.8 \text{ kN} \cdot \text{m/m}$$

With the angle of the compression strut and the moment distribution across the slab, the NIC length  $l_{NIC}$  is equal to 233 mm. The contribution of the UHPFRC layer is finally obtained with equation 11.

$$v_U = \frac{2m_{UR}}{l_{NIC}} = 84 \text{ kN/m}$$

Finally, the total shear resistance is the addition of the concrete and the UHPFRC contribution:

$$v_{Rd} = 170 \text{ kN/m} + 84 \text{ kN/m} = 254 \text{ kN/m} > v_{Ed} = 198 \text{ kN/m}$$

## 4 Punching shear resistance of composite slabs

### 4.1 Punching shear resistance of RU-RC composite slabs

A series of 6 composite slabs were submitted to a point force to study their resistance to punching shear [4.6]. These tests showed that the layer of UHPFRC carries part of the shear by activating its out-of-plane bending capacity similarly to what was observed for one-way members. As developed in paragraph 2.1, punching shear resistance in a RC slab is mainly due to the direct strut action enhanced by the contribution of tangential compressive strains. At ultimate resistance, the inclined shear crack develops through this strut. This inclined crack cannot propagate through the UHPFRC layer. Instead, the layer follows the movement of the crack lips by bending out-of-plane. This mechanism creates tensile stresses in the

concrete, perpendicularly to the layer. These stresses can lead to the horizontal development of limited NIC in the concrete below the interface (Figure 8a) [4.9].

## 4.2 Analytical model

### 4.2.1 Overview

Based on the experimental observations, a composite model was developed in [4.9] to predict the load-rotation behaviour of a composite slab and its punching shear resistance. To take into account the state of deformation due to the bending efforts, punching shear resistance is calculated as a combination of the force-rotation curve and a composite strain-based failure criterion (Figure 8b). This model was also validated with test results and gives reliable results [4.9]. The main equations of this model are recalled herein.

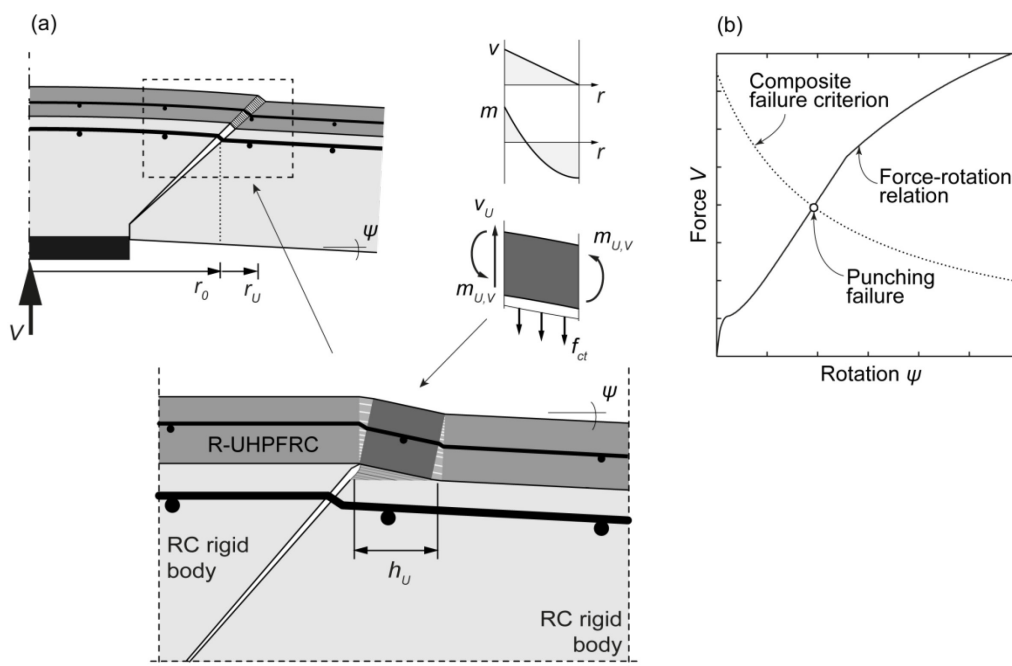


**Figure 8** Punching shear resistance of composite RU-RC slabs [4.9]: (a) failure mechanisms; (b) calculation of punching shear resistance with a failure criterion

### 4.2.2 Composite failure criterion

The punching shear resistance of a composite slab  $V_R$  is the superposition of the concrete contribution  $V_c$  and the UHPFRC layer contribution  $V_U$  to shear resistance:

$$V_R(\psi) = V_c(\psi) + V_U \quad (13)$$

The contribution of transverse reinforcement can also be added to the previous relation by verifying the different potential failure modes of shear reinforced slabs: failure within or outside the shear-reinforced area or failure close to the column by crushing of the concrete [4.25, 26]. The relations to calculate the contribution of the transverse reinforcement for these different types of failure are described in detail in [4.25]. In all cases, the presence of transverse reinforcement does not modify the contribution of the UHPFRC layer.

The concrete contribution is calculated with the critical shear crack theory (CSCT) formulation [4.15]. According to this theory, the state of deformation due to bending can be related to the global rotation of the slab  $\psi$ . The failure criterion is semi-empirical and calculates the punching shear resistance of a RC slab as a function of its rotation.

$$\frac{V_c}{b_0 d_{sc} \sqrt{f_c}} = \frac{3/4}{1 + 15 \frac{\psi d_{sc}}{d_{g0} + d_g}} \quad (14)$$

The contribution of the UHPFRC layer is linked to the radial activation of its out-of-plane bending resistance at the mouth of the inclined shear crack, at radius  $r_U$ , measured at the top of the slab at a distance  $b_c + b_U$  of the column side. The tensile stresses induced by this mechanism in the concrete below the interface with the UHPFRC layer must reach the tensile strength of concrete  $f_{ct}$  before NIC starts developing. The maximum contribution of the UHPFRC layer to punching shear resistance thus depends on  $f_{ct}$ . Based on experimental observations, it is supposed that the developing length of NIC is limited prior to failure. It is thus supposed that the out-of-plane bending mechanism activates over the minimum required length, equal to the height of the layer  $h_U$  [4.8]. By equilibrating the efforts on the small UHPFRC sector element (Figure 8a), the shear contribution of the UHPFRC layer is expressed as follows:

$$V_U = 2\pi f_{ct} h_U \left( r_U + \frac{h_U}{2} \right) \quad (15)$$

$$m_{U,V} = \frac{h_U^2 f_{ct}}{4} \leq m_{UR} \quad (16)$$

The value of  $V_U$  is limited by the maximum bending resistance of the layer,  $m_{UR}$ , which can be calculated with equations 5 and 6. For typical thickness of the UHPFRC layer, its bending resistance is rarely reached and the steel rebars in the layer do not yield [4.9]. To simplify equation 16, the conservative assumption that the tangential moments  $m_t$  do not significantly contribute to the punching shear resistance is made.

The equation used to obtain the UHPFRC contribution (equation 15) implicitly considers the material properties of UHPFRC. First, UHPFRC has rigidity higher than the concrete and prevents the inclined shear crack from propagating through the layer. Second, the moments induced in the layer by the out-of-plane bending efforts (equation 16) are at levels higher than the elastic limit of UHPFRC. Its hardening capacity is thus activated even if the maximum bending resistance is not reached. Finally, the tensile properties of UHPFRC have a strong influence on the force-rotation behavior of the slab and thus on the shear contribution of the concrete section.

#### 4.2.3 Force-rotation behavior

The composite failure criterion expressed by equation 13 has to be used in combination with the force-rotation curve of the slab, describing its bending behavior under a point force. This method allows taking into account the state of deformation in the slab. Kinnunen and Nylander [4.27] developed a sector model to simulate the behavior of an axisymmetric slab submitted to a point force. It is assumed that slab sectors rotate around the edge of the column. Based on this kinematics, a simplified distribution of the radial and tangential moments was proposed in [4.15]. With these distributions and the multilinear moment-

curvature relation proposed for composite slabs (paragraph 2.2), the complete force-rotation curve can be derived [4.9].

To directly obtain the rotation of the slab for a given load, it was proposed in [4.15] to estimate the force-rotation curve with a parabola and a cap at the theoretical bending resistance of the slab,  $V_{flex}$ . This bending resistance can be calculated using yield-line method. For a continuous slab, radius  $r_s$  is the distance between the point force (or column) and the point of counter-flexion where moments are equal to zero.

$$\psi = 1.5r_s\kappa_{sy} \left( \frac{V}{V_{flex}} \right)^{3/2} \quad (18)$$

In the *fib* Model Code [4.19], using the same formulation, the rotation around the support is directly estimated for the given action effects in the slab. The available punching shear resistance is then calculated with equation 13.

$$\psi = 1.5r_s\kappa_{sy} \left( \frac{m_{Ed}}{m_{sy}} \right)^{3/2} \quad (19)$$

In the previous equations,  $m_{Ed}$  is the average value of the moment acting in the support strip,  $m_{sy}$  is the maximum bending resistance of the composite section (Figure 3) and  $\kappa_{sy}$  is the related curvature.

### 4.3 Parametric study

In order to assess how the properties of the UHPFRC layer influence the punching shear resistance of a composite slab, a parametric study is realized for the case of an isolated slab, such as the ones tested in [4.6]. The slabs are 3×3 m squares and are placed over a 260×260 mm square column with the UHPFRC layer on top. The following parameters are varied: the reinforcement ratio in the layer  $\rho_{sU}$ , the height of the layer  $h_U$  and the tensile strength of UHPFRC  $f_{Um}$ . All other parameters are kept constant to the reference values given in Table 7. The punching shear resistance is calculated using the equations previously proposed.

**Table 7 Reference values for parametric study on punching shear resistance of composite slabs**

UHPFRC layer		Concrete section		Steel reinforcement		Loading and slab geometry	
Para.	Ref. value	Para.	Ref. value	Para.	Ref. value	Para.	Ref. value
$h_U$	Var.	$b_c$	200 mm	$\rho_{sU}$	Var.	$c$	260 mm
$E_U$	50 GPa	$E_c$	30 GPa	$\rho_{sc}$	1%	$B$	3000 mm
$f_{Um}$	Var.	$f_c$	30 MPa	$E_s$	210 GPa	$r_q$	1500 mm
$f_{Ute}$	$f_{Utu} - 2 \text{ MPa}$	$f_d$	$0.3 \cdot f_c^{2/3}$ [4.19]	$f_{sy}$	500 MPa		
$\epsilon_{Um}$	2.5‰						
$f_{Uc}$	150 MPa						

For varying values of UHPFRC tensile strength,  $f_{Um}$ , Figure 9 relates the height of the layer  $h_U$  to the total punching shear resistance  $V_R$  as well as the ratio between the UHPFRC contribution  $V_U$  and the total resistance. These results demonstrate that although the



UHPFRC material properties are not implicitly considered in equation 15, they modify the force-rotation behavior of the layer and thus influence the punching shear resistance.

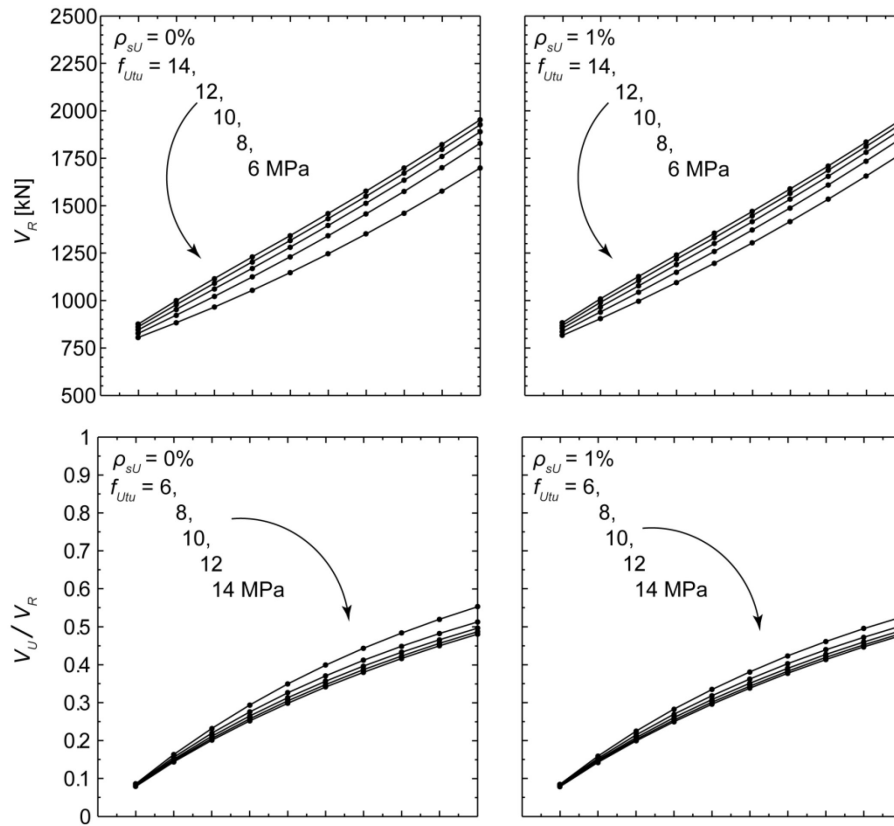


Figure 9 Influence of UHPFRC layer parameters on the punching resistance

#### 4.4 Design example

In the following, the punching shear resistance of a composite flat slab will be calculated for the case of an inner column (column C5, Figure 10). The factored design properties as well as the geometry and steel layout of the slab are given in Table 8. In a first approximation, moment redistribution and compressive membrane action are not considered. This is reasonable for a first approximation as these phenomena increase the punching shear resistance of flat slabs [4.28].

The factored design load including the self-weight of the structural element and the surcharge is  $15 \text{ kN/m}^2$ . The design load is estimated based on contributive areas [4.29].

$$V_{Ed} = (2 \cdot 0.6 \cdot L_x) \times (2 \cdot 0.6 \cdot L_y) \times q_d = 648 \text{ kN}$$

The contribution of the concrete is evaluated based on the state of deformation in the slab. For the applied load  $V_{Ed}$ , the rotation is calculated using equation 18. The radius of the slab  $r_s$  is estimated as proposed in the *fib* Model Code [4.19].

$$r_{sx} = 0.22 \cdot L_x = 1320 \text{ mm}$$

$$r_{sy} = 0.22 \cdot L_y = 1100 \text{ mm}$$

The largest value,  $r_{xx}$ , governs. The bending resistance is then estimated with yield lines and the rotation is calculated.

$$V_{flex} = 1579 \text{ kN}$$

$$\psi = 1.5 r_s \kappa_{sy} \left( \frac{V_d}{V_{flex}} \right)^{3/2} = 1.5 \cdot 1320 \text{ mm} \cdot (2.2 \cdot 10^{-5}) \text{ mm}^{-1} \cdot \left( \frac{648 \text{ kN}}{1579 \text{ kN}} \right)^{3/2} = 0.01$$

The critical perimeter  $b_0$  where the punching shear resistance of concrete is checked is set at  $d_{sc}/2$  from the column face, as prescribed in [4.19].

$$b_0 = 4 \cdot c + \pi \cdot d_{sc} = 1628 \text{ mm}$$

$$V_c = \frac{0.75 \cdot b_0 d_{sc}}{1 + 15 \frac{\psi d_{sc}}{d_{go} + d_g}} \cdot \frac{\sqrt{f_{ck}}}{\gamma_c} = 461 \text{ kN} < V_{Ed}$$

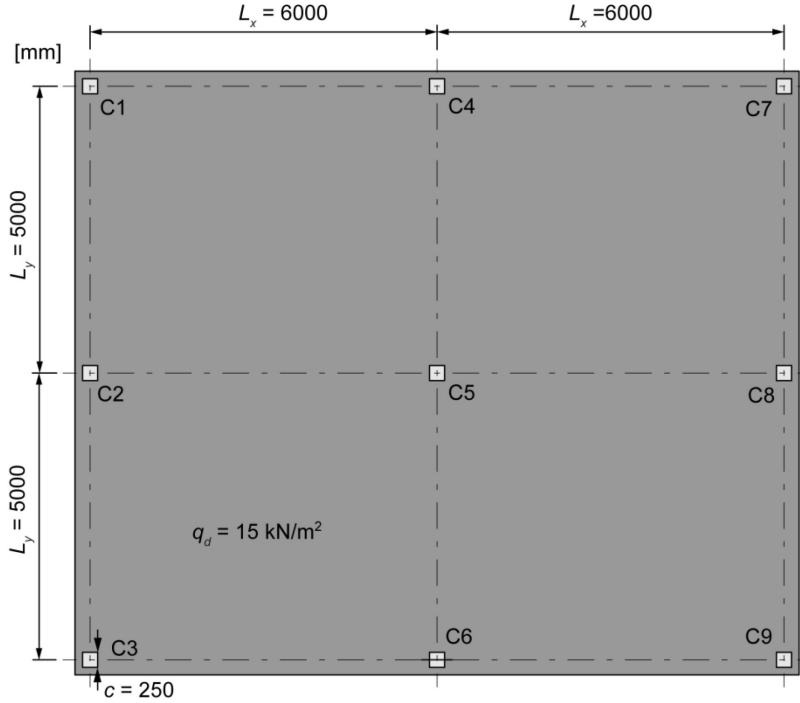


Figure 10 Design example: floor plan

The contribution of the UHPFRC layer is calculated with equation 15. Then, the activated moment in the layer  $m_{U,V}$  is compared to the maximum bending resistance of the layer  $m_{UR}$  to verify that the latter is not exceeded.

$$r_U = \frac{2c}{\pi} + h_c + h_U = 419 \text{ mm}$$

$$V_U = 2\pi f_{ctd} h_U \left( r_U + \frac{h_U}{2} \right) = 2\pi \cdot 1.7 \text{ MPa} \cdot 50 \text{ mm} \cdot \left( 419 \text{ mm} + \frac{50 \text{ mm}}{2} \right) = 237 \text{ kN}$$

$$m_{U,V} = \frac{h_U^2 f_{ctd}}{4} = \frac{(50 \text{ mm})^2 \cdot 1.7 \text{ MPa}}{2} = 1.1 \text{ kN} \cdot \text{m/m}$$

$$x_U = \frac{\rho_{sU} h_U f_{sd,U}}{0.5 f_{Ucd}} = \frac{0.78\% \cdot 50 \text{ mm} \cdot 435 \text{ MPa}}{0.5 \cdot 150 \text{ MPa}} = 2.3 \text{ mm}$$

$$m_{UR} = f_{sd,U} \rho_{sU} h_U \left( \frac{h_U}{2} - \frac{x_U}{2} \right) + f_{Utud} (h_U - x_U) \left( \frac{h_U}{2} - x_U \right) = 12.7 \text{ kN} \cdot \text{m/m} > m_{U,V} \rightarrow \text{ok}$$

**Table 8 Main parameters for the punching shear design example**

UHPFRC layer		Concrete section		Steel reinforcement	
Para.	Ref. value	Para.	Ref. value	Para.	Ref. value
$h_U$	50 mm	$h_c$	210 mm	$\rho_{sU}$	Ø8@200mm: 0.78%
$E_U$	50 GPa	$d_{sc}$	200 mm	$\rho_{sc}$	Ø14@125mm: 0.54%
$f_{Utd}$	8 MPa	$E_c$	30 GPa	$E_s$	210 GPa
$f_{Utd}$	6 MPa	$f_{ck}$	30 MPa	$f_{sd}$	435 MPa
$\varepsilon_{Utu}$	2.5‰	$f_{ad}$	1.7 MPa		
$f_{Ucd}$	150 MPa	$d_g$	16 mm		

The total punching shear resistance is the sum of the UHPFRC and concrete contributions.

$$V_{Rd} = 237 \text{ kN} + 461 \text{ kN} = 698 \text{ kN} > V_{Ed} = 648 \text{ kN}$$

The addition of the UHPFRC layer is sufficient to ensure the punching shear resistance of the slab.

## 5 Discussion

It has been demonstrated in the previous paragraphs that a layer of UHPFRC resists shear forces by bending out-of-plane. This mechanism is analogous to the dowel action of longitudinal steel rebars along a shear crack. It is accompanied by NIC in the concrete below the interface with the UHPFRC layer. The contribution of the UHPFRC layer to the shear or punching shear resistance depends on the state of cracking and the length of NIC. Some differences can be noted between the mechanism implied in shear resistance of composite slender beams and in punching shear resistance of composite slabs.

For slender composite beams, significant flexural cracking first develops in the concrete section. After the appearance of the inclined shear crack, NIC will quickly develop from the mouth of the crack towards the point of counter-flexion. At failure, NIC is fully developed and plastic hinges have formed in the UHPFRC layer. The moments in these hinges reach  $m_{UR}$ , the maximum bending resistance of the UHPFRC layer.

In the case of slabs submitted to a point force, the RC section resists by direct strut action. As was experimentally observed, the development of NIC is limited prior to punching shear failure [4.6]. NIC is thus an ongoing process controlled by the tensile strength of concrete. At failure, it is supposed that the NIC length is equal to the height of the UHPFRC layer

(Figure 8), which is the minimal value for the out-of-plane bending mechanism to activate. The bending efforts created in the layer are below  $m_{UR}$ , the maximum bending resistance of the UHPFRC layer.

Besides carrying shear by this out-of-plane bending mechanism, the UHPFRC layer, as a longitudinal tensile reinforcement, also improves the shear carrying mechanism in the RC section by modifying its bending behavior. First, the rotation of the member or the slab is proportional to the opening of the shear crack [4.15]. By increasing the bending rigidity, the layer of UHPFRC hinders the widening of the inclined shear crack. Second, in the cases of beams, the uncracked compression zone carries part of the shear. The addition of the layer increases the height of the compression zone and thus increases its carrying capacity.

## 6 Conclusions

This paper demonstrated that the addition of a UHPFRC layer is an efficient method to strengthen an RC slab in both bending and shear. The following points can be outlined:

1. A UHPFRC layer carries shear by an out-of-plane bending mechanism accompanied by NIC, similarly to dowel action of rebars.
2. For slender composite beams submitted to shear, NIC fully develops and plastic hinges are created in the UHPFRC layer to carry part of the shear forces.
3. For composite beams submitted to a point force, RC carries shear mainly by direct strut action and NIC is an ongoing process controlled by the tensile strength of concrete. Its length is limited to the height of the UHPFRC layer.
4. The UHPFRC layer improves the shear carrying mechanisms of the concrete section by increasing the bending rigidity of the element.
5. Models to predict the shear and punching shear resistance of composite sections are presented and validated.
6. A parametric study on the shear resistance model showed the strong dependence to the shear-span to depth ratio. In some cases, a layer of UHPFRC can also rule out the risk of a shear failure.

## 7 References

- [4.1] Brühwiler E, Denarie E. Rehabilitation and Strengthening of Concrete Structures Using Ultra-High Performance Fibre Reinforced Concrete. *Structural Engineering International*. 2013;23(4):450-7.
- [4.2] Habel K, Denarie E, Brühwiler E. Structural Response of Elements Combining Ultrahigh-Performance Fiber-Reinforced Concretes and Reinforced Concrete. *Journal of Structural Engineering*. 2006;132(11):1793-800.

- [4.3] Habel K, Denarie E, Brühwiler E. Experimental investigation of composite ultra-high-performance fiber-reinforced concrete and conventional concrete members. *ACI Structural Journal*. 2007;104(1):93-101.
- [4.4] Oosterlee C. Structural Response of Reinforced UHPFRC and RC Composite Members. Doctoral thesis EPFL no. 4848. Lausanne: Ecole Polytechnique Fédérale de Lausanne; 2010; 136 p.
- [4.5] Noshiravani T, Brühwiler E. Experimental investigation on reinforced ultra-high-performance fiber-reinforced concrete composite beams subjected to combined bending and shear. *ACI Structural Journal*. 2013;110(2):251-61.
- [4.6] Bastien-Masse M, Brühwiler E. Experimental Investigation on Punching Resistance of R-UHPFRC – RC Composite Slabs. *Materials and Structures*. 2015: doi:10.1617/s11527-015-0596-4.
- [4.7] Denarié E, Brühwiler E. Strain Hardening of Ultra-high Performance Fibre Reinforced Concrete: Deformability versus Strength Optimization. *International Journal of Restoration of Buildings and Monuments*. 2012;17(6):397-410.
- [4.8] Noshiravani T. Structural Response of R-UHPFRC - RC Composite Members Subjected to Combined Bending and Shear. Doctoral Thesis EPFL no. 5246. Lausanne: Ecole Polytechnique Federale de Lausanne; 2012; 188 p.
- [4.9] Bastien-Masse M, Brühwiler E. Composite model for predicting the punching resistance of R-UHPFRC - RC composite slabs. Submitted to *Engineering Structures*. [Research paper]. 2015.
- [4.10] Kani GNJ. The Riddle of Shear Failure and its Solution. *ACI Journal Proceedings*. 1964;61(4):441-67.
- [4.11] Reineck K-H. Ultimate shear force of structural concrete members Without Transverse Reinforcement Derived From a Mechanical Model (SP-885). *Structural Journal*.88(5).
- [4.12] Muttoni A, Fernández Ruiz M. Shear Strength of Members without Transverse Reinforcement as Function of Critical Shear Crack Width. *ACI Structural Journal*. 2008;105(2):163-72.
- [4.13] Campana S, Fernández Ruiz M, Muttoni A. Analysis of shear-transfer actions on one-way RC members based on measured cracking pattern and failure kinematics. *Magazine of Concrete Research*. [Research Article]. 2013;65(6):386-404.
- [4.14] Collins MP, Bentz EC, Sherwood EG, Xie L. An adequate theory for the shear strength of reinforced concrete structures. *Magazine of Concrete Research*. 2008;60(9):635-50.
- [4.15] Muttoni A. Punching Shear Strength of Reinforced Concrete Slabs without Transverse Reinforcement. *ACI Structural Journal*. 2008;105(4):440-50.
- [4.16] Muttoni A, Fernández Ruiz M. Shear in slabs and beams: should they be treated in the same way? Shear and punching shear in RC and FRC elements. Lausanne: Fédération Internationale du Béton; 2010. p. 105-28.
- [4.17] Marti P. *Theory of Structures: Fundamentals, Framed Structures, Plates and Shells*. First ed. Berlin: Ernst & Sohn; 2013; 696 p.
- [4.18] Stoffel P. Zur Beurteilung der Tragsicherheit bestehender Stahlbetonbauten. Doctoral thesis 13692. Zürich, Switzerland: ETHZ; 2000; 186 p.
- [4.19] fib. *Model Code for Concrete Structures 2010*. Fédération Internationale du Béton ed. Lausanne: Ernst & Sohn; 2013; 434 p.
- [4.20] Fernandez Ruiz M, Plumey S, Muttoni A. Interaction between Bond and Deviation Forces in Spalling Failures of Arch-Shaped Members without Transverse Reinforcement. *ACI Structural Journal*. 2010;107(03).

- [4.21] Bastien-Masse M, Brühwiler E. Concrete bridge deck slabs strengthened with UHPFRC. IABSE Conference 'Assessment, Upgrading and Refurbishment of Infrastructures'; Rotterdam: IABSE; 2013.
- [4.22] Noshiravani T, Brühwiler E. Rotation capacity and stress redistribution ability of R-UHPFRC-RC composite continuous beams: an experimental investigation. *Materials and Structures*. 2013;46(12):2013-28.
- [4.23] Bastien-Masse M, Denarié E, Brühwiler E. Effect of fiber orientation on the in-plane tensile response of UHPFRC reinforcement layers. Submitted to *Cement and Concrete Composites*. [Research paper]. 2015.
- [4.24] Brühwiler E, Bastien-Masse M, Mühlberg H, Houriet B, Fleury B, Cuennet S, et al. Strengthening the Chillon viaducts deck slabs with reinforced UHPFRC. IABSE Conference 'Structural Engineering: Providing Solutions to Global Challenges'; Geneva: IABSE; 2015. p. 1171-8.
- [4.25] Fernández Ruiz M, Muttoni A. Applications of Critical Shear Crack Theory to Punching of Reinforced Concrete Slabs with Transverse Reinforcement. *ACI Structural Journal*. 2009;106(4):485-94.
- [4.26] Lips S, Fernandez Ruiz M, Muttoni A. Experimental Investigation on Punching Strength and Deformation Capacity of Shear-Reinforced Slabs. *ACI Structural Journal*. 2012;109(6):889-900.
- [4.27] Kinnunen S, Nylander H. Punching of concrete slabs without shear reinforcement. *Transactions of the Royal Institute of Technology No.158*. Stockholm:1960; 112 p.
- [4.28] Einpaul J, Fernández Ruiz M, Muttoni A. Influence of moment redistribution and compressive membrane action on punching strength of flat slabs. *Engineering Structures*. 2015;86:43-57.
- [4.29] Muttoni A, Ruiz MF, Bentz E, Foster S, Sigrist V. Background to fib Model Code 2010 shear provisions – part II: punching shear. *Structural Concrete*. 2013;14(3):204-14.

## Conclusions

---

## CONCLUSIONS



## 1 Overview

This thesis aimed at extending the current knowledge on composite RU-RC members to the case of two-way spanning slabs. The work combined material and structural engineering with the final aim of correctly predicting the behavior and resistance of a composite RU-RC slab submitted to combined bending and shear, with a certain focus on punching shear resistance. Experimental investigations, both at the material and structural level, were carried out and served as basis for the development of analytical models. This final section of the thesis summarizes the main contributions of this work and gives an outlook on future research on the topic of composite RU-RC slabs.

## 2 Summary of contributions

### 2.1 Representative tensile response of a UHPFRC layer

The first part of the thesis focused on establishing a method to define the representative in-plane tensile properties for a UHPFRC layer using the results of a material characterization campaign. The following points were achieved.

1. Using stereological principles, the relation between fiber orientation factors in the orthogonal directions of a UHPFRC layer and the relation between the orientation factor and the average fiber efficiency factor were established.
2. Any type of bending or tensile tests can be carried out in order to identify the material's tensile response as the effect of fiber orientation on the results can afterwards be identified. With the relation between the average fiber efficiency factor and the fiber orientation factor, fiber efficiency at pull-out can correctly be taken into account when analyzing the results.
3. The material characterization campaign clearly demonstrated that there is no intrinsic tensile response for UHPFRC, as it depends on the geometry of the tested specimen and on the casting process which both influence the final fiber orientation. It is thus proposed to scale the whole tensile response of UHPFRC to the intended application using average orientation factors. This can be done with the proposed meso-mechanical model.
4. The relation between fiber orientation factors in orthogonal directions was validated with test results. Using these test results, the average fiber orientation factors expected in a layer cast with conventional tools were estimated and the tensile response was scaled accordingly.
5. The average orientation factor in specimens with a thickness of between 20 and 50 mm, obtained with experimental data, is 0.58 with a standard deviation of 0.15. It is thus expected that in a layer of UHPFRC, the average orientation factor should be between the perfect 3D case (0.50) and the perfect 2D case (0.63).

## 2.2 Experimental investigation on the punching shear resistance of composite slabs

A total of six composite slabs were tested in a punching test setup. These tests aimed at studying the behavior of a two-way spanning slab submitted to a point force. With the test results, the following conclusions could be made.

1. The layer of UHPFRC increases the rigidity of the slab, as an added flexural reinforcement is expected to do. However, as the UHPFRC layer also carries part of the shear, it also allows the RC section to deform more. Shear deformation and crack opening of the RC section are larger than for the reference RC slab. This allows for the composite slab to fail in punching shear at a higher force than the RC section alone, but for rotations close to what is expected for the unreinforced section.
2. The layer of UHPFRC provides shear resistance to the cracked RC section by out-of-plane bending. At the mouth of the critical shear crack, bending efforts are introduced in the layer due to the relative movement of the critical shear crack lips.
3. Final failure happens due to the failure of the RC section. This happens prior to the yielding of the reinforcement in the UHPFRC layer. Thus, the use of reinforcement in the UHPFRC layer does not significantly influence the final punching shear resistance of the composite slab. Yet, the addition of rebars in UHPFRC improves its tensile behavior. It makes a significant difference in the bending resistance of the composite slab and should always be considered when designing composite sections.
4. Only limited Near Interface Cracking (NIC) was observed prior to punching shear failure, over the column and near the inclined crack. NIC over the column is due to an upward deflection of the UHPFRC layer and is due to the incompatibility between the deformations of the cracked UHPFRC layer and the RC section at this point of high bending efforts. After the punching shear failure of the RC section, as the inclined crack cannot develop through the UHPFRC layer, NIC propagates away from the punching cone.

## 2.3 Modelling the behavior and punching shear resistance of composite slabs

Based on experimental observations, a model to predict the behavior and punching shear resistance of composite slabs was developed. The following points can be outlined.

1. A multilinear moment-curvature relation for composite RU-RC section is proposed. This relation is based on the plane section theory and supposes a rigid bond between the layer of UHPFRC and the RC section. It also takes into account tension stiffening of the RC tension chord. Using this relation and the sector model for axisymmetric slabs, the force-rotation behavior of a composite slab submitted to a point force can be predicted.
2. The contribution of a RC section to the punching shear resistance of a composite slab is calculated with the critical shear crack theory (CSCT) criterion [C.1]. This criterion relates the punching shear resistance of a slab to its state of deformation expressed with its rotation.

3. The UHPFRC layer contributes to the punching shear resistance by out-of-plane bending, activated radially at the perimeter of the punching cone. By doing so, tensile stresses are created in the concrete below the interface with the UHPFRC layer. Once the tensile strength of concrete is reached, NIC starts developing. As only limited NIC was observed experimentally prior to failure, it is supposed that the out-of-plane bending mechanism activates over the smallest possible length, which is equal to the height of the UHPFRC layer. The contribution of the UHPFRC layer to punching shear resistance is thus calculated as a function of its height and the tensile strength of concrete. The tensile properties of UHPFRC are considered implicitly and its strain hardening capacity is activated.
4. Punching shear resistance is obtained at the intersection between the force-rotation curve and the composite failure criterion. The latter is the sum between the CSCT criterion and the UHPFRC contribution. The model predictions are in good agreement with the test results
5. A procedure is proposed to calculate the punching shear resistance of a RC slab with pre-existing deformations in the concrete section when the UHPFRC layer is installed. A modified moment-curvature relation can be used to calculate the force-rotation behavior for this case. The same composite failure criterion can be used.

#### **2.4 Influence of parameters on the shear resistance of composite sections**

In the last part of the thesis, the existing model to predict shear resistance of composite beams is presented and a parametric study is carried out on both the shear and punching shear resistance model. Finally, the analyses of the mechanisms involved in the RC section and UHPFRC layer allowed clearly exposing how the layer of UHPFRC influences the shear resistance of a composite beam or slab. The following conclusions were drawn.

1. In punching or one-way shear, the UHPFRC layer carries part of the shear forces by bending out-of-plane in double curvature, similarly to dowel action of longitudinal steel rebars along a shear crack. This contribution to the shear or punching shear resistance depends on the length of NIC which develops in the concrete below the interface.
2. For slender composite beams submitted to shear, NIC fully develops and plastic hinges are created in the UHPFRC layer. The contribution of the UHPFRC layer to shear resistance is thus proportional to the maximum bending resistance and inversely proportional to the NIC length. This length is measured between the mouth of the inclined crack and the point of counter-flexure.
3. In the case of slabs submitted to a point force, the RC section resists by direct strut action. NIC is an ongoing process controlled by the tensile strength of concrete. Its length is limited to the height of the UHPFRC layer
4. The UHPFRC layer, as a longitudinal tensile reinforcement, also improves the shear carrying mechanism in the RC section by modifying its bending rigidity. By doing so, it controls the widening of the inclined shear crack. Moreover, the addition of the

layer increases the height of the compression zone and thus increases the carrying capacity of the uncracked compression zone.

### 3 Perspectives and future works

#### 3.1 UHPFRC properties

In this work, a detailed procedure was proposed to identify the in-plane representative tensile response for a UHPFRC layer based on fiber orientation. The fiber orientation in the tested specimens must be identified and the tensile response can then be scaled to the fiber orientation expected in the structure. To improve this procedure, the following points need to be studied and further developed:

1. Reliable and systematic testing methods specific to UHPFRC need to be selected, from specimen geometry to casting process. Although this work showed that any test can be used to predict the tensile response of UHPFRC, systematizing the testing procedure for the material characterization phase would greatly simplify test interpretation. A first proposition has been made in the recent guidelines for UHPFRC design in France [C.2] and Switzerland [C.3]. The procedure proposed in both documents should be compared and tested through a new large testing campaign.
2. To estimate fiber orientation in an element to be designed, various procedures are possible. Representative testing such as what was realised in this work is a first option. Mock-up elements are another possibility. However, both methods are fastidious. Reliable and straight forward numerical and analytical tools need to be developed and tested to easily predict and estimate fiber orientation factors in structural element depending on geometry, rheology and casting process.
3. For cast-on-site UHPFRC, on-site specimen preparation for later material testing should be avoided as they are time consuming and costly. To verify that fiber orientation in a UHPFRC layer or structural element corresponds to what was predicted during the design phase, reliable non-destructive techniques need to be developed. Techniques such as AC-impedance spectroscopy [C.4], electrical resistivity measurement [C.5] or magnetic measurements [C.6, 7] have been developed in the recent years, but they still need to be systematized and applied to real scale structures.

Regarding the actual tensile response and strength of UHPFRC, the following point can still be addressed in the future:

1. Besides fiber orientation, fiber efficiency and maximum pull-out stress have a strong influence on the hardening phase and maximum tensile strength of the material. Both should be influenced by the type of fiber and the matrix properties. Little research has been done on the relation between the fiber inclination and the efficiency factor and it was carried out on various types of fibers and mixes. Moreover, only little tests have been done on UHPFRC mixes

to evaluate the maximum pull-out stress and fiber efficiency. A better estimation of the maximum pull-out stress and its relation with the inclination of the fiber for the specific case of UHPFRC mixes would help in the predictions of tensile strength.

2. The tensile elastic limit of UHPFRC is mainly governed by the strength of the matrix. However, other factors such as a very unfavorable fiber orientation or the presence of defects in the matrix such as pores can influence its value. A rigorous method to establish the elastic limit from test results is needed.
3. In a UHPFRC layer, the material is submitted to biaxial tensile stress. However, there is very little experimental work [C.8] on the behavior of UHPFRC under biaxial solicitations, whether biaxial tension, compression-tension or biaxial compression. More research is needed to understand the behavior of UHPFRC under these types of solicitations which are common in structural elements.

### 3.2 Structural behavior of RU-RC elements

Although a lot of work has been done in the past years to understand the behavior of RU-RC composite sections and to develop models to predict their behavior, some experimental followed by modelling work could still be carried to precise and extend the knowledge.

1. NIC strongly influences the contribution of a UHPFRC layer to shear resistance. The length of this NIC was estimated with the tensile strength of concrete. However, a series of direct shear tests or tests reproducing the out-of-plane bending action of the layer would allow identifying exactly the bond behavior of the interface. The presence of pre-existing cracks in the concrete could also be studied.
2. Slabs submitted to point forces near linear supports, such as box-girder bridge deck slabs, have a behavior different from beams submitted to one-way shear or slabs submitted to punching shear [C.9, 10]. Transversal redistribution of forces can occur prior to failure which is a combination of punching and one-way shear failure. An experimental campaign on composite RU-RC cantilever slabs submitted to point forces near linear supports would help to study how the out-of-plane bending mechanism of the UHPFRC layer contributes to this type of failure and how it affects transversal redistribution.
3. In the case of ribbed slabs, T-beams and I-beams the shear failure will happen in the RC webs. It would be interesting to know how a layer of UHPFRC added on the top flange contributes the shear resistance of such beams.
4. The method developed herein is intended for the strengthening of existing structures. A moment-curvature relation was proposed to take into account pre-existing strains in the RC section. However, these pre-existing deformations or cracks can also influence the shear resistance capacity of the RC section as well as the bond between the UHPFRC layer and the existing section. Tests on pre-damaged members or slabs could help identifying the influence of pre-existing strains and cracks.

5. All studies have been carried out on the behavior of composite RU-RC sections with the UHPFRC layer acting as a tensile reinforcement. However, in the case of continuous beams, the layer can also be in the compression zone. Using plane section analysis, the bending behavior and resistance of such a configuration can quite simply be identified [C.11]. Nonetheless, an investigation should be carried on how compression in the UHPFRC layer can influence the behavior of the interface with the RC section and the shear resistance of the composite section.

### 3.3 Reinforcing with UHPFRC

UHPFRC could also be used to reinforce steel girders or steel slabs to increase the ultimate limit state resistance or the fatigue life of the element. Some first tests have been carried out on small specimens to investigate how the connection could be made between the new UHPFRC layer and a steel plate [C.12, 13]. However, more research needs to be done to investigate how the composite UHPFRC-steel section behaves.

## 4 References

- [C.1] Muttoni A. Punching Shear Strength of Reinforced Concrete Slabs without Transverse Reinforcement. *ACI Structural Journal*. 2008;105(4):440-50.
- [C.2] AFGC. Ultra High Performance Fibre-reinforced Concretes – Recommendations. Paris: Association Française de Génie Civil; 2013; 358 p.
- [C.3] SIA. CT 2052 : Béton fibré ultra-performant (BFUP) - Matériaux, dimensionnement et exécution. Zürich: Société suisse des Ingénieurs et Architectes; 2015.
- [C.4] Ozyurt N, Mason TO, Shah SP. Non-destructive monitoring of fiber orientation using AC-IS: An industrial-scale application. *Cement and Concrete Research*. 2006;36(9):1653-60.
- [C.5] Lataste JF, Behloul M, Breyse D. Characterisation of fibres distribution in a steel fibre reinforced concrete with electrical resistivity measurements. *NDT & E International*. 2008;41(8):638-47.
- [C.6] Ferrara L, Faifer M, Toscani S. A magnetic method for non destructive monitoring of fiber dispersion and orientation in steel fiber reinforced cementitious composites—part 1: method calibration. *Materials and Structures*. 2012;45(4):575-89.
- [C.7] Nunes S, Ribeiro F, Carvalho A, Pimentel M, Brühwiler E, Bastien-Masse M. Non-destructive measurements to evaluate fiber dispersion and content in UHPFRC reinforcement layers. In: Pacheco P, Magalhaes F, editors. *Multi-Span Large Bridges*; 01-03 July 2015; Porto, Portugal: Taylor & Francis Group; 2015. p. 1001-8.
- [C.8] Astudillo E, Bernier G, Plé O. Le BPR fibré sous sollicitation biaxiale - Étude expérimentale du comportement mécanique en bitraction du Béton de Poudres Réactives (BPR) fibré. *Revue française de génie civil*. 2002;6(5):709-22.
- [C.9] Lantsoght EOL, Veen C, Walraven J. Shear in One-Way Slabs under Concentrated Load Close to Support. *ACI Structural Journal*. 2013;110(2):275-84.
- [C.10] Natário F, Fernández Ruiz M, Muttoni A. Shear strength of RC slabs under concentrated loads near clamped linear supports. *Engineering Structures*. 2014;76:10-23.
- [C.11] Habel K. Structural behaviour of elements combining ultra-high performance fibre reinforced concretes (UHPFRC) and reinforced concrete. Doctoral thesis EPFL no. 3036. Lausanne: Ecole Polytechnique Fédérale de Lausanne; 2004; 195 p.

[C.12] Duan L, Noukpo Houankpo TO, Dong P, Wang CS, Brühwiler E. UHPFRC Strengthening Method for Existing Bridges. IABSE Conference 'Structural Engineering: Providing Solutions to Global Challenges'; Geneva: IABSE; 2015. p. 1179-86.

[C.13] Duan L, Brühwiler E, Wang CS. Experimental Investigation of Steel – UHPFRC Composite Behaviour. IABSE Workshop 'Exploring the Potential of Hybrid Structures for Sustainable Construction'; Fribourg, Switzerland: IABSE; 2014.





# Appendix A

## Characterization of the UHPFRC S3-13

---

This test report contains 53 pages that are independently numbered from the thesis. It gives all the details and results of the characterization campaign carried out on the UHPFRC mix S3-13.

The report is available online at [DOI:10.5075/epfl-thesis-6841](https://doi.org/10.5075/epfl-thesis-6841)



# **Appendix B**

## **Punching Tests on R-UHPFRC-RC Composite Slabs without Shear Reinforcement**

---

This test report contains 78 pages that are independently numbered from the thesis. It gives all the details and results of the punching tests carried out on the four PBM composite slabs.

The report is available online at [DOI:10.5075/epfl-thesis-6841](https://doi.org/10.5075/epfl-thesis-6841)



# Curriculum Vitae

---

## Maléna BASTIEN-MASSE

Civil Engineer, M.A.Sc.

[malena.bastien.masse@gmail.com](mailto:malena.bastien.masse@gmail.com)

Date of Birth: 01.08.1985

Nationality: Canadian



## EDUCATION

---

- 2011-2015:**      **Doctoral candidate, Structural Engineering**  
École Polytechnique Fédérale de Lausanne  
Title: Structural Behavior of R-UHPFRC – RC Composite Slabs  
Director: Prof. E BRÜHWILER
- 2008-2010:**    **Master in Applied Sciences (M.A.Sc), Civil Engineering**  
École Polytechnique de Montréal  
Title: Time-dependant strain behavior of repair concretes  
Director: Prof. JP CHARRON
- 2004-2008:**    **Bachelor in Civil Engineering (B.Eng.)**  
Specialisation in infrastructures and construction  
École Polytechnique de Montréal  
Academic distinction from the school chairman

## WORK EXPERIENCE

---

- 2011-2015:**      **Research and teaching assistant, EPFL**  
Research and consulting projects on composite R-UHPFRC – RC structures  
Teaching assistant for “Security and Reliability of Structures”, “Existing Structures” and “Aesthetics of Structures” as well as supervision of master projects
- 2010-2011:**    **Junior Engineer, Civil Engineering Department, AECOM, Montréal**  
Design of structures auxiliary to hydropower plants
- 2009-2010:**    **Research trainee, Laboratoire Central des Ponts et Chaussées, Paris**  
Experimental and numerical work on time-dependant behavior of UHPFRC

**2006-2007: Research trainee, École Polytechnique de Montréal**  
Experimental work on the early age mechanical properties of UHPFRC

**Summers 2006 and 2007: Trainee Engineer, Transport Department  
VIA Rail Canada Inc., Montréal**  
Management and maintenance of railway tracks  
Upgrading of all crossings on 250 km of countryside tracks

## **OTHER EXPERIENCES**

---

**2014-2015: Scientific Committee Secretary, IABSE Geneva Conference 2015**  
With the chair of the Scientific Committee, coordination of all the peer-review process for the conference, from initial abstract submission to the preparation of the final conference proceedings: 500 submitted abstracts, 300 accepted and published papers, 500 conference participants.

## **PUBLICATIONS**

---

### **Internationally peer-reviewed journal papers:**

Bastien-Masse M, Brühwiler E. Experimental Investigation on Punching Resistance of R-UHPFRC – RC Composite Slabs. *Materials and Structures*. 2015: doi:10.1617/s11527-015-0596-4.

Rossi P, Charron JP, Bastien-Masse M, Tailhan JL, Le Maou F, Ramanich S. Tensile basic creep versus compressive basic creep at early ages: Comparison between normal strength concrete and a very high strength fibre reinforced concrete. *Materials and Structures*. 2014;47(10):1773-85.

### **International conference peer-reviewed contributions:**

Brühwiler E, Bastien-Masse M, Mühlberg H, Houriet B, Fleury B, Cuennet S, et al. Strengthening the Chillon viaducts deck slabs with reinforced UHPFRC. IABSE Conference 'Structural Engineering: Providing Solutions to Global Challenges'; Geneva: IABSE; 2015.

Bastien-Masse M, Brühwiler E. Ultra high performance fiber reinforced concrete for strengthening and protecting bridge deck slabs. In: Chen A, Frangopol D, Ruan X, editors. IABMAS Conference 'Bridge Maintenance, Safety, Management and Life Extension'; Shanghai: CRC Press; 2014. p. 2176-82.

Bastien-Masse M., Brühwiler E., Makita, T. Analytical modelling of R-UHPFRC - RC composite members subjected to combined bending and shear, In: F. T, J. R, editors. RILEM-fib-AFGC International Symposium on Ultra-High Performance Fibre-Reinforced Concrete; 2013; Marseille, France: RILEM; 2013. p.177-86

Bastien-Masse M, Brühwiler E. Concrete bridge deck slabs strengthened with UHPFRC. IABSE Conference 'Assessment, Upgrading and Refurbishment of Infrastructures'; Rotterdam: IABSE; 2013.

## **AWARDS AND SCHOLARSHIPS**

---

**2013: IABSE Young Engineer Award for Outstanding Contribution**

IABSE Rotterdam Conference 2013

**2008-2010: Canada Graduate Scholarship - Master's Program**

Natural Sciences and Engineering Research Council of Canada

Two years of funding during the graduate master studies awarded to high level students

**2007-2008: De Vinci Distinction, École Polytechnique de Montréal**

Distinction attributed to students who have diversified their experiences during their bachelor degree while maintaining high grades

## **SKILLS**

---

**Professional:** Characterization, design and application of UHPFRC; Design of reinforced concrete; Examination, upgrading and reinforcement of existing structures

**Softwares:** Microsoft Office, MATLAB, ATENA (finite elements), AutoCAD, Adobe Illustrator

**Languages:** French (mother tongue), English (fluent), Spanish (basic knowledge, level B1), German (basic knowledge, level A2).

## **PERSONAL INTERESTS**

---

Classical and contemporary dance, practiced for over 20 years

